UNIVERSIDAD MICHOACANA DE SAN NICOLÁS DE HIDALGO

Instituto de Física y Matemáticas

INDUCED BOUND STATES BY MONOPOLE AND POINT DIPOLE ELECTRIC IMPURITIES IN STRAINED GRAPHENE

Tesis que para obtener el grado de
Maestro en Ciencias en el Área de Física

Presenta:
JULIO CÉSAR PÉREZ PEDRAZA

Asesor:
Dr. Alfredo Raya Montaño

MORELIA, MICH., FEBRERO DEL 2020.

"La imaginación es más inportante que el conocimiento. El conocimiento es limitado. La imaginación circunda al mundo."

-A. Einstein

Agradecimientos

Con este trabajo “culmina” una etapa de mi vida, pero tambien “arranca” una nueva. Los dos pilares fundamentales a lo largo de mi historia, y a quienes les debo mayormente en lo que me he convertido, han sido mis padres, Esteban y Araceli, quienes siempre me han inculcado el trabajo, esfuerzo y responsabilidad con sus propias acciones, pero también el cariño, el apoyo y la felicidad como parte fundamental del éxito en cualquier cosa. Por todo eso les quiero y agradezco infinitamente.

Siempre he considerado a esta profesión como una de las mas bellas y adictivas, pero también algo “peligrosa” en el sentido de que es fácil perderse de la vida diaria y de momentos que no se recuperan después. Es por eso que valoro demasiado el tiempo y los momentos que durante prácicamente toda esta etapa compartiste conmigo, Gaby. De corazón te agradezco por ellos, buenos, malos o extraños, pero has sido un gran equilibrio en mis días.

Quiero además agradecer a mis hermanos, Ivonne y Beto, por su cariño, confidencia y hasta por su carrilla desde que eramos pequeños y hasta la fecha, son parte importante de lo que soy ahora. Además de que, Ivonne, trajiste a “gordita” a alegrar la familia. Y obvio aquí entran también Ludo, Alberta y Yeska, siempre incondicionales.

No puedo dejar de mencionar a todos mis amigos que, para no ser injusto, prefiero no mencionarlos por su nombre. Ustedes saben quienes son.

Quiero agradecer a la UMSNH, mi alma máter, al IFM, y en particular al Dr. Alfredo por darme la oportunidad de hacer lo que me gusta e intentar “vivir” de ello. Gracias Dr. por todos los conocimientos y charlas compartidas conmigo que sin duda me han ayudado a mejorar como estudiante y como persona.

Al CONACyT por el apoyo económico para realizar estos estudios.

Finalmente agradecer a todas las personas que se me han escapado, pero que en

alguna etapa de mi vida han colaborado a hacerme crecer como persona. Gracias totales!

Resumen

El grafeno ha acaparado los reflectores de la comunidad científica debido a sus intrigantes propiedades nunca antes vistas en materiales convencionales. En particular, su resistencia mecánica lo hace capaz de soportar deformaciones mayores a 20%, lo cual abre la posibilidad de modificar sus propiedades electrónicas mediante deformaciones mecánicas (*Straintronics*). Las deformaciones en el grafeno pueden producir adicionalmente campos *pseudo-magnéticos* intensos, los cuales juegan un rol importante por ejemplo en la aparición de niveles de Landau sin un campo magnético externo aplicado. También, el fenómeno de colapso atómico, predicho por la Mecánica Cuántica Relativista, fue recientemente logrado en grafeno con una impureza cargada y ha sido mostrado que dicho fenómeno puede ocurrir en condiciones menos demandantes mediante la inclusión de un campo magnético externo. En este trabajo estudiamos el problema de los estados ligados en grafeno bajo la influencia de los potenciales de un monopolo eléctrico y un dipolo eléctrico puntual, extendido al caso en el cual la membrana de este material es deformada. Considerando una velocidad de Fermi anisótropa, resolvemos analíticamente la ecuación de Dirac resultante para cada potencial. Observamos que el efecto de la anisotropía es promover o inhibir el comportamiento crítico que se conoce ocurre para cada tipo de impureza, dependiendo de la dirección sobre la que se aplica la deformación: Tanto el colapso atómico para el caso de una impureza monopolar, como la emergencia de cascadas de infinitos estados ligados con un escalamiento universal de tipo Efimov para la impureza dipolar, son fenómenos que ocurren bajo menores o mayores condiciones restrictivas debido a la deformación.

Palabras clave: *Deformación en grafeno, estados ligados, monopolo eléctrico, dipolo eléctrico puntual, colapso atómico, escalamiento tipo Efimov.*

Abstract

Graphene lies on the spotlight for the scientific community because of its intriguing properties never seen before in conventional materials. In particular, it mechanical resistance makes it able to sustain strains larger than 20%, which opens the possibility to tune its electronic properties by strain (*Straintronics*). Strain in graphene additionally produces intense *pseudo-magnetic* fields, which play an important role for example in the development of Landau levels without an external applied magnetic field. Also, the atomic collapse phenomenon, predicted by Relativistic Quantum Mechanics, was recently achieved with a charged impurity center in graphene and it has been shown that such phenomenon can happen under less restrictive conditions by the inclusion of an external magnetic field. In this work, we study the problem of bound states in graphene under the influence of point electric monopole and dipole impurity potentials extended to the case in which the membrane of this material strained. By considering an anisotropic Fermi velocity, we analytically solve the resulting Dirac equation for each potential. We observe that the effect of the anisotropy is to promote or inhibit the critical behavior known to occur for each kind of impurity, depending on the direction along which strain is applied: Both the atomic collapse in the case of a monopole impurity, and the emergence of cascades of infinitely many bound states with a universal Efimov-like scaling for dipole impurity, are phenomena that occur under lesser or greater restrictive conditions due to strain.

Keywords: *Strained graphene, bound states, electric monopole, point electric dipole, atomic collapse, Efimov-like scaling.*

Contents

Chapter 1

Introduction

In the past century (1935-1937) some outstanding physicists like L. Landau [1], R. E. Peierls [2] and N. D. Mermin [3] argued that 2D materials were thermodynamically unstable due to thermal fluctuations. Back in 1947, the idea of a monolayer of Carbon was considered by P. R. Wallace from a theoretical point of view exploring the applicability of graphite in nuclear reactors [4]. This apparent problem with low-dimensional materials was left behind when, in 2004, A. Geim and K. Novoselov (Fig. 1.1) were able to synthesize graphene [5]. The physical explanation was almost immediately reached [6, 7], arguing that in this of material, there is an elastic energy gain, but thermal vibration energy is suppressed, making it stable.

Figure 1.1: Andre Geim (left) and Konstantin Novoselov (right), Nobel Prize in Physics 2010.

In the past few years graphene, as the principal representative of 2D materials, has gained special attention in Condensed Matter Physics. This is so because of the surprising electronic and mechanical properties that it possesses, such as being very strong but malleable at the same time, resistant to strains and deformations

[8]. Its charge carriers present a very high mobility, and anomalous QHE can be produced, both at room-temperature. If that was not enough, because of the form of the equation of motion governing its charge carriers at low energies (a Dirac-like equation), graphene can be thought and used as a mini QED lab, where it is possible to measure effects as the Klein paradox, *Zitterbewegung*, and some effects of QED in curved spaces can be tested too [8]. More recently, experiments have found that strains in a graphene lattice can produce high intensity *pseudo-magnetic* fields [9]. Additionally, the old relativistic prediction of atomic collapse [10] has been experimentally measured recently in graphene by Y. Wang *et al.* [11]. The theoretical explanation was given a few years earlier using energy considerations of relativistic particles [12, 13, 14, 15, 16, 17], predicting manifestations as strong oscillations in the local density of states in the supercritical regime [12], as measured by Wang.

In this thesis we introduce and study graphene, starting with its main properties to later focus in the effects of strain in the electronic and magnetic properties, with special attention in the predicted and recently accomplished atomic collapse in graphene, but with strain under consideration. The structure of the thesis is as follows: In Chapter 2, we introduce and discuss the basic properties of graphene, focusing in two aspects which are of relevance for this thesis: Crystallographic and electronic properties. In the third Chapter, we address the Landau problem in two cases: Non-relativistic charged particles and relativistic charged particles (massless Dirac Fermions) as in graphene. In both cases, the Landau and the Symmetric gauges are considered to define the external magnetic field. The results are useful in comparing with the Landau levels in strained graphene that we obtain below, in Chapter 5. But before reaching to this point, in Chapter 4, we first consider the case of strain in graphene. We briefly introduce the notions of strain in crystals, and then, we tackle the issue of the *pseudo-magnetic* field generation by strain, focusing in uniaxial and triaxial strains in graphene. For both cases, we discuss the effect of these deformations in the Landau levels. Then, in Chapter 5, the atomic collapse phenomenon in graphene is discussed. In the first section, an introduction of the subject is given. Then, we consider the case of graphene in the field of a Coulomb impurity, immersed in a homogeneous magnetic field perpendicular to the plane of graphene, and considering uniaxial strains of the lattice. It is known [15] that by regularizing the Coulomb potential by a spherical potential well, a critical strength of the potential is required to induce collapse, and that such critical potential is diminished as an external magnetic field is turned on. We obtain some expressions and curves of the energy and critical potential with explicit dependence of the strain effects in this case. We also consider qualitatively the case of the Coulomb center with no external magnetic field, but with a strained- generated *pseudomagnetic* field. In the same order of ideas, in Chapter 6 we treat the case of a point electric dipole placed in a graphene sheet. This configuration give rise to bound states, and can be used to

provoke atomic collapse in graphene [18, 19]. First, the electric dipole is introduced, obtaining the point electric dipole expression for large distances. Then, using this expression, the corresponding Dirac equation for the point dipole in graphene including strain is solved, obtaining expressions for the eigenstates and energies depending on the strain strength and the electric dipolar moment. Plots for different values of the strain strength are included. Finally, in Chapter 7 we discuss the results and point out the conclusions obtained during the thesis, finishing with some possible future works in the subject. Additionally, two appendices are presented. In Appendix A, the Dirac equation is introduced, which is the equation ruling the behavior of the fermions in two-dimensional systems like graphene. In Appendix B, we develop and get some useful expressions used throughout the thesis.

Chapter 2

Graphene: A two-dimensional material

In this Chapter we briefly introduce graphene, an amazingly interesting material due to its properties and potential applications. It is the mother of all Carbon graphitic structures, as shown in Fig. 2.1. Fullerenes, nanotubes and multilayers of graphene are of great relevance in technological applications and fundamental physics research nowadays. We introduce and discuss the basic properties of graphene, focusing in two aspects which are of relevance for this thesis: Crystallographic and electronic properties.

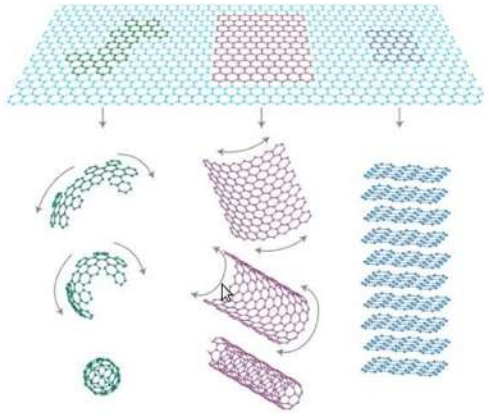

Figure 2.1: Some structures based in graphene. Graphene can be wrapped to form fullerenes, rolled up to form Carbon nanotubes, or piled up to form graphite. Figure adapted from [8].

2.1 Crystallographic properties

In this Section we follow the discussion given in [20]. Graphene is the name of an array of Carbon atoms tightly packed in a one-atom thick honeycomb (hexagonal) lattice (Fig. 2.2(a)). The honeycomb array itself is not a Bravais lattice (it is not invariant under arbitrary translations), so, graphene crystalline structure is considered in practice as a bipartite lattice, consisting of two triangular sublattices A and B, whose unitary cell is shown in Fig. 2.2(a) (these cells contain both kind of atoms A and B).

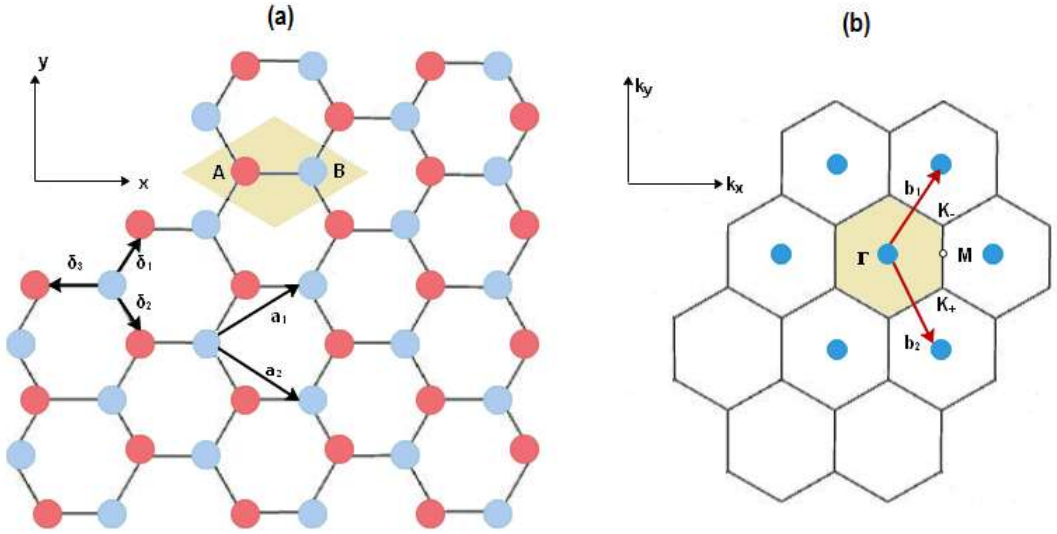

Figure 2.2: (a) Hexagonal graphene lattice formed by two triangular sublattices A and B. The primitive vectors $\mathbf{a}_1$ and $\mathbf{a}_2$, along with the vectors that join both sublattices, $\boldsymbol{\delta}_i$ are shown. (b) FBZ of the graphene lattice. Some important points ($\mathbf{\Gamma}$, $\mathbf{K}_-$, $\mathbf{K}_+$, $\mathbf{M}$) are also drawn.

For pristine graphene, the Bravais lattice is generated by the primitive vectors (shown in Fig. 2.2(a))

$$\mathbf{a}_1 = \frac{a}{2}(3, \sqrt{3}), \qquad \mathbf{a}_2 = \frac{a}{2}(3, -\sqrt{3}), \tag{2.1}$$

where a represents the inter-atomic distance (in graphene $a \approx 1.42$Å) [4, 21]. Any site in real (position) space can be written as a linear combination of these vectors

$$\mathbf{R} = n\mathbf{a}_1 + m\mathbf{a}_2 \ , \tag{2.2}$$

with n and m integers. Also, the vectors that join one kind of atoms (A or B) with

its three nearest neighbors (Fig. 2.2(a)) are

$$\boldsymbol{\delta}_1 = \mathbf{a}_1 + \boldsymbol{\delta}_3 = \frac{a}{2}(1, \sqrt{3}), \quad \boldsymbol{\delta}_2 = \mathbf{a}_2 + \boldsymbol{\delta}_3 = \frac{a}{2}(1, -\sqrt{3}), \quad \boldsymbol{\delta}_3 = -a(1, 0) \ , \tag{2.3}$$

where we use the fact that the underlying lattice (honeycomb) can be generated by the two vectors $\mathbf{a}_1$, $\mathbf{a}_2$, and one of the $\boldsymbol{\delta}_i$ vectors, which, for simplicity, is taken to be $\boldsymbol{\delta}_3$. Thus, any point in the honeycomb lattice can be reached by a translation

$$\mathbf{T} = n\mathbf{a}_1 + m\mathbf{a}_2 - \boldsymbol{\delta}_3 \ . \tag{2.4}$$

In addition, we can see that graphene lattice has two principal directions: *Zig-zag* and *armchair* (Fig. 2.3). These directions repeat alternately every 30°, and they are of great importance in the the discussion of strained graphene.

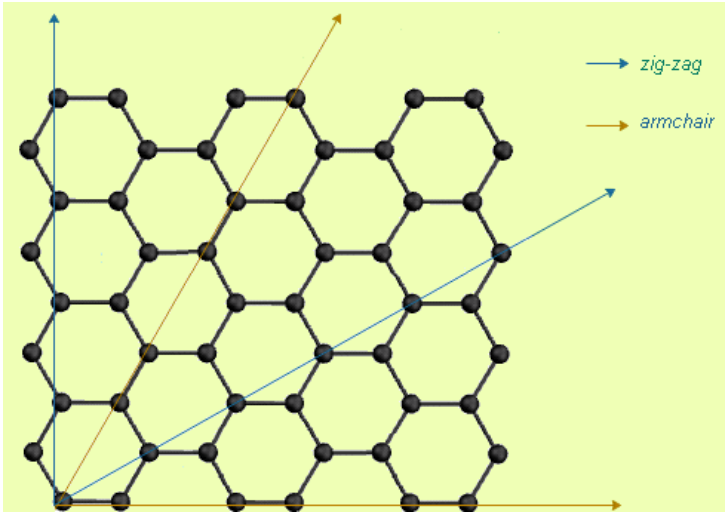

Figure 2.3: *Zig-zag* and *armchair* directions in graphene. They repeat alternately every 30°.

To define the reciprocal lattice, according with the definition in classical textbooks [22], we introduce the basis vectors $\mathbf{b}_i$ that verify

$$\mathbf{a}_i \cdot \mathbf{b}_j = 2\pi\delta_{ij}, \tag{2.5}$$

and they are explicitly obtained to be:

$$\mathbf{b}_1 = \frac{2\pi}{3a}(1, \sqrt{3}), \quad \mathbf{b}_2 = \frac{2\pi}{3a}(1, -\sqrt{3}). \tag{2.6}$$

The First Brillouin Zone (FBZ), which is the analogue to the Wigner-Seitz cell in the reciprocal space, is hexagonal as well (Fig. 2.2(b)), but rotated 90°. In this

FBZ we locate the high-symmetry points: $\mathbf{K}_+$, $\mathbf{K}_-$[1], $\mathbf{M}$ and $\mathbf{\Gamma}$ as:

$$\mathbf{K}_+ = \frac{2\pi}{3a}\left(1, -\frac{1}{\sqrt{3}}\right),\ \mathbf{K}_- = \frac{2\pi}{3a}\left(1, \frac{1}{\sqrt{3}}\right),\ \mathbf{M} = \frac{2\pi}{3a}(1,0),\ \mathbf{\Gamma} = (0,0)\ . \qquad (2.7)$$

The points $\mathbf{K}_\pm$ are called Dirac points, and they are of central importance in the properties exhibited by graphene since, as we discuss below, the dispersion relation of graphene has critical points (minimum and maximum respectively to the signs + and -) at these points, where the valence and conduction bands intersect. $\mathbf{\Gamma}$ is the point located at the center of the FBZ, and $\mathbf{M}$ is the midpoint between the $\mathbf{K}_+$ and $\mathbf{K}_-$ points.

2.2 Electronic properties and dispersion relation

Based in the discussion given in [20, 23], when atoms are arranged in crystals (solids), the system can decrease its ground state energy by overlapping the wave functions of the "free" electrons. In the case of Carbon, whose electronic configuration is $1s^2\ 2s^2\ 2p^2$, electrons in the $1s$ layer (we call them "$1s$ electrons") are very near the nucleus, so that they are strongly bounded to it and they do not interact (create bonds) with the other electrons; they are considered bonded electrons. The energy of the Carbon crystal decreases by promoting one of the $2s$ electrons to the $2p$ orbital (Fig. 2.4), producing four equivalent states denoted by $|2s\rangle$, $|2p_x\rangle$, $|2p_y\rangle$ and $|2p_z\rangle$ [24], and creating hybrid orbitals between them. Depending on the number of orbitals involved in the hybridization, the Carbon structure gets different physical properties. The superposition of n $|p_i\rangle$ orbitals with the orbital $|2s\rangle$ constitute an sp^n hybridization [25]. For example, when the four orbitals mix, hybridization sp^3, they form orbitals in an icosahedric array (Fig. 2.5), forming strong covalent bonds (σ bonds) because of the large overlap of the wave functions. This explains why diamond is one of the hardest materials in nature. On the other hand, when just two of the $|2p\rangle$ states (usually taken $|2p_x\rangle$ and $|2p_y\rangle$) and the $|2s\rangle$ state mix, they form hybrid sp^2 orbitals lying on a plane (Fig. 2.6) forming σ bonds, with the remaining non-interacting $|2p_z\rangle$ electron forming a weaker bond (usually called π bond) perpendicular to the plane of the σ bonds. This is the structure of graphite (constituted by many graphene layers), where the σ bonds are responsible of the mechanical properties whereas the π bonds are responsible of the electronic properties.

Let us compute the dispersion relation in graphene within the tight-binding approach (to nearest-neighbors). Let us consider only the π states, with *hopping* parameter t ($\sim$ 2.97eV for graphene [23]) giving the probability for an electron to

[1]The $\mathbf{K}_+$, $\mathbf{K}_-$ points are also usually called $\mathbf{K}$, $\mathbf{K}'$ points, respectively.

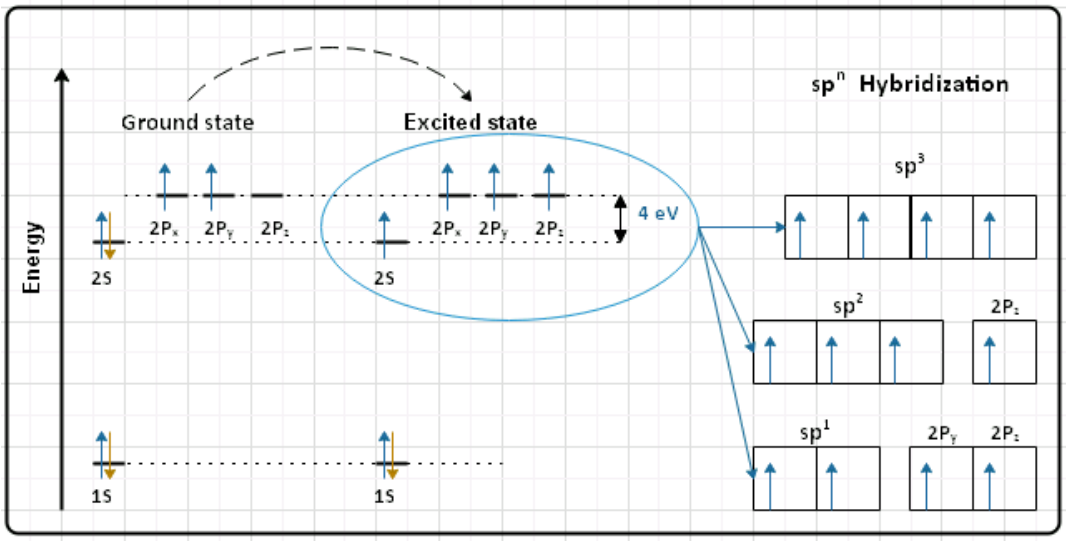

Figure 2.4: In Carbon lattices, one of the $2s$ electrons is promoted to the $2p_z$ state, creating an excited state with an increase of energy of approximately 4eV. This configuration gives rise to four equivalent states which can hybridize among them, forming different kind of bonds. They are called sp^n hybridizations depending on the number of p electrons involved.

hop from one site A to one nearest-neighbor site B (in this nearest-neighbors TB approach there is no hopping within the same sublattice). So, the Schrödinger equation describing the system is

$$E\psi_A(\mathbf{r}_A) = t\psi_B(\mathbf{r}_B) + t\psi_B(\mathbf{r}_B - \mathbf{a}_1) + t\psi_B(\mathbf{r}_B - \mathbf{a}_2), \tag{2.8}$$

$$E\psi_B(\mathbf{r}_B) = t\psi_A(\mathbf{r}_A) + t\psi_A(\mathbf{r}_A + \mathbf{a}_1) + t\psi_A(\mathbf{r}_A + \mathbf{a}_2). \tag{2.9}$$

As we are dealing with a periodic potential of periodicity $\mathbf{T}$, using Bloch's theorem:

$$\psi_k(\mathbf{r} + \mathbf{T}) = \psi_k(\mathbf{r})e^{\mathbf{k}\cdot\mathbf{T}}, \tag{2.10}$$

and exploiting the fact that $\mathbf{a}_1 = -\boldsymbol{\delta}_3 + \boldsymbol{\delta}_1$, $\mathbf{a}_2 = -\boldsymbol{\delta}_3 + \boldsymbol{\delta}_2$, the Schrödinger equation can be written as

$$\hat{H}(k)\begin{pmatrix}\psi_A\\ \psi_B\end{pmatrix} = \begin{pmatrix}0 & tS(\mathbf{k})\\ tS^*(\mathbf{k}) & 0\end{pmatrix}\begin{pmatrix}\psi_A\\ \psi_B\end{pmatrix}, \tag{2.11}$$

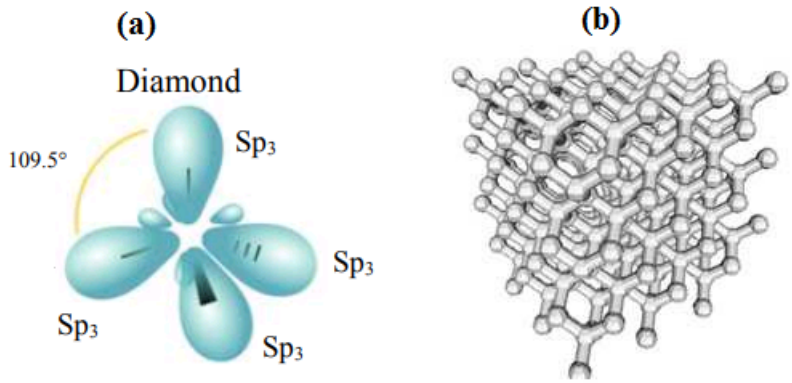

Figure 2.5: (a) Hybridization sp^3 in Carbon, forming an icosahedric array of strong σ bonds. (b) Diamond lattice formed by only σ bonds, making the lattice very resistant and strong. Figure adapted from [26].

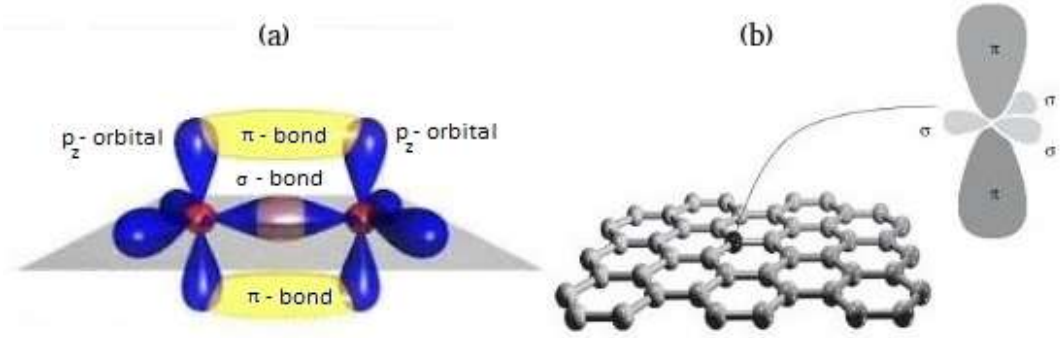

Figure 2.6: (a) sp^2 hybridization in Carbon, where three strong σ bonds in a plane, and two weak π bonds perpendicular to this plane are formed. (b) Graphene lattice formed by σ bonds. Figure (b) adapted from [27].

where

$$S(\mathbf{k}) = \sum_{\delta} e^{i\mathbf{k}\cdot\boldsymbol{\delta}} = e^{i\frac{a}{2}(k_x+\sqrt{3}k_y)} + e^{i\frac{a}{2}(k_x-\sqrt{3}k_y)} + e^{-iak_x}$$
$$= 2\cos\left(\frac{\sqrt{3}}{2}ak_y\right) e^{i\frac{a}{2}k_x} + e^{-iak_x}, \tag{2.12}$$

where the definitions of $\boldsymbol{\delta}_i$ are given by Eq. (2.3). From this expression, it is easy to obtain the energy-momentum relation

$$E(\mathbf{k}) = \pm t\ |S(\mathbf{k})| = \pm t\left\{S(\mathbf{k})S^*(\mathbf{k})\right\}^{1/2},$$

with $S(\mathbf{k})$ given in Eq. (2.12), and $S^*(\mathbf{k})$ its complex conjugate. Thus, the energy-momentum dispersion relation is given by

$$E(\mathbf{k}) = \pm t\sqrt{4\cos^2\left(\frac{\sqrt{3}}{2}ak_y\right) + 2\cos\left(\frac{\sqrt{3}}{2}ak_y\right)e^{i\frac{3a}{2}k_x} + 2\cos\left(\frac{\sqrt{3}}{2}ak_y\right)e^{-i\frac{3a}{2}k_x} + 1}$$

$$= \pm t\sqrt{4\cos^2\left(\frac{\sqrt{3}}{2}ak_y\right) + 4\cos\left(\frac{\sqrt{3}}{2}ak_y\right)\cos\left(\frac{3}{2}ak_x\right) + 1}$$

$$= \pm t\sqrt{2\cos\left(\sqrt{3}ak_y\right) + 4\cos\left(\frac{\sqrt{3}}{2}ak_y\right)\cos\left(\frac{3}{2}ak_x\right) + 3}. \tag{2.13}$$

In the Dirac point $\mathbf{K}_+$ (given in Eq. (2.7)):

$$E(\mathbf{K}_+) = \pm t\sqrt{2\cos\left(\sqrt{3}a\frac{2\pi}{3\sqrt{3}a}\right) + 4\cos\left(\frac{\sqrt{3}}{2}a\frac{2\pi}{3\sqrt{3}a}\right)\cos\left(\frac{3}{2}a\frac{2\pi}{3a}\right) + 3}$$

$$= \pm t\sqrt{2\cos\left(\frac{2\pi}{3}\right) + 4\cos\left(\frac{\pi}{3}\right)\cos(\pi) + 3} = 0. \tag{2.14}$$

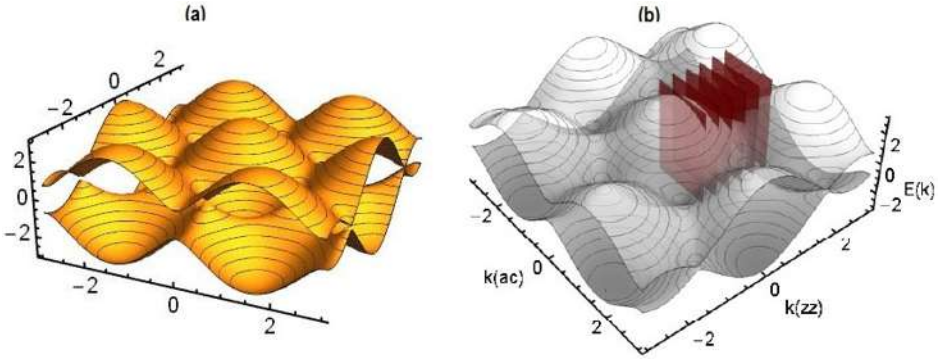

Figure 2.7: (a) Energy-momentum dispersion relation in graphene (Eq.(2.13)). The upper band corresponds to the conduction band and the lower to the valence band. It can be seen that both bands touch at the Dirac points $\mathbf{K}$, $\mathbf{K}'$. (b) Transverse cuts in the 3D energy-momentum scheme.

Similarly, $E(\mathbf{K}_-) = 0$. This means that both, the valence and the conducting bands, touch each other at these points. Thus, graphene is said to be a zero-gap semiconductor. The dispersion relation given by Eq. (2.13) is shown in Fig. 2.7(a), where the behavior just seen in the Dirac points is represented clearly. If we take notice of the transverse cuts in the energy-momentum relation scheme (Fig. 2.7(b)), in 2D they are represented in Fig. 2.8(a) as red lines. We can construct the typical band structure plot by taking the path shown in Fig. 2.8(b) ($\mathbf{\Gamma} \to \mathbf{K} \to \mathbf{M} \to \mathbf{\Gamma}$). The

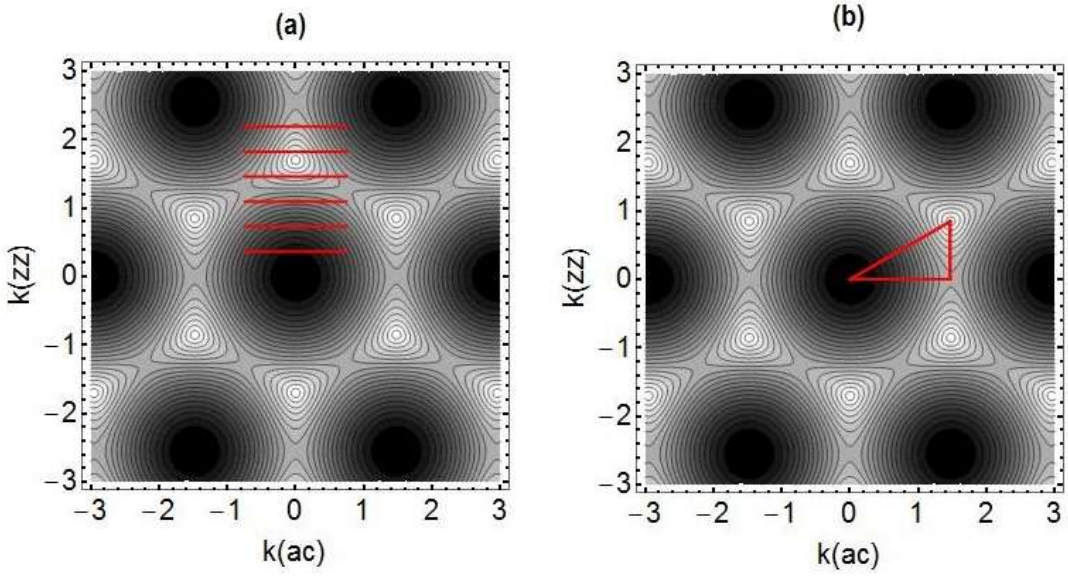

Figure 2.8: (a) 2D representation of a transverse cut of the energy-momentum relation scheme. (b) 2D transverse cut showing the typical path for diagrams in band structure model.

band structure model scheme obtained through this path is depicted in Fig. 2.9, where just the conduction electrons (π-electron) were considered. The π states form a single band of conical self-crossing point in $\mathbf{K}$ (and $\mathbf{K}'$). These cones (Dirac cones), first obtained by Wallace in 1947 [4], give rise to the peculiar electronic properties of graphene.

The band structure of graphene, including the effects of the σ-electrons, was recently computed [28], and it is shown in Fig. 2.10. It can be seen that the sp^2 hybridized states (σ bonds) form occupied and empty valence and conducting bands separated by a huge gap, so that, these states do not contribute to conduction (as we already knew).

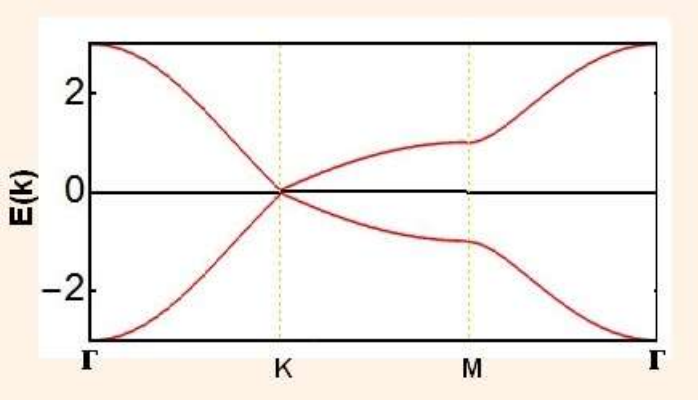

Figure 2.9: Band theory diagram for graphene, where only were considered the conducting π-electrons. The spectrum near the Dirac points is very similar to cones (Dirac cones). Both bands intersect in these Dirac points, having a zero-gap semiconductor behavior.

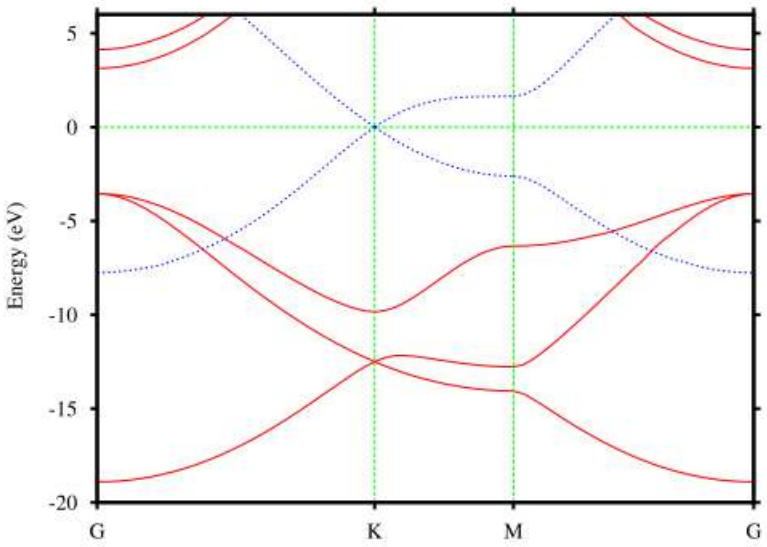

Figure 2.10: Band structure of a single graphene layer. Solid red lines represent σ bands and dotted blue lines represent π bands. The horizontal green line represents the Fermi level. Figure adapted from [28].

It is possible to expand the Hamiltonian near the Dirac points [23] by taking

$\mathbf{K} = \mathbf{k} + \mathbf{q}$ (such expansion is valid for energies less than 1eV [29]) as

$$\hat{H}_{\mathbf{K}_+,\mathbf{K}_-}(\mathbf{q}) = \hbar v_F \begin{pmatrix} 0 & q_x \mp i q_y \\ q_x \pm i q_y & 0 \end{pmatrix}, \tag{2.15}$$

with v_F the Fermi velocity given by [30]

$$v_F = \frac{3at}{2\hbar} \approx \frac{c}{300}. \tag{2.16}$$

This equation has the same mathematical form as the 2D massless Dirac Hamiltonian (Appendix A), but replacing the speed of light c by the Fermi velocity v_F:

$$\hat{H}_{\mathbf{K}_+} = v_F \left(\boldsymbol{\sigma} \cdot \mathbf{p}\right), \tag{2.17}$$

$$\hat{H}_{\mathbf{K}_-} = \sigma_1 \hat{H}_{\mathbf{K}_+} \sigma_1 = \hat{H}^T_{\mathbf{K}_+}. \tag{2.18}$$

Hence, the equation of motion is a Dirac-like equation

$$\hat{H}\Psi = E\Psi, \tag{2.19}$$

with the complete Hamiltonian

$$\hat{H} = \begin{pmatrix} \hat{H}_{\mathbf{K}_+} & 0 \\ 0 & \hat{H}_{\mathbf{K}_-} \end{pmatrix}, \tag{2.20}$$

and the spinor

$$\Psi = \begin{pmatrix} \psi_{\mathbf{K}_+,A} \\ \psi_{\mathbf{K}_+,B} \\ \psi_{\mathbf{K}_-,A} \\ \psi_{\mathbf{K}_-,B} \end{pmatrix}, \tag{2.21}$$

where $\psi_{\mathbf{K}_+,A}$, represents the wave function corresponding to the $\mathbf{K}_+$ valley and the sublattice A, and analogously the other functions.

As it is discussed in [23], the parameter t' of the next-to nearest-neighbors[2] in the tight-binding model has been computed by Reich *et al.* [32], finding $t' = 0.073$eV, a very small value compared with t. So, inside the FBZ, the next-to nearest-neighbors do not affect considerably to electronic properties near the Dirac points, making our model a good approximation (the second-next-to nearest-neighbors contribution is much bigger $t'' = 0.33$eV, but they lay outside of the FBZ).

In the next Chapter we analyze the Landau problem in graphene. For that purpose, the Dirac-like Hamiltonian of Eq. (2.15) is used, and a valley-dependence ($\mathbf{K}$ or $\mathbf{K}'$) appears in the solution.

[2]The Hamiltonian in this case is anisotropic [31].

Chapter 3

The Landau problem

When we confine a gas of charged particles to a plane (say, the $x-y$ plane) and observe the effect of an external uniform magnetic field directed perpendicularly to the plane ($\hat{k}$ direction), the resulting energy spectrum results to be discrete as shown in Fig. 3.1(b), (c). These discrete levels of energy are called Landau levels. In this Chapter we present the resulting Landau levels for two cases: Non-relativistic charged particles as in the original calculation [33] and relativistic charged particles (Dirac Fermions of zero mass) in graphene. In both cases, the Landau and the Symmetric gauges are considered to describe the external field. The results are useful in comparing with the Landau levels in strained graphene obtained in Chapter 4.

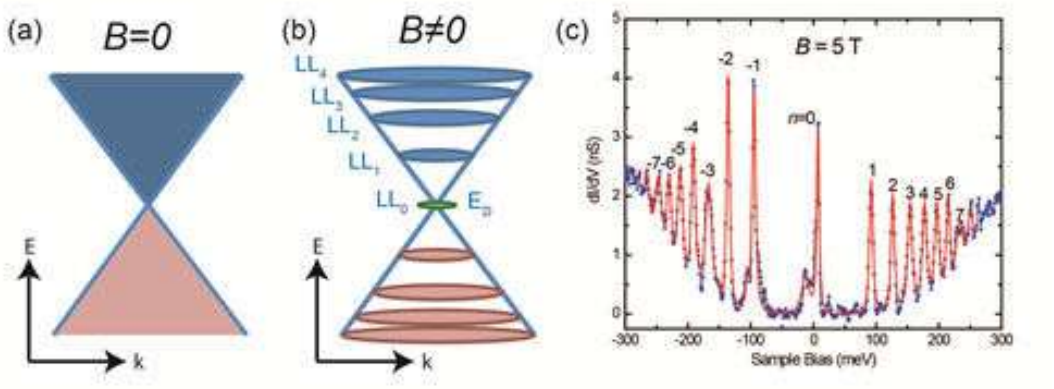

Figure 3.1: Landau levels in graphene. (a) Available states for $B = 0$. (b) Available states (Landau states) for $B \neq 0$. (c) LDOS for $B = 5$T. Adapted from [34].

3.1 The non-relativistic Landau problem

Let us consider a charged particle immersed in a constant, uniform magnetic field pointing in the $\hat{k}$ direction,

$$\mathbf{B} = B_0\hat{k}. \tag{3.1}$$

We neglect the spin degree of freedom in the following discussion, so that the Hamiltonian of the system is described by the Pauli Hamiltonian

$$H = \frac{1}{2M}\left(\boldsymbol{\pi} + \frac{e}{c}\mathbf{A}\right)^2, \tag{3.2}$$

where M is the mass of the particle, $\boldsymbol{\pi} = \mathbf{p} + \frac{e}{c}\mathbf{A}$ is the canonical momentum, which satisfies the commutation relations $[r_i, \pi_j] = i\hbar\delta_{i,j}$, and $\mathbf{A}$ is the magnetic vector potential, such that

$$\mathbf{B} = \nabla \times \mathbf{A}. \tag{3.3}$$

For this magnetic field $\mathbf{B}$ (Eq. (3.1)), we choose two different forms of the vector potential $\mathbf{A}$, given by two different elections of the gauge

$$\mathbf{A} = (0, B_0x, 0), \longrightarrow \text{Landau gauge} \tag{3.4}$$

$$\mathbf{A'} = \mathbf{A} + \nabla\Phi = \frac{B_0}{2}(-y, x, 0), \longrightarrow \text{Symmetric gauge} \tag{3.5}$$

where $\Phi = -\frac{B_0}{2}xy$ is used to apply a gauge transformation to the Landau gauge vector potential. We can easily see that both gauges satisfy the Coulomb condition:

$$\nabla \cdot \mathbf{A} = 0\ . \tag{3.6}$$

3.1.1 Landau gauge

In this case, the vector potential $\mathbf{A}$ is given by Eq. (3.4), so, the 2-D Hamiltonian, Eq. (3.2) is

$$H = \frac{1}{2M}\left[p_x^2 + \left(p_y + \frac{e}{c}B_0x\right)^2\right]\ . \tag{3.7}$$

Thus, the Schrödinger equation becomes

$$H\Psi(x,y) = \frac{1}{2M}\left[p_x^2 + \left(p_y + \frac{e}{c}B_0x\right)^2\right]\Psi(x,y) = E\Psi(x,y). \tag{3.8}$$

It is easy to get the energy spectrum [20], which corresponds to a simple harmonic oscillator given by

$$E_n = \hbar\omega_B \left(n + \frac{1}{2}\right), \qquad n = 0, 1, 2, ..., \tag{3.9}$$

where $\omega_B = \dfrac{eB_0}{M}$ is the cyclotron frequency. We observe directly that the discrete energy levels (Landau levels) are equidistant, and are labeled by an integer number n.

3.1.2 Symmetric gauge

In this case, $\mathbf{A}$ is given in Eq. (3.5). So, the corresponding Hamiltonian is

$$\begin{aligned} H &= \frac{1}{2M}\left[p_z^2 + \left(p_x - \frac{eB_0}{2c}y\right)^2 + \left(p_y + \frac{eB_0}{2c}B_0 x\right)^2\right] \\ &= \frac{p_x^2}{2M} + \frac{p_y^2}{2M} + \frac{p_z^2}{2M} + \frac{\omega}{2}\hat{L}_z + \frac{M\omega^2}{8}\left(x^2 + y^2\right), \end{aligned} \tag{3.10}$$

where the relations

$$[p_i, x_j] = 0 \ , i \neq j, \qquad \hat{L}_z = \hat{x}\hat{p}_y - \hat{y}\hat{p}_x, \tag{3.11}$$

and ω_B, defined in the last subsection, were used. Also, using that $p_i = \dfrac{\hbar}{i}\dfrac{\partial}{\partial x_i}$, the Schrödinger equation takes the form

$$\left[-\frac{\hbar^2}{2M}\left(\frac{\partial^2}{\partial x^2} + \frac{\partial^2}{\partial y^2}\right) + \frac{\omega}{2}\hat{L}_z + \frac{M\omega^2}{8}\left(x^2 + y^2\right)\right]\psi(x, y) = E\psi(x, y). \tag{3.12}$$

Using cylindrical coordinates, and after some algebra (see Appendix B), Eq. (3.11) can be cast in the form

$$\xi R'' + R' + \left[\beta - \frac{m^2}{4\xi} - \frac{\xi}{4}\right]R = 0, \tag{3.13}$$

where m is the angular momentum eigenvalue (in this case $\mathbf{L} = L_z$), and where we have introduced the change of variables $\xi = \dfrac{M\omega}{2\hbar}\rho^2$, $R' = \dfrac{dR}{d\xi}$ and $\beta = \dfrac{E}{\hbar\omega} - \dfrac{m}{2}$. Now, the function R is written as

$$R(\xi) = \xi^{-1/2}y(\xi), \tag{3.14}$$

so that, Eq. (3.12) takes the final form:

$$y''(\xi) + \left[\frac{-1}{4} + \frac{\beta}{\xi} + \frac{\frac{1}{4} - \frac{m^2}{4}}{\xi^2} \right] y(\xi) = 0. \tag{3.15}$$

Eq. (3.15) corresponds to a Whittaker equation [35], which has the solutions

$$y(\xi) = Ae^{-\xi/2}\xi^{|m|/2} M\left(\frac{|m|}{2} + \frac{1}{2} - \beta, |m| + 1; \xi \right), \tag{3.16}$$

where $M(a, c; x)$ is the solution of the confluent-hypergeometric equation. For this solution to be normalizable, we must impose

$$n_\rho = \frac{E}{\hbar\omega_B} - \frac{m}{2} - \frac{|m|}{2} - \frac{1}{2} \quad \in \mathbb{N}, \tag{3.17}$$

so, the energy spectrum results to be

$$E_n = \hbar\omega_B \left(n_\rho + \frac{|m|}{2} + \frac{m}{2} + \frac{1}{2} \right). \tag{3.18}$$

We see that in this case the energy depends on the eigenvalue of the angular momentum m, but, in general has the same form as in Eq. (3.8). Further computational details of the Landau levels in the Symmetric gauge are carried out in Appendix B.

3.2 The Landau problem in pristine graphene

In pristine graphene, as we have seen earlier in Chapter 2, for low energies and near the Dirac point, the equation governing the dynamics of its charge carriers is the 2D Dirac equation (a historical review of the development of Dirac equation is presented in Appendix A). Let us consider the equation corresponding to the $\mathbf{K}_+$ point

$$\hbar v_F \left(\boldsymbol{\sigma} \cdot \boldsymbol{\pi} \right) \Psi = E\Psi, \tag{3.19}$$

where $\boldsymbol{\pi}$ is the 2D canonical momentum defined earlier, $\boldsymbol{\sigma} = (\sigma_1, \sigma_2)$ with σ_i the ith Pauli matrix (Appendix A), and $\boldsymbol{\Psi} = \begin{pmatrix} \Psi_A \\ \Psi_B \end{pmatrix}$. Explicitly:

$$\hbar v_F \begin{pmatrix} 0 & \hat{\pi}_x - i\hat{\pi}_y \\ \hat{\pi}_x + i\hat{\pi}_y & 0 \end{pmatrix} \begin{pmatrix} \Psi_A \\ \Psi_B \end{pmatrix} = E \begin{pmatrix} \Psi_A \\ \Psi_B \end{pmatrix}, \tag{3.20}$$

which, after decoupling yields two equations

$$\left(\hat{\pi}_x^2 + \hat{\pi}_y^2 + i\left[\hat{\pi}_x, \hat{\pi}_y\right]\right)\Psi_A = \left(\frac{E}{\hbar v_F}\right)^2 \Psi_A, \tag{3.21}$$

$$\left(\hat{\pi}_x^2 + \hat{\pi}_y^2 - i\left[\hat{\pi}_x, \hat{\pi}_y\right]\right)\Psi_B = \left(\frac{E}{\hbar v_F}\right)^2 \Psi_B. \tag{3.22}$$

3.2.1 Landau gauge

In this case, the vector potential $\mathbf{A}$ is given in Eq. (3.4). So, using the minimal coupling $\boldsymbol{\pi} = \mathbf{p} + e\mathbf{A}$, we have

$$\hat{\pi}_x = \hat{p}_x, \qquad \hat{\pi}_y = \hat{p}_x + eB_0\hat{x}, \tag{3.23}$$

and

$$[\hat{\pi}_x, \hat{\pi}_y] = [\hat{p}_x, \hat{p}_y + eB_0\hat{x}] = eB_0\left[\hat{p}_x, \hat{x}\right] = -ieB_0\ . \tag{3.24}$$

Thus, we obtain two harmonic oscillator equations

$$\left[\hat{p}_x + eB_0\left(\frac{\hat{p}_y}{eB_0} + \hat{x}\right)^2\right]\Psi_A = \left(\frac{E^2}{\hbar^2 v_F^2} - eB_0\right)\Psi_A, \tag{3.25}$$

$$\left[\hat{p}_x + eB_0\left(\frac{\hat{p}_y}{eB_0} + \hat{x}\right)^2\right]\Psi_B = \left(\frac{E^2}{\hbar^2 v_F^2} + eB_0\right)\Psi_B, \tag{3.26}$$

for which the energy spectrum is respectively

$$E_{A,n} = \hbar v_F\sqrt{2eB_0\left(n+1\right)} \tag{3.27}$$

and

$$E_{B,n} = \hbar v_F\sqrt{2eB_0 n}. \tag{3.28}$$

In this case, unlike the non-relativistic case, even though the Landau levels depend only in an integer number n, they are no longer equidistant, and the dependence goes as $\sqrt{n}$.

3.2.2 Symmetric gauge

In this case, the vector potential **A** is given in Eq. (3.5). The resulting Landau levels (which are computed in detail in Appendix B) are given by

$$E_{A,n} = \hbar v_F \sqrt{2eB_0 \left(n_\rho + 1 + \frac{|m|}{2} + \frac{m}{2} \right)} \tag{3.29}$$

and

$$E_{B,n} = \hbar v_F \sqrt{2eB_0 \left(n_\rho + \frac{|m|}{2} + \frac{m}{2} \right)}. \tag{3.30}$$

Similarly to the non-relativistic case, the energies at each site for the Symmetric gauge depend on the angular momentum eigenvalue m, but in both gauges the behavior of the energies is proportional to $\sqrt{n}$. This spectrum was obtained for the first time in Condensed Matter Physics by J. W. McClure [36], when he developed the theory of diamagnetism in graphite, and has been recently experimentally confirmed [37, 38, 39].

The Landau levels in graphene present two remarkable differences with respect to the non-relativistic case:

- In graphene, they are not equidistant as they go as $\sqrt{n}$, while in the non-relativistic case they grow $\sim n$.
- Unlike the non-relativistic case, in graphene the energy spectrum presents a zero-energy level for $n = 0$, which has important implications in graphene transport properties. This $n = 0$ state explains the occurrence of the semi-integer Quantum Hall Effect (QHE) [37, 38], where, unlike the usual values for the Hall conductivity ($\sigma_{xy} = \pm \frac{4e^2}{h} n$), in this material the values are $\sigma_{xy} = \pm \frac{4e^2}{h}(n+1/2)$. This semi-integer shift is associated to the fact that the ground state ($n = 0$) has half of the degeneracy than all other energy levels [40].

The next Chapter is devoted to the study of strain in a graphene crystal. As we shall shortly see, strain affects directly the electronic and magnetic properties of graphene. In particular, the Landau levels suffer a distortion.

Chapter 4

Strained graphene: Pseudo-magnetic field generation

In this Chapter we treat the case of strain in graphene. In the first Section, we briefly introduce the notions of strain in crystals supported by elasticity theory [41]. Then, we tackle the *pseudo-magnetic* field generation by strain, focusing in uniaxial and triaxial strain in graphene. For both cases, we discuss its effect in the Landau levels, where we define a tensor Fermi velocity referring to the deformation of the lattice.

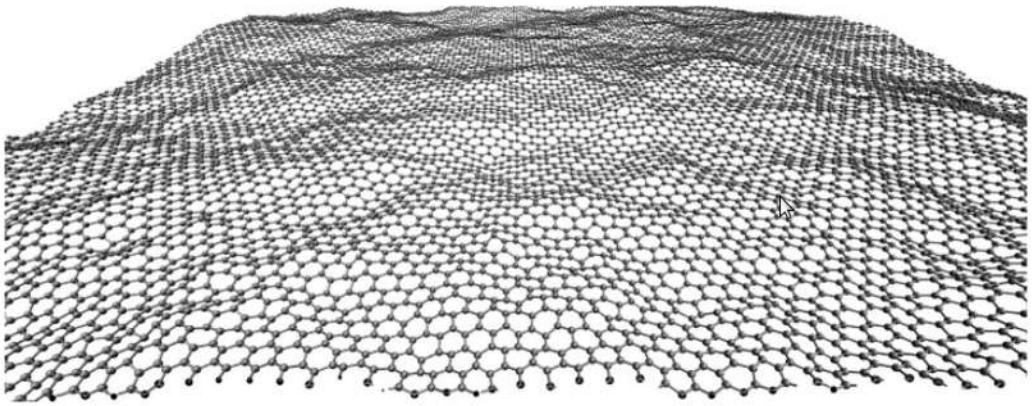

Figure 4.1: Atom configuration for graphene at room temperature. The plot was made by atomistic Monte Carlo simulations. Adapted from [42].

It is well known that, at room temperature, graphene is unavoidable corrugated

as shown in Fig. 4.1. In addition, owing to the forms graphene is synthesized, that is, through mechanical processes or by growing it on substrates with different lattice parameters or structure, graphene usually presents tensions and corrugation [43]. As a result, the three bonds of each atom with its nearest neighbors are no longer

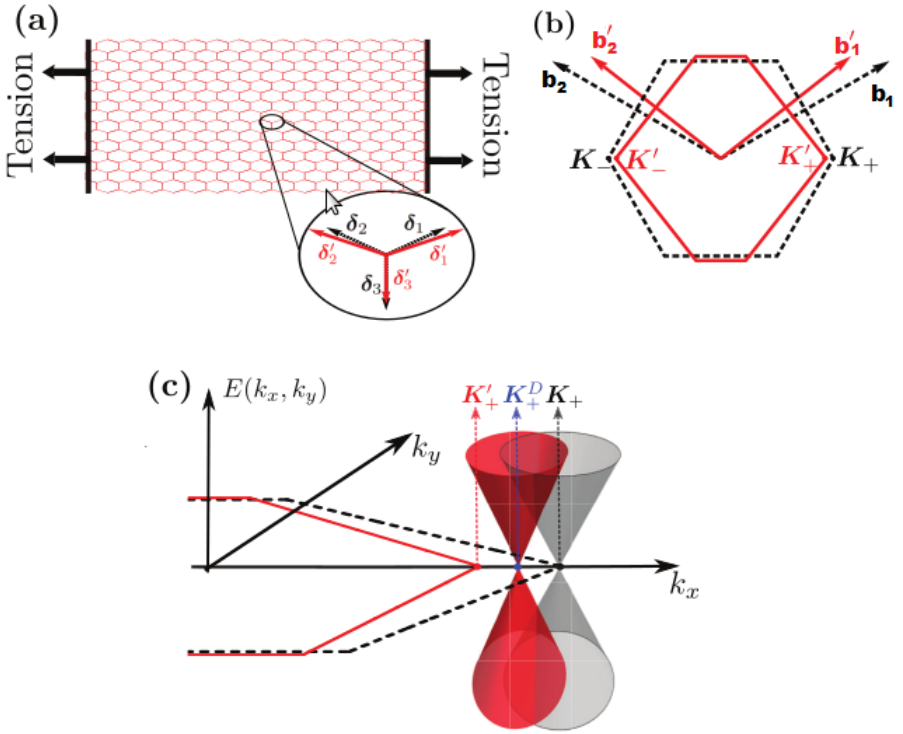

Figure 4.2: (a) Uniform strain in graphene. The $\boldsymbol{\delta}_i$ vectors joining the sites of both sublattices, A and B, are distorted to $\boldsymbol{\delta}'_i$ vectors. (b) Corresponding strained reciprocal lattice, where the new reciprocal vectors $\mathbf{b}'_1$ and $\mathbf{b}'_2$, as well as the new positions of the Dirac points, $\mathbf{K}'_+$ and $\mathbf{K}'_-$, are shown. (c) Distorted energy bands. The new Dirac cones are now directional dependent Fermi velocity. The new position of the Dirac cone vertex, $\mathbf{K}^D_+$, does not coincide with the new $\mathbf{K}'_\pm$ points. The vector displacement is directly given by the pseudomagnetic vector potential. Image adapted from [44].

equivalent, leading to different electronic properties of the material. More dramatic effects are produced when the graphene lattice is strained (in one or more directions), corrugated or bent [45]. Following the discussion in [46], *ab initio* calculations, as well as tight-binding models, have shown that in the case of an uniaxial strain, Dirac cones K and K' shift apart for "small" strains (less than 20%) [47] (Figs. 4.2), whereas a gap is opened between them for larger strains ($> 20\%$) [48, 49, 50]. A sim-

ilar behavior is found for shear strains, with a smaller threshold ($\sim 16\%$) [51]. Such strain-based electronic effects are studies by a recent field dubbed as *Straintronics* [52].

Another novel effect turns out of straining the graphene lattice: A *pseudo-magnetic* field generation. This effect arises from the shifting of the $\mathbf{K}$ and $\mathbf{K}'$ points in opposite directions. Such effect can be introduced as a covariant derivative into the Dirac hamiltonian through a minimal coupling of a vector potential, inducing a gauge field which acts as a magnetic field [53, 54] (Fig. 4.2(c)).

4.1 Modelling strain

We follow the discussion presented in [45]. In order to describe mechanical deformations (under the elasticity theory assumptions [41]), we consider the positions of atoms of the lattice under a strain

$$\mathbf{r}' = \mathbf{r} + \mathbf{u}(\mathbf{r}), \tag{4.1}$$

where $\mathbf{u}(\mathbf{r})$ is the displacement field. It is useful to define the symmetric and antisymmetric tensors

$$\tilde{\varepsilon}(\mathbf{r})_{ij} = \left(\partial_i u_j(\mathbf{r}) + \partial_j u_i(\mathbf{r})\right)/2, \quad i,j = x,y, \tag{4.2}$$

and

$$\tilde{\omega}(\mathbf{r})_{ij} = \left(\partial_i u_j(\mathbf{r}) - \partial_j u_i(\mathbf{r})\right)/2, \quad i,j = x,y. \tag{4.3}$$

The symmetric tensor $\tilde{\varepsilon}$ (deformation tensor) measures the deformations in the lattice discarding rigid motions such as rotations and translations, which are described by the antisymmetric tensor $\tilde{\omega}$ [55]. The vectors connecting the nearest neighbors of each atom of the strained lattice, $\boldsymbol{\delta}'_n$, become space-dependent, and within the Cauchy-Born approximation [56], are given by

$$\boldsymbol{\delta}'_n \approx \boldsymbol{\delta}_n + \left(\boldsymbol{\delta}_n \cdot \nabla\right)\mathbf{u}(\mathbf{r}) = \left(I + \nabla\mathbf{u}(\mathbf{r})\right)\cdot\boldsymbol{\delta}_n, \tag{4.4}$$

where I is the identity matrix. Using that the components of the displacement field

$$\left[\nabla\mathbf{u}(\mathbf{r})\right]_{ij} = \tilde{\varepsilon}(\mathbf{r})_{ij} + \tilde{\omega}(\mathbf{r})_{ij}, \tag{4.5}$$

and that we are only considering deformations in the lattice ($\tilde{\omega}(\mathbf{r})_{ij} = 0$), we are lead to

$$\delta'_n \approx \left(I + \tilde{\varepsilon}(\mathbf{r})\right)\cdot\delta_n. \tag{4.6}$$

The deformation tensor in the plane is given by

$$\tilde{\varepsilon} = \begin{pmatrix} \varepsilon_{xx} & \varepsilon_{xy} \\ \varepsilon_{yx} & \varepsilon_{yy} \end{pmatrix}. \tag{4.7}$$

It is important to notice that for uniform deformations, that is, for deformations where the new positions do not depend explicitly on the original position without strain, the deformation tensor is a constant.

In the case of graphene, taking the x-direction as the *zig-zag* direction,

$$\tilde{\varepsilon} = \begin{pmatrix} \varepsilon_Z & \gamma_s \\ \gamma_s & \varepsilon_A \end{pmatrix}, \tag{4.8}$$

where ε_Z, ε_A, denote uniaxial strains applied along *zig-zag* and *armchair* directions respectively, and γ_s represents the shear strain [45].

4.2 *Pseudomagnetic* field generation

As a consequence of lattice strain, because the hopping integrals t_i change, it is found that the effective Hamiltonian near the Dirac points [23] is given by:

$$\hat{H} = v_F \boldsymbol{\sigma} \cdot \left(\hat{\boldsymbol{\pi}} - e\hat{\mathbf{A}} \right) \quad , \tag{4.9}$$

where the operator $\hat{\mathbf{A}}$ represents a quantity similar to the magnetic vector potential $\mathbf{A}$ [53]. The corresponding magnetic field $\mathbf{B}$ produced by this vector potential acts on the *pseudo-spin* of the charge carriers in the material. So, it has been dubbed *pseudo-magnetic* field, whereas $\hat{\mathbf{A}}$ is called *pseudo-magnetic* vector potential [1].

In graphene, a strain allows to define the *pseudo-magnetic* vector potential [53, 57]

$$\mathbf{A} = \frac{\beta}{a}(\varepsilon_Z - \varepsilon_A, -2\gamma_s) \ , \tag{4.10}$$

where a is the lattice constant, $\beta = -\dfrac{\partial ln(t)}{\partial ln(a)}$ is the electron Grüneisen parameter, which describes the dependence of the nearest neighbor hopping integrals, t_i, on interatomic distances ($\beta \approx 2 - 3$ for graphene [58, 59]). This *pseudo-magnetic* field has been experimentally measured in graphene nanobubbles [9], finding really big intensities up to 300 T. It is important to notice that the *pseudo-magnetic* field obtained acts with opposite sign for the two valleys K, K' [53]. So, it is useful to define

$$\mathbf{B}_\xi = \begin{cases} \mathbf{B}_s, & \text{in } K \\ -\mathbf{B}_s, & \text{in } K' \end{cases} \quad . \tag{4.11}$$

[1] It is important to note that the *pseudo-magnetic* field is not produced by motion of charges, as magnetic fields should produce in Electrodynamics.

This condition tells us that the system as a whole remains time-reversal invariant, resulting in the existence of two counter-propagating edge states from the valleys K and K' without charge transfer. This effects is denominated "Valley QHE" [60, 61].

4.3 Uniaxial strain

In this case, the effect of the strain is angular-dependent as can be seen in Fig. 4.3. So, the strain tensor can be written as [47]

$$\tilde{\varepsilon} = \varepsilon \begin{pmatrix} \cos^2\theta - \nu \sin^2\theta & (1+\nu)\cos\theta \sin\theta \\ (1+\nu)\cos\theta \sin\theta & \sin^2\theta - \nu \cos^2\theta \end{pmatrix} , \tag{4.12}$$

where θ is the angle respect the x-axis (that we have taken to be the *zig-zag* direction), ε is the normalized strain parameter, and ν is the Poisson ratio (~ 0.165 for graphite [47]). This tensor is used under the assumption of elastic isotropy with $\nu = const.$ [47].

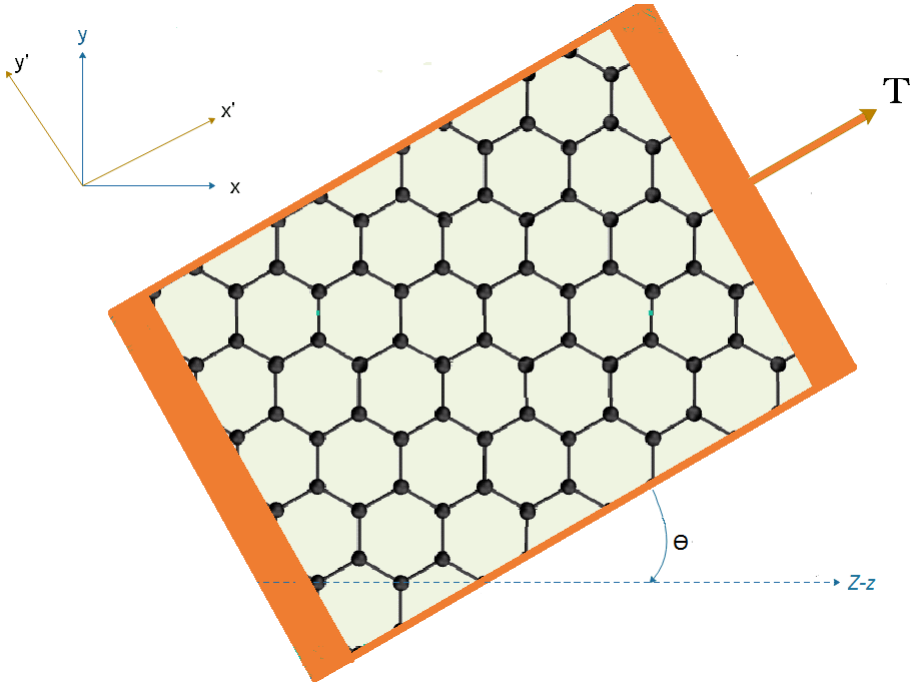

Figure 4.3: Tension geometry considered. The *zig-zag* direction is considered parallel to the x-axis.

From this expression of the strain tensor, we observe that in the cases of uniaxial strain in the *zig-zag* ($\theta = 0$) and *armchair* ($\theta = \pi/2$) directions, the strain tensor

is constant. Thus, strains in these directions are uniform and no *pseudo-magnetic* field is produced. For an arbitrary angle, the *pseudo-magnetic* vector potential Eq. (4.10) is

$$\begin{aligned}\mathbf{A} &= \frac{\beta}{a}\,(\varepsilon_Z - \varepsilon_A, -2\gamma_s) \\ &= \frac{\beta}{a}\,\varepsilon\,(1+\nu)\,(\cos^2\theta - \sin^2\theta, -2\,\mathrm{sen}\theta\,\cos\theta, 0) \\ &= \frac{B_0}{\rho^2}(x^2 - y^2, -2xy, 0),\end{aligned} \tag{4.13}$$

where we take $B_0 = \dfrac{\beta}{a}\,\varepsilon\,(1+\nu)$, and we have used cilindrical cordinates: $x = \rho\,\cos\theta$, $y = \rho\,\sin\theta$, $z = z$. The resulting *pseudomagnetic* field is

$$\mathbf{B} = \nabla \times \mathbf{A} = 0. \tag{4.14}$$

So, even though the strain tensor representing an arbitrary uniaxial strain is not necessarily constant, such strain never generates a *pseudo-magnetic* field.

4.3.1 Landau problem in uniaxial-strained graphene

It has been found that subjecting graphene to an arbitrary strain generates a displacement and a tilting of the Dirac cones with respect to the cones of unstrained sample [62] so that the transverse section of such cones turns to be elliptical. The anisotropy in the Dirac cones affects directly the electric and magnetic properties of the material. From the physical point of view, it can be understood as if the charge carriers move easily or faster in a certain direction, and more difficult or slower in the other. That is, Fermi velocity acquires a tensorial character

$$v_F \longmapsto \mathbf{v_F} = v_F \begin{pmatrix} a(x,y) & 0 \\ 0 & b(x,y) \end{pmatrix}, \tag{4.15}$$

where a and b are dimensionless parameters related to the semi-axes of the ellipses of the transverse section of the inclined Dirac cones. Thus, under strain, the canonical momentum $\boldsymbol{\pi}$ is given by [62]

$$\boldsymbol{\pi} = \begin{pmatrix} a(x,y)\pi_x \\ b(x,y)\pi_y. \end{pmatrix}. \tag{4.16}$$

In this thesis we consider the parameters a and b constants, so the Hamiltonian given by Eq. (3.19) becomes

$$\hbar v_F \begin{pmatrix} 0 & a\hat{\pi}_x - i\ b\ \hat{\pi}_y \\ a\hat{\pi}_x + i\ b\ \hat{\pi}_y & 0 \end{pmatrix} \begin{pmatrix} \Psi_A \\ \Psi_B \end{pmatrix} = E \begin{pmatrix} \Psi_A \\ \Psi_B \end{pmatrix}, \tag{4.17}$$

from which, proceeding in the same way as in unstrained case, we obtain the decoupled equations

$$\left(a^2\pi_x^2 + b^2\pi_y^2 + i\ ab\ [\pi_x, \pi_y]\right)\Psi_A = \left(\frac{E}{\hbar v_F}\right)^2 \Psi_A, \tag{4.18}$$

and

$$\left(a^2\pi_x^2 + b^2\pi_y^2 - i\ ab\ [\pi_x, \pi_y]\right)\Psi_B = \left(\frac{E}{\hbar v_F}\right)^2 \Psi_B. \tag{4.19}$$

It is important to note that when we use the minimal coupling $\boldsymbol{\pi} = \mathbf{p} + e\mathbf{A}$, in the case of strained graphene the vector potential $\mathbf{A} = \mathbf{A}_{ext} + \mathbf{A}_{pseudo}$, where $\mathbf{A}_{ext}$ represents the effect of the external magnetic field, and $\mathbf{A}_{pseudo}$ represents the pseudomagnetic field generated by the strain. Having said that, we notice that for uniform uniaxial strains, from which no pseudomagnetic field is produced, it is required an external magnetic field to find the quantization of the energy levels in graphene (Landau levels), which is shown in Fig. 4.4 [62]. Nevertheless, there exist some kinds of strains which certainly produce a non-zero pseudomagnetic field (as we will see in the next section), and exhibit an energy quantization (Landau levels) without the application of an external magnetic field.

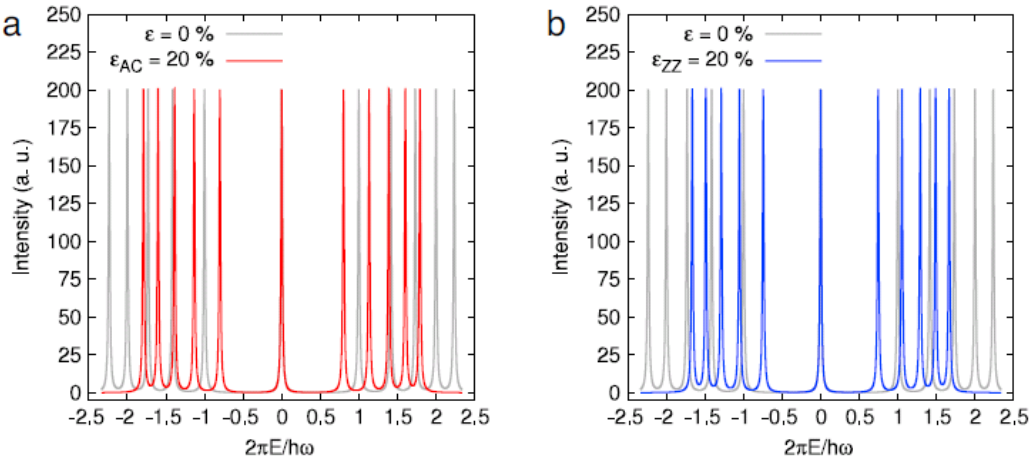

Figure 4.4: Distorted Landau levels density of states (DOS) for graphene strained in the (a) *armchair* (red) and (b) *zig-zag* (blue) directions with respect to the unstrained graphene DOS (gray). It can be seen immediately the contraction of the LL's distances, showing clearly the strain-dependence of the LL's spectra. Adapted from [62].

In addition, it can be seen that in the presence of an external magnetic field directed in the $\hat{k}$ direction, for the sublattice A the total magnetic field is the sum

of $B_0 + B_{pseudo}$, magnifying the total intensity, and therefore, making larger the separation between the Landau levels. On the other hand, for atoms in sublattice B, the pseudomagnetic fields is in opposite direction to the external field, so they counteract diminishing the total intensity of the magnetic field, making smaller the separation between Landau levels. There is a critical value $B_0 = B_{pseudo}$ in which the total magnetic field vanish for this sublattice, so there is no quantization of the energy.

From Eqs. (4.18) and (4.19) the Landau levels are easily obtained [20]

$$E_{A,n} = \lambda\sqrt{2e|B|(n+1)} \quad \text{and} \quad E_{B,n} = \lambda\sqrt{2e|B|n}, \tag{4.20}$$

where $\lambda = \sqrt{ab}$ measures the contraction ($\lambda < 1$) or the expansion ($\lambda > 1$) of the Landau levels separation[2], and

$$B = \begin{cases} B_0 + B_{pseudo}, & \text{in sublattice } A \\ B_0 - B_{pseudo}, & \text{in sublattice } B \end{cases}, \tag{4.21}$$

where $B_{pseudo} = 0$ for uniform strains.

4.4 Triaxial strain

If we are interested in creating intentionally a uniform pseudomagnetic field pointing in the $\hat{k}$ direction, this in order to manipulate the electronic properties via "*strain engineering*" [9, 59], we can use the relations given in Eq. (4.10) for the pseudomagnetic vector potential, which creates, in general, a pseudomagnetic field given by

$$\mathbf{B}_{pseudo} = \left(\frac{\partial A_y}{\partial x} - \frac{\partial A_x}{\partial y}\right)\hat{k}. \tag{4.22}$$

From Eq. (4.10)

$$A_s = \frac{\beta t}{a}\left(u_{xx} - u_{yy}, -2u_{xy}\right) = B_0(0, x), \tag{4.23}$$

where the last equality is considering the pseudomagnetic field in the Landau gauge which would produce the desired uniform pseudomagnetic field. The symbols u_{ij} with $1, i = x, y$ are given in Eq. (4.2). Explicitly,

$$u_{xx} = \frac{\partial u_x}{\partial x};\ u_{yy} = \frac{\partial u_y}{\partial y};\ 2u_{xy} = \frac{\partial u_x}{\partial y} + \frac{\partial u_y}{\partial x}. \tag{4.24}$$

[2]Let us not lose sight that there is also a hidden term $\zeta = a/b$ which is related to the direction in which the strain is applied, and thus, to the velocity of the Dirac fermions in each ZZ and AC direction: If the material is tensed in the ZZ direction, the velocity in this direction $a = v_{xx}$ is lower than the velocity in the AC direction $b = v_{yy}$, thus $\zeta < 1$. Reciprocally, for tension in the AC direction we have $\zeta > 1$. Talking about λ, as it is shown in [63], a value $\lambda < 1$ ($\lambda > 1$) not necessarily indicates a compression (expansion) of the lattice in a particular direction (ZZ or AC).

So, from Eq. (4.23), in Laundau gauge

$$u_{xx} - u_{yy} = 0 \Rightarrow u_{xx} = u_{yy} \;\text{ and }\; 2u_{xy} = -Cx, \tag{4.25}$$

where $C = B_0 a/\beta t$. Considering the simplest case in which the geometry is plane, and also the strains in the x and y directions are identical, that is, $u_{xy} = u_{yx}$, then, from the last expression in Eq. (4.24)

$$2u_{xy} = -Cx \Rightarrow \begin{cases} u_x = -\dfrac{C}{2}xy + A(x), \\ u_x = -\dfrac{C}{2}\dfrac{x^2}{2} + B(y). \end{cases}$$

$$\Rightarrow \begin{cases} u_{xx} = -\dfrac{C}{2}y + A'(x) \\ u_{yy} = B'(y) \end{cases} \Rightarrow \begin{cases} A'(x) = 0 \Rightarrow A(x) = A = const. \\ B'(y) = -\dfrac{C}{2}y \Rightarrow B(y) = -\dfrac{C}{4}y^2 + const. \end{cases}$$

$$\Rightarrow \mathbf{u}(\mathbf{r}) = (u_x, u_y) = -\frac{B_0 a}{2\beta t}\left(xy, \frac{x^2+y^2}{2}\right), \tag{4.26}$$

where we have chosen the constants as zero. Eq. (4.26) represents the strain which creates a uniform pseudomagnetic field in the $\hat{k}$ direction. Such strain is depicted in Fig. 4.5(a).

Despite it is a very particular strain, what is really important in order to generate a *quasi*-uniform pseudomagnetic field in much more realistic situations is to keep the triagonal symmetry of the strain [53, 54]. This is shown in Fig. 4.5(b), where it can be seen that a triaxial strain (strain over the three not-adjacent sides) creates a very uniform magnetic field at the center of the hexagonal cell [53]. As a result, the local density of (electronic) states (LDOS) given by [64]

$$\rho(\mathbf{r}, E) = -\frac{1}{\pi}\text{Tr ImG}(\mathbf{r}, \mathbf{r}'; E), \tag{4.27}$$

which gives the number of states in a interval of energy $[E, E+\Delta E]$, exhibits Landau levels without an external magnetic field in this central region, just because of the effect of the pseudomagnetic field created by strain [53] (Fig. 4.6). Here, $G(\mathbf{r}, \mathbf{r}'; E)$ is the Green function corresponding to the Dirac equation of the system. These results have been verified experimentally in nanobubbles by scanning tunnelling microscopy, obtaining very intense pseudomagnetic fields of approximately 300T [9].

Applying the same procedure in order to construct a uniform magnetic field using the symmetric gauge, we obtain the deformation

$$\mathbf{u}(\mathbf{r}) = (u_x, u_y) = \frac{B_0 a}{4\beta t}\left(-xy, \frac{-x^2+y^2}{2}\right). \tag{4.28}$$

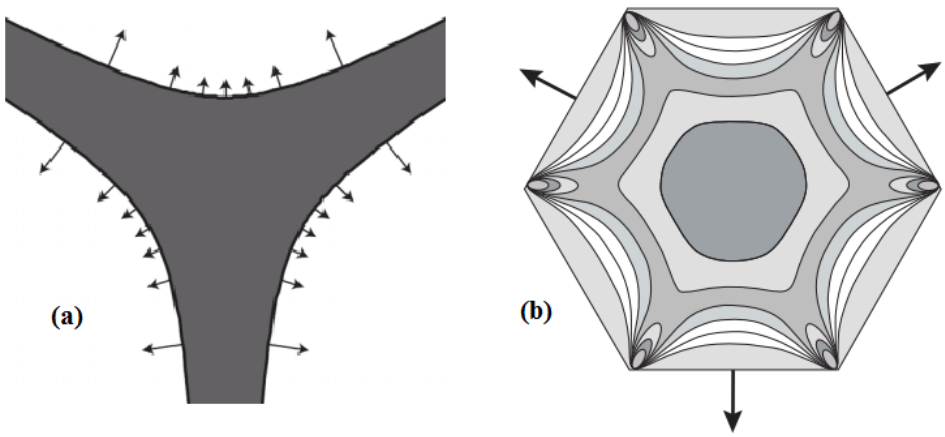

Figure 4.5: (a) Shape describing Eq. (4.26), producing a uniform magnetic field in graphene. (b) *quasi*-uniform pseudomagnetic field generated by triaxial strain. The maximum strain of 20% creates an effective field of about 10T at the center of the hexagon, and it is lowering from inside to outside to correspondent values of 8, 6, 4, 2, 0, and −2T. Images adapted from [53].

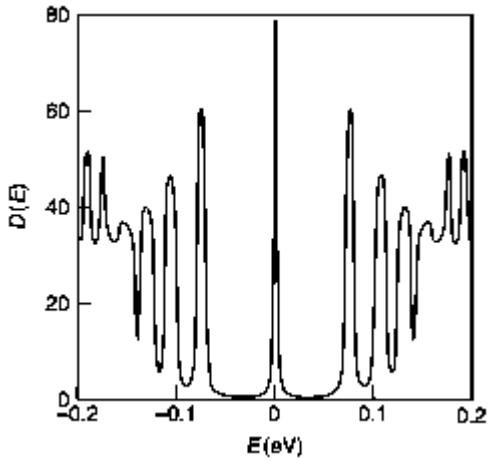

Figure 4.6: Average DOS in the central region of the hexagon in Fig. 4.5(b). Adapted from [53].

In the next Chapter we study the phenomenon of atomic collapse predicted in Relativistic Quantum Mechanics (RQM). Specially, we treat the case of a Coulomb impurity in graphene immersed in an external magnetic field and under strain effects.

Chapter 5

Atomic Collapse

In this Chapter, the atomic collapse phenomenon in graphene is discussed. In the first Section, an introduction of the subject is presented. Then, we consider the case of graphene in the field of a Coulomb impurity, immersed in a homogeneous magnetic field perpendicular to the plane of graphene. We further consider an uniaxial strain of the lattice. For that purpose, we use the approximation of the Coulomb potential as a constant potential well, and the model of the tensor Fermi velocity described in last Chapter. We obtain some expressions and curves of the energy and critical potential with explicit dependence of the strain effects.

5.1 Introduction

Following the discussion in [11], atomic collapse has been long predicted by Relativistic Quantum Mechanics (RQM) [65]. In this phenomenon, an electron falls into the atomic nucleus emitting a positron. This is theoretically assumed to happen when the charge of a super-heavy nucleus exceeds certain threshold, Z_c [10, 65], so the resulting intense Coulomb field causes the electron wave function component to fall into the center of the nucleus (with a finite lifetime [66]), and, at the same time, the positron component escapes to infinity. Such supercritical quantum states depict the semiclassical idea of the electron-component trajectory spiralling inward toward the nucleus-atomic collapse- while the positron-component trajectory spiralling outward away from the nucleus, propagating to infinity (Fig. 5.1). The mentioned threshold $Z_c = 137$ for punctual nucleus (for Hydrogen atom the fine structure constant is $\alpha = 1/137$), and, for extended nucleus, where screening effects appear, $Z_c \simeq 170$ [10, 65, 66]. Nevertheless, because super-heavy nucleus have not been observed up to date, experimental evidence of this phenomena can not be obtained in this context. In the past few years, some efforts to observe atomic collapse have been developed by colliding heavy ions and searching for positrons [66, 67, 68, 69], but the resulting

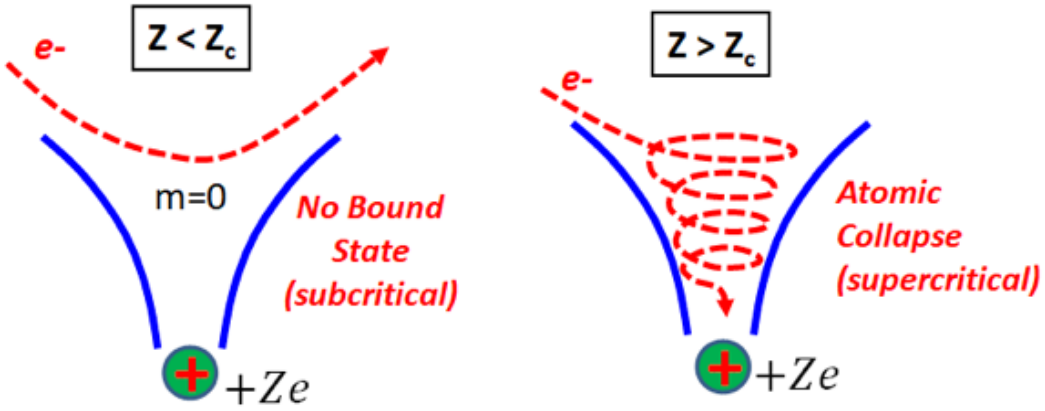

Figure 5.1: Atomic collapse phenomenon for relativistic systems in supercritical states: the electron trajectory goes inward toward the nucleus, and the positron trajectory escapes outward away, both describing an spiral trajectory. Adapted from [70].

data is difficult to analyze as the amount of interactions is enormous, making it impossible to have satisfactory conclusions.

Based on the discussion in [15], in graphene, where, as we have seen in Chapter 2, its charge carriers (massless Dirac electrons) are described by a linear energy dispersion relation near the Dirac points, and whose electrons move with velocity $v_F \simeq c/300$, the coupling constant is given by:

$$\beta = \frac{Z\alpha_g}{\kappa}, \tag{5.1}$$

where κ is the dielectric constant ($\kappa \approx 1.104859$ for graphene [71]), and $\alpha_g = \dfrac{e^2}{v_F\hbar} \simeq 2.2$ exceeds unity. It has been found that the Hamiltonian of the system turns not self-adjoint for $\beta > \beta_c \simeq 1/2$ [12, 13, 14, 72, 73], decreasing considerably the value of the critical charge Z_c of artificial nuclei [12, 13, 14, 74], and, in consequence, making the atomic collapse in graphene easily achieved theoretically by adding highly charged impurities in pristine graphene. Despite this prediction, fast charge recombination was a problem to produce collapse. This difficulty was recently overcome by Wang, et. al., in 2013 [11], by using the tip of a scanning tunnelling microscope (STM) to create clusters of charged calcium dimmers, creating supercritical Coulomb potentials (Fig. 5.2). They measured the local density of states (LDOS) through STM dI/dV spectroscopy. The spectrum shows two important results: First, a sys-

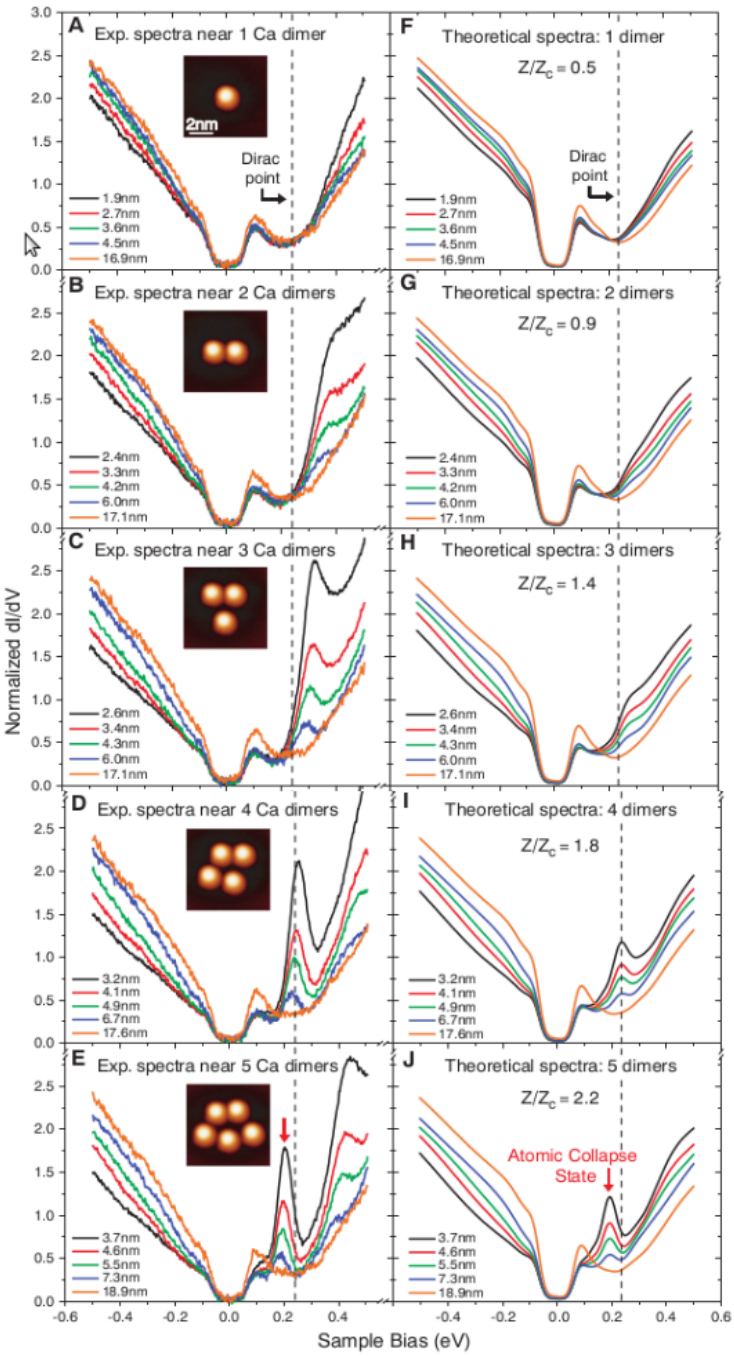

Figure 5.2: Atomic collapse by Wang [11]. (Left) experimental measurements of the LDOS in the presence of one-five calcium dimmers. As the number of dimmers increases, a resonance in the electron-spectrum LDOS increases, until it passes to the hole-spectrum for five dimmers, meaning atomic collapse. (Right) same results carried out theoretically.

tematic electron-hole asymmetry owing to the positive charge of the dimmers [75]. The second, and the most important fact, is the appearance of a resonance (a quasi-bound state) increasing and shifting toward lower energies as the number of dimmers increases from one to five (Figs. 5.2 A-E). For five dimmers, the resonance shifted below the Dirac point (Fig. 5.2 E), representing the atomic collapse of the electron in graphene. These experimental results are in agreement with the theoretical computations (Figs. 5.2 F-J), observing the same behavior of the resonance appearing in each multi-dimmer system.

The experimental plot obtained by Wang, *et al.* [11], of the spatial distribution of the atomic collapse around the artificial nucleus of five calcium dimmers is shown in Fig. 5.3. The calcium dimmers appear as little dark disks.

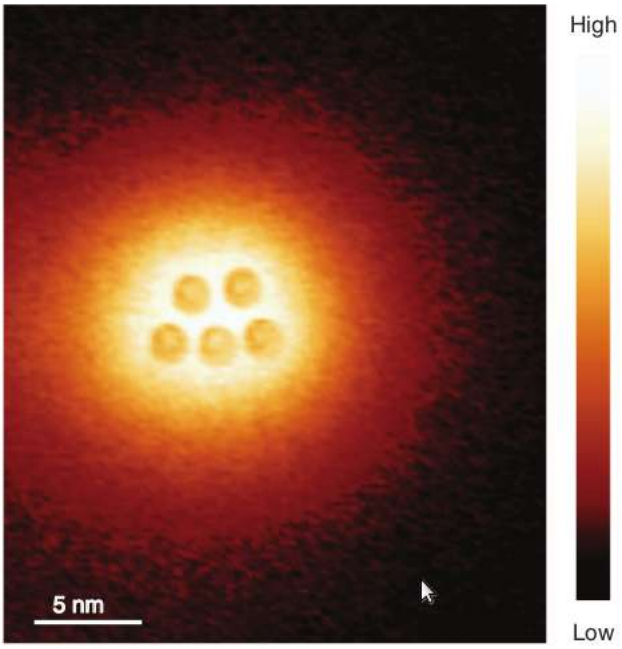

Figure 5.3: Experimental image of the distribution of the atomic collapse around the dimmers. Adapted from [11].

In the next section we model the atomic collapse in graphene under strain effects by means of a (2+1) inhomogeneous Dirac equation.

5.2 Coulomb impurity in graphene under uniaxial strain and in a magnetic field

In all this section we follow the discussion given in [15]. As we have just seen, atomic collapse develops in graphene when a high-charge impurity is placed in the graphene lattice. Even more, it has been demonstrated that the effect of a homogeneous magnetic field perpendicular to the graphene sheet catalyzes the gap generation for gapless fermions in relativistic-like systems [15, 76, 77], playing an important role in quantum Hall effect in graphene [78, 79, 80, 81, 82, 83, 84], lifting the degeneracy of the Landau levels. Also, consistent with magnetic catalysis phenomenon, with the presence of a magnetic field B, as electrons and holes get closer to the nucleus than in free atoms [85, 86], Coulomb impurity gets supercritical ($Z > Z_c$) for any Z, that is, atomic collapse is always present [76]. On the other hand, as we have seen in the previous Chapter, strain in graphene can induce different electric and magnetic effects. In the case of an uniaxial strain, we have seen that this changes can be thought as given by a change of the charge carriers velocity depending on the direction of motion (Eq. (4.15)). Let us consider then (2+1) Dirac Hamiltonian describing a Coulomb impurity in graphene immersed in a perpendicular magnetic field $\mathbf{B}$. Considering the tensorial character of the Fermi velocity, $\mathbf{v}_F = v_F \mathrm{diag}(a, b)$,

$$H_D = \hbar \mathbf{v}_F \cdot \boldsymbol{\sigma} \cdot \boldsymbol{\pi} + \xi \Delta \sigma_3 + V(r), \tag{5.2}$$

where $V(r)$ corresponds to the $1/r$ Coulomb potential, a, b are the strain parameters, $\pi_i = -i\partial_i + (e/\hbar c)A_i$ with $i = x, y$, is the $i-th$ component of the canonical momentum (covariant derivative), $\mathbf{A} = \dfrac{B_0}{2}(-y, x)$ is the vector potential corresponding to the external magnetic field $\mathbf{B}$ in the symmetric gauge, σ_i are the Pauli matrices, and Δ is the quasiparticle gap. The two component spinor $\Psi_{\xi s}$ carries the valley ($\xi = \pm$) and spin ($s = \pm$) indices. Also, the standard convention $\Psi_{+s} = (\psi_A, \psi_B)_{K^T_{+s}}$ whereas $\Psi_{-s} = (\psi_B, \psi_A)_{K^T_{-s}}$ is used, where A, B refer to the two sublattices of a hexagonal graphene lattice. Since the interaction $V(r)$ does not depend on spin, it is omitted. Then, by defining the parameters

$$\lambda = \sqrt{ab} \quad \text{and} \quad \zeta = a/b, \tag{5.3}$$

the equation governing the system can be written as

$$\begin{pmatrix} \xi\Delta & \hbar v_F(a\pi_x - ib\pi_y) \\ \hbar v_F(a\pi_x + ib\pi_y) & -\xi\Delta \end{pmatrix} \Psi(\mathbf{r}) = [E - V(r)]\Psi(\mathbf{r}),$$

$$\Rightarrow \begin{pmatrix} 0 & \zeta^{1/2}\pi_x - i\zeta^{-1/2}\pi_y \\ \zeta^{1/2}\pi_x + i\zeta^{-1/2}\pi_y & 0 \end{pmatrix} \Psi(\mathbf{r}) = \left(\frac{E - V(r) - \xi\Delta\sigma_z}{\sqrt{2}\lambda\hbar v_F} \right) \Psi(\mathbf{r}),$$

$$\Rightarrow \begin{pmatrix} 0 & -iS^- \\ iS^+ & 0 \end{pmatrix} \Psi(\mathbf{r}) = \begin{pmatrix} \epsilon^- & 0 \\ 0 & \epsilon^+ \end{pmatrix} \Psi(\mathbf{r}), \tag{5.4}$$

where we have defined the differential operators

$$S^{\pm} = \mp i \frac{l_B}{\sqrt{2}} \left(\zeta^{1/2} \pi_x \pm i \zeta^{-1/2} \pi_y \right), \quad [S^-, S^+] = 1, \tag{5.5}$$

and the quantities

$$\epsilon^{\pm} = \frac{l_B [E - V(r) \pm \xi \Delta]}{\sqrt{2} \lambda \hbar v_F}. \tag{5.6}$$

Here $l_B = \sqrt{\hbar c / |eB_0|}$ is the magnetic lenght. Thus, we get two coupled equations

$$-i \; S^- \psi_B = \epsilon^- \psi_A, \qquad\qquad i \; S^+ \psi_A = \epsilon^+ \psi_B. \tag{5.7}$$

In order to obtain explicit expressions for $\zeta^{1/2} \; \pi_x \; \pm \; i \; \zeta^{-1/2} \; \pi_y$, we can define the following azimuthal-symmetric relations

$$\begin{cases} x = \zeta^{1/2} \; r \; \cos\phi \\ y = \zeta^{-1/2} \; r \; \sin\phi \end{cases} \quad , \quad \Rightarrow \begin{cases} \partial_x = \zeta^{-1/2} \left(\cos\phi \; \partial_r - \frac{\sin\phi}{r} \; \partial_\phi \right) \\ \partial_y = \zeta^{1/2} \left(\sin\phi \; \partial_r + \frac{\cos\phi}{r} \partial_\phi \right) \end{cases} \quad , \tag{5.8}$$

which describe an ellipse

$$\frac{x^2}{\zeta r^2} + \frac{y^2}{\zeta^{-1} r^2} = 1. \tag{5.9}$$

Thus, we have

$$\zeta^{1/2}\pi_x \pm i\zeta^{1/2}\pi_y = \zeta^{1/2}\left(-i\partial_x + \frac{e}{\hbar c}A_x\right) \pm i\zeta^{-1/2}\left(-i\ \partial_y + \frac{e}{\hbar c}A_y\right)$$

$$= \zeta^{1/2}\left(-i\ \partial_x - \frac{1}{2l_B^2}y\right) \pm i\ \zeta^{-1/2}\left(-i\ \partial_y + \frac{1}{2l_B^2}x\right)$$

$$= \left(-i\ \cos\phi\ \partial_r + i\ \frac{\sin\phi}{r}\partial_\phi - \frac{r\ \sin\phi}{2l_B^2}\right)$$

$$\pm i\left(-i\ \sin\phi\ \partial_r - i\ \frac{\cos\phi}{r}\partial_\phi + \frac{r\ \cos\phi}{2l_B^2}\right)$$

$$= (\cos\phi \pm i\ \sin\phi)\left(-i\ \partial_r \pm \frac{1}{r}\partial_\phi \pm \frac{ir}{2l^2}\right)$$

$$= e^{\pm i\phi}\left(-i\ \partial_r \pm \frac{\partial_\phi}{r} \pm \frac{ir}{2l_B^2}\right), \tag{5.10}$$

obtaining the following form of the differential operators

$$S^{\pm} = \mp\frac{1}{\sqrt{2}}e^{\pm i\phi}\left(\ \partial_\rho \pm \frac{i\ \partial_\phi}{\rho} \mp \frac{\rho}{2}\right), \tag{5.11}$$

with the substitution $\rho = r/l_B$ in the last equality. Unfortunately, with this (Coulomb) potential it is not possible to solve exactly the resulting differential equation [15]. So, in order to take into account the finite size of the impurity, R, it is necessary to replace the $1/r$ Coulomb potential by a regularized potential. So, we use the approximation the spherical potential well

$$V(r) = -V_0\theta(r_0 - r). \tag{5.12}$$

Decoupling Eqs. (5.7), we get

$$S^-S^+\psi_A = \epsilon^+\epsilon^-\psi_A, \qquad S^+S^-\psi_B = \epsilon^+\epsilon^-\psi_B, \tag{5.13}$$

where

$$\epsilon^+\epsilon^- = p'^2 = \begin{cases} p_v^2 = \dfrac{l_B^2[(E+V_0)^2 - \Delta^2]}{2(\lambda\hbar v_F)^2}, & \text{if } r < r_0 \\ \\ p^2 = \dfrac{l_B^2[E^2 - \Delta^2]}{2(\lambda\hbar v_F)^2}, & \text{if } r > r_0 \end{cases}. \tag{5.14}$$

The spinor $\Psi(\mathbf{r})$ can be written in terms of the eigenfunctions of the conserved angular momentum $J_z = L_z + \sigma_z/2 = -i\partial_\phi + \sigma_z/2$ as follows:

$$\Psi(\rho) = \frac{1}{\rho}\begin{pmatrix} e^{i(j-1/2)\phi}\ f(\rho) \\ \\ i\ e^{i(j+1/2)\phi}\ g(\rho) \end{pmatrix}, \tag{5.15}$$

with $j = \pm 1/2,\ \pm 3/2, ...$ Substituting this in Eq. (5.14), we have for the component ψ_A

$$\begin{aligned}
S^-S^+\psi_A &= S^-\left\{-\frac{1}{\sqrt{2}}e^{i\phi}\left(\partial_\rho + \frac{i}{\rho}\partial_\phi - \frac{\rho}{2}\right)\left(\frac{1}{\rho}e^{i(j-1/2)\phi}f(\rho)\right)\right\} \\
&= \hat{S}^-\left\{-\frac{1}{\sqrt{2}}e^{i\phi}\left[\left(\frac{-f(\rho)}{\rho^2} + \frac{f'(\rho)}{\rho} + i\frac{f(\rho)}{\rho^2}i(j-1/2) - \frac{f(\rho)}{2}\right)e^{i(j-1/2)\phi}\right]\right\} \\
&= \frac{1}{\sqrt{2}}e^{-i\phi}\left(\partial_\rho + \frac{i}{\rho}\partial_\phi - \frac{\rho}{2}\right)\left\{-\frac{1}{\sqrt{2}}\left(\frac{-f(\rho)}{\rho^2}(j+1/2) + \frac{f'(\rho)}{\rho} - \frac{f(\rho)}{2}\right)e^{i(j+1/2)\phi}\right\} \\
&= -\frac{1}{2}e^{-i\phi}\left\{\left[\frac{-f'(\rho)}{\rho^2} + \frac{f''(\rho)}{\rho} + \frac{2f(\rho)}{\rho^3}(j+1/2) - \frac{f'(\rho)}{\rho^2}(j+1/2) - \frac{f'(\rho)}{2}\right]\right. \\
&\quad -\frac{i}{\rho}\left[\frac{-f(\rho)}{\rho^2}(j+1/2) + \frac{f'(\rho)}{\rho} - \frac{f(\rho)}{2}\right]i(j+1/2) \\
&\quad \left.+\left[\frac{-f(\rho)}{\rho^2}(j+1/2) + \frac{f'(\rho)}{\rho} - \frac{f(\rho)}{2}\right]\right\}e^{i(j+1/2)\phi} \\
&= -\frac{1}{2\rho}e^{i(j-1/2)\phi}\left\{f''(\rho) - \frac{f'(\rho)}{\rho} + \left[-\frac{(j^2-j-3/4)}{\rho^2} - (j+1/2) - \frac{\rho^2}{4}\right]f(\rho)\right\} \\
&= p'^2\frac{1}{\rho}e^{i(j-1/2)\phi}f(\rho),
\end{aligned}$$

from where we get

$$\Rightarrow f'' - \frac{1}{\rho}f' + \left[2p'^2 - j - \frac{1}{2} - \frac{1}{\rho^2}(j^2-j-3/4) - \frac{\rho^2}{4}\right]f = 0, \tag{5.16}$$

with p'^2 given in Eq. (5.14).

Equation (5.16) is a confluent hypergeometric differential equation, which, with the additional change of variable $x = \rho^2/2 \Rightarrow \rho = \sqrt{2x}$,

$$\frac{df}{d\rho} = \sqrt{2x}\frac{df}{dx},$$

$$\frac{d^2f}{d\rho^2} = \sqrt{2x}\frac{d}{dx}\left(\sqrt{2x}\frac{df}{dx}\right) = 2x\frac{d^2f}{dx^2} + \frac{df}{dx},$$

turns into

$$f'' + \left[\frac{p'^2 - j/2 - 1/4}{x} + \frac{1/4 - (j/2 - 1/4)^2}{x^2} - \frac{1}{4}\right] f = 0, \tag{5.17}$$

which corresponds to the Whittaker equation, whose solutions are [35]

$$f(x) = e^{-x/2}x^{j/2+1/4}\left[C_1 M\left(j + 1/2 - p'^2, j + 1/2; x\right) + \right.$$

$$\left. C_2 U\left(j + 1/2 - p'^2, j + 1/2; x\right)\right], \tag{5.18}$$

where $M(a, c; x)$ and $U(a, c; x)$, are the confluent hypergeometric functions, and C_1, C_2 are normalization constants. The function $U(a, c; x)$ blows up at $r = 0$, whereas $M(a, c; x)$ diverges as $r \longrightarrow \infty$. So, the regular solutions are

$$f_{int}(\rho) = e^{-\rho^2/4}\rho^{j+1/2}\frac{C_1}{\Gamma(j + 1/2)}M\left(j + \frac{1}{2} - p_v^2, j + \frac{1}{2}; \frac{\rho^2}{2}\right), \quad (r < r_0) \tag{5.19}$$

$$f_{ext}(\rho) = e^{-\rho^2/4}\rho^{j+1/2}C_2 U\left(j + \frac{1}{2} - p^2, j + \frac{1}{2}; \frac{\rho^2}{2}\right), \quad (r > r_0). \tag{5.20}$$

Proceeding at the same way, we obtain the solutions of $g(\rho)$

$$g_{int}(\rho) = \frac{l_B(E + V_0 - \xi\Delta)}{\sqrt{2}\lambda\hbar v_F}e^{-\rho^2/4}\rho^{j+3/2}\frac{C_1}{\Gamma(j + 3/2)}M\left(j + \frac{1}{2} - p_v^2, j + \frac{3}{2}; \frac{\rho^2}{2}\right), \quad (r < r_0) \tag{5.21}$$

$$g_{ext}(\rho) = \frac{\sqrt{2}\lambda\hbar v_F C_2}{l_B(E + \xi\Delta)}e^{-\rho^2/4}\rho^{j+3/2}U\left(j + \frac{1}{2} - p^2, j + \frac{3}{2}; \frac{\rho^2}{2}\right), \quad (r > r_0). \tag{5.22}$$

These expressions are valid for all $j = \pm 1/2, \pm 3/2, \pm 5/2$,... The boundary condition

$$\left.\frac{f_{int}(\rho)}{f_{ext}(\rho)}\right|_{\rho=\rho_0} = \left.\frac{g_{int}(\rho)}{g_{ext}(\rho)}\right|_{\rho=\rho_0}, \tag{5.23}$$

gives a transcendental relation for the energies of the bound states with total angular momentum j

$$\frac{e^{-\rho_0^2/4}\rho_0^{j+1/2}\dfrac{C_1}{\Gamma(j+1/2)}\ M\left(j+\dfrac{1}{2}-p_v^2, j+\dfrac{1}{2}; \rho_0^2/2\right)}{e^{-\rho_0^2/4}\rho_0^{j+1/2}C_2\ U\left(j+\dfrac{1}{2}-p^2, j+\dfrac{1}{2}; \rho_0^2/2\right)} =$$

$$\frac{\dfrac{l_B(E+V_0-\xi\Delta)}{\sqrt{2}\lambda\hbar v_F}e^{-\rho_0^2/4}\rho_0^{j+3/2}\dfrac{C_1}{\Gamma(j+3/2)}\ M\left(j+\dfrac{1}{2}-p_v^2, j+\dfrac{3}{2}; \rho_0^2/2\right)}{\dfrac{\sqrt{2}\lambda\hbar v_F C_2}{l_B(E+\xi\Delta)}\ e^{-\rho_0^2/4}\ \rho_0^{j+3/2}\ U\left(j+\dfrac{1}{2}-p^2, j+\dfrac{3}{2}; \rho_0^2/2\right)}$$

$$\Rightarrow\frac{\dfrac{1}{\Gamma(j+1/2)}M\left(j+\dfrac{1}{2}-p_v^2, j+\dfrac{1}{2}; \rho_0^2/2\right)}{U\left(j+\dfrac{1}{2}-p^2, j+\dfrac{1}{2}; \rho_0^2/2\right)} =$$

$$\frac{l_B^2(E+V_0-\xi\Delta)(E+\xi\Delta)}{2(\lambda\hbar v_F)^2}\frac{\dfrac{1}{\Gamma(j+3/2)}M\left(j+\dfrac{1}{2}-p_v^2, j+\dfrac{3}{2}; \rho_0^2/2\right)}{U\left(j+\dfrac{1}{2}-p^2, j+\dfrac{3}{2}; \rho_0^2/2\right)}$$

$$\Rightarrow \frac{2(\lambda\hbar v_F)^2(j+\frac{1}{2})M\left(j+\dfrac{1}{2}-p_v^2, j+\dfrac{1}{2}; \rho_0^2/2\right)}{l_B^2(E+V_0-\xi\Delta)M\left(j+\dfrac{1}{2}-p_v^2, j+\dfrac{3}{2}; \rho_0^2/2\right)} = (E+\xi\Delta)\frac{U\left(j+\dfrac{1}{2}-p^2, j+\dfrac{1}{2}; \rho_0^2/2\right)}{U\left(j+\dfrac{1}{2}-p^2, j+\dfrac{3}{2}; \rho_0^2/2\right)}, \tag{5.24}$$

where the Gamma function $\Gamma(n+1) = n!$ This equation matches with the case of a Coulomb impurity in graphene immersed in a perpendicular homogeneous external magnetic field in absence of strain, $\lambda = 1$, treated in [15].

Because of the definition of the functions $M(a, c; x)$ and $U(a, c; x)$:

$$M(a, c; x) = {}_1F_1(a, c; x) = 1 + \frac{a}{c}\frac{x}{1!} + \frac{a(a+1)}{c(c+1)}\frac{x^2}{2!} + ..., \tag{5.25}$$

$$U(a, c; x) = \frac{\pi}{\sin\pi c}\left[\frac{M(a, c; x)}{\Gamma(a-c+1)\Gamma(c)} - \frac{x^{1-c}M(a+1-c, 2-c; x)}{\Gamma(a)\Gamma(-c)}\right], \tag{5.26}$$

the functions are not well defined for $c = 0,\ -1,\ -2...$, or in our case $c = j + 1/2$ and $j + 3/2$, that is, for negative values of j ($j = -1/2,\ -3/2,\ -5/2,...$). Thus, expressions (5.25) and (5.26) have to be cast in a different form for those values of j. For this purpose, we use the relations

$$\lim_{c\to -m} \frac{M(a,c;x)}{\Gamma(c)} = \frac{\Gamma(a+m+1)}{\Gamma(a)(m+1)!} x^{m+1} M(a+m+1, m+2; x), \quad m = 0,\ 1, ... \tag{5.27}$$

$$U(a,c;x) = x^{1-c} U(a-c+1, 2-c; x). \tag{5.28}$$

Then, for $j = -1/2$, relations (5.27) and (5.28) can be written as

$$\lim_{c\to 0} \frac{M\left(-p_v^2, c; \rho_0^2/2\right)}{\Gamma(j+1/2)} = \frac{\Gamma(1-p_v^2)}{\Gamma(-p_v^2)(1)!} \frac{\rho_0^2}{2} M\left(1-p_v^2, 2; \rho_0^2/2\right),$$

and

$$U\left(j+1/2-p^2, j+1/2; \rho_0^2/2\right) = \frac{\rho_0^2}{2} U\left(1-p^2, 2; \rho_0^2/2\right),$$

respectively. So, Eq. (5.24) for $j = -1/2$ becomes

$$\frac{2(\hbar\lambda v_F)^2 \Gamma\left(-\frac{1}{2}+\frac{3}{2}\right)(-p_v^2)\frac{\rho_0^2}{2} M\left(1-p_v^2, 2; \rho_0^2/2\right)}{l_B^2 (E+V_0-\xi\Delta) M\left(-p_v^2, 1; \rho_0^2/2\right)} = (E+\xi\Delta)\frac{\rho_0^2}{2}\frac{U\left(1-p^2, 2; \rho_0^2/2\right)}{U\left(-p^2, 1; \rho_0^2/2\right)},$$

$$\Rightarrow \frac{2(\hbar\lambda v_F)^2 \left(-\frac{l_B^2[(E+V_0)^2-\Delta^2]}{2(\hbar\lambda v_F)^2}\right) M\left(1-p_v^2, 2; \rho_0^2/2\right)}{l_B^2 (E+V_0-\xi\Delta) M\left(-p_v^2, 1; \rho_0^2/2\right)} = (E+\xi\Delta)\frac{U\left(1-p^2, 2; \rho_0^2/2\right)}{U\left(-p^2, 1; \rho_0^2/2\right)},$$

$$\Rightarrow \frac{(-(E+V_0-\xi\Delta)(E+V_0+\xi\Delta))\, M\left(1-p_v^2, 2; \rho_0^2/2\right)}{(E+V_0-\xi\Delta) M\left(-p_v^2, 1; \rho_0^2/2\right)} = (E+\xi\Delta)\frac{U\left(1-p^2, 2; \rho_0^2/2\right)}{U\left(-p^2, 1; \rho_0^2/2\right)},$$

$$\Rightarrow \left(\frac{E}{\Delta}+\frac{V_0}{\Delta}+\xi\right)\frac{M\left(1-p_v^2, 2; \rho_0^2/2\right)}{M\left(-p_v^2, 1; \rho_0^2/2\right)} = -\left(\frac{E}{\Delta}+\xi\right)\frac{U\left(1-p^2, 2; \rho_0^2/2\right)}{U\left(-p^2, 1; \rho_0^2/2\right)}, \tag{5.29}$$

where we have used the identity

$$\frac{\Gamma(a+1)}{\Gamma(a)} = a. \tag{5.30}$$

In particular,

$$\left(j+\frac{1}{2}\right)=\frac{\Gamma\left(j+\frac{3}{2}\right)}{\Gamma\left(j+\frac{1}{2}\right)} \quad \text{and} \quad -p_v^2=\frac{\Gamma\left(1-p_v^2\right)}{\Gamma\left(-p_v^2\right)}. \tag{5.31}$$

For $j=-3/2$, relations (5.31) and (5.32) become

$$\lim_{c\to -1}\frac{M\left(-1-p_v^2,c;\rho_0^2/2\right)}{\Gamma(j+1/2)}=\frac{\Gamma(1-p_v^2)}{\Gamma(-1-p_v^2)(2)!}\left(\frac{\rho_0^2}{2}\right)^2 M\left(1-p_v^2,3;\rho_0^2/2\right),$$

$$\lim_{c\to 0}\frac{M\left(-1-p_v^2,c;\rho_0^2/2\right)}{\Gamma(j+3/2)}=\frac{\Gamma(-p_v^2)}{\Gamma(-1-p_v^2)(1)!}\frac{\rho_0^2}{2}M(-p_v^2,2;\rho_0^2/2),$$

$$U\left(j+1/2-p^2,j+1/2;\rho_0^2/2\right)=\left(\frac{\rho_0^2}{2}\right)^2 U\left(1-p^2,3;\rho_0^2/2\right),$$

and

$$U\left(j+1/2-p^2,j+3/2;\rho_0^2/2\right)=\frac{\rho_0^2}{2}U\left(-p^2,2;\rho_0^2/2\right).$$

Correspondingly, Eq. (5.24) for $j=-3/2$ can be expressed as

$$\frac{2(\hbar\lambda v_F)^2(-p_v^2)\frac{\rho_0^2}{4}M\left(1-p_v^2,3;\rho_0^2/2\right)}{l_B^2(E+V_0-\xi\Delta)M\left(-p_v^2,2;\rho_0^2/2\right)}=(E+\xi\Delta)\frac{\rho_0^2}{2}\frac{U\left(1-p^2,3;\rho_0^2/2\right)}{U\left(-p^2,2;\rho_0^2/2\right)}.$$

$$\Rightarrow\frac{(-(E+V_0-\xi\Delta)(E+V_0+\xi\Delta))\frac{1}{2}M\left(1-p_v^2,3;\rho_0^2/2\right)}{(E+V_0-\xi\Delta)M\left(-p_v^2,2;\rho_0^2/2\right)}=(E+\xi\Delta)\frac{U\left(1-p^2,3;\rho_0^2/2\right)}{U\left(-p^2,2;\rho_0^2/2\right)},$$

$$\Rightarrow\left(\frac{E}{\Delta}+\frac{V_0}{\Delta}+\xi\right)\frac{1}{2}\frac{M\left(1-p_v^2,3;\rho_0^2/2\right)}{M\left(-p_v^2,2;\rho_0^2/2\right)}=-\left(\frac{E}{\Delta}+\xi\right)\frac{U\left(1-p^2,3;\rho_0^2/2\right)}{U\left(-p^2,2;\rho_0^2/2\right)}. \tag{5.32}$$

For $j=-5/2$ relations (5.31) and (5.32) are

$$\lim_{c\to -2}\frac{M\left(-2-p_v^2,c;\rho_0^2/2\right)}{\Gamma(j+1/2)}=\frac{\Gamma(1-p_v^2)}{\Gamma(-2-p_v^2)(3)!}\left(\frac{\rho_0^2}{2}\right)^3 M\left(1-p_v^2,4;\rho_0^2/2\right),$$

$$\lim_{c\to -1}\frac{M\left(-2-p_v^2,c;\rho_0^2/2\right)}{\Gamma(j+3/2)}=\frac{\Gamma(-p_v^2)}{\Gamma(-2-p_v^2)(2)!}\left(\frac{\rho_0^2}{2}\right)^2 M\left(-p_v^2,3;\rho_0^2/2\right),$$

$$U\left(j+1/2-p^2,j+1/2;\rho_0^2/2\right)=\left(\frac{\rho_0^2}{2}\right)^3 U\left(1-p^2,4;\rho_0^2/2\right),$$

and

$$U\left(j+1/2-p^2,j+3/2;\rho_0^2/2\right)=\left(\frac{\rho_0^2}{2}\right)^2 U\left(-p^2,3;\rho_0^2/2\right).$$

Thus, Eq. (5.24) for $j=-5/2$ is simply

$$\left(\frac{E}{\Delta}+\frac{V_0}{\Delta}+\xi\right)\frac{1}{3}\frac{M\left(1-p_v^2,4;\rho_0^2/2\right)}{M\left(-p_v^2,3;\rho_0^2/2\right)}=-\left(\frac{E}{\Delta}+\xi\right)\frac{U\left(1-p^2,4;\rho_0^2/2\right)}{U\left(-p^2,3;\rho_0^2/2\right)}. \tag{5.33}$$

Proceeding in the same way we get for $j=-7/2$ and $j=-9/2$

$$\left(\frac{E}{\Delta}+\frac{V_0}{\Delta}+\xi\right)\frac{1}{4}\frac{M\left(1-p_v^2,5;\rho_0^2/2\right)}{M\left(-p_v^2,4;\rho_0^2/2\right)}=-\left(\frac{E}{\Delta}+\xi\right)\frac{U\left(1-p^2,5;\rho_0^2/2\right)}{U\left(-p^2,4;\rho_0^2/2\right)}, \tag{5.34}$$

and

$$\left(\frac{E}{\Delta}+\frac{V_0}{\Delta}+\xi\right)\frac{1}{5}\frac{M\left(1-p_v^2,6;\rho_0^2/2\right)}{M\left(-p_v^2,5;\rho_0^2/2\right)}=-\left(\frac{E}{\Delta}+\xi\right)\frac{U\left(1-p^2,6;\rho_0^2/2\right)}{U\left(-p^2,5;\rho_0^2/2\right)}, \tag{5.35}$$

respectively. In general, for $j\leq -1/2$, we have the formula

$$\left(\frac{E}{\Delta}+\frac{V_0}{\Delta}+\xi\right)\left(\frac{1}{\frac{1}{2}-j}\right)\frac{M\left(1-p_v^2,\frac{3}{2}-j;\rho_0^2/2\right)}{M\left(-p_v^2,\frac{1}{2}-j;\rho_0^2/2\right)}=-\left(\frac{E}{\Delta}+\xi\right)\frac{U\left(1-p^2,\frac{3}{2}-j;\rho_0^2/2\right)}{U\left(-p^2,\frac{1}{2}-j;\rho_0^2/2\right)}. \tag{5.36}$$

with the quantities p_v^2 and p^2 given by

$$p_v^2=\frac{l_B^2[(E+V_0)^2-\Delta^2]}{2(\lambda\hbar v_F)^2}\quad\text{and}\quad p^2=\frac{l_B^2[E^2-\Delta^2]}{2(\lambda\hbar v_F)^2}. \tag{5.37}$$

The general equation (Eq. (5.36)) is now well defined for values $j\leq -1/2$. Below we analyze the behaviour of this energy relation on strained graphene. First, we analyze the case in absence of an external magnetic field, and then, with an external

magnetic field acting on the system. We derive expressions for the energy and the critical potential $V_{0,cr}$ in both cases, sketching them graphically as well. We show an asymptotic difference of the lower energy states caused by the application of the magnetic field, and the effects of the strain on this behaviour.

5.2.1 Collapse in absence of an external magnetic field

Let us first analyze the case of the potential well in graphene without an external magnetic field ($B = 0 \Rightarrow l_B \to \infty \Rightarrow p_v^2 \to \infty$), which is a benchmark to compare with the case with $B \neq 0$. In this case, by using the relations

$$M(a, c; x) = e^x U(c - a, c; -x), \tag{5.38}$$

$$\lim_{a\to\infty} M(a, c; x) = \Gamma(c)\ x^{\frac{1-c}{2}} J_{c-1}(2\sqrt{x}), \tag{5.39}$$

$$\lim_{a\to\infty} \left[\Gamma(1 + a - c)\ U(a, c; -x/a)\right] = -i\ \pi e^{i\pi c} x^{\frac{1-c}{2}} H^{(1)}_{c-1}(2\sqrt{x}), \quad \mathrm{Im}x > 0, \tag{5.40}$$

and $|\arg a| < \pi$ for the two last equations, and taking $z = p_v^2\ (\rho_0^2/2) \Rightarrow \rho_0^2/2 = z/p_v^2$, Eq. (5.24) turns into

$$\lim_{p_v^2,\ p^2\to\infty} \left\{ \frac{2(\lambda\hbar v_F)^2(j + \frac{1}{2})\ M\left(p_v^2, j + \frac{1}{2}; -\frac{z}{p_v^2}\right)}{l_B^2(E + V_0 - \xi\Delta)\ M\left(p_v^2, j + \frac{3}{2}; -\frac{z}{p_v^2}\right)} = \right.$$

$$\left. (E + \xi\Delta)\frac{U\left(j + \frac{1}{2} - p^2, j + \frac{1}{2}; -\frac{z}{p^2}\right)}{U\left(j + \frac{1}{2} - p^2, j + \frac{3}{2}; -\frac{z}{p^2}\right)} \right\},$$

$$\Rightarrow \frac{2(\lambda\hbar v_F)^2(j + \frac{1}{2})\ \Gamma(j + 1/2)\ \left(\frac{p_v^2 r_0^2}{2l_B^2}\right)^{\frac{-j+1/2}{2}} J_{j-1/2}\left(\frac{\sqrt{(E+V_0)^2-\Delta^2}\ r_0}{\hbar\lambda v_F}\right)}{l_B^2(E + V_0 - \xi\Delta)\ \Gamma(j + 3/2)\ \left(\frac{p_v^2 r_0^2}{2l_B^2}\right)^{\frac{-j-1/2}{2}} J_{j+1/2}\left(\frac{\sqrt{(E+V_0)^2-\Delta^2}\ r_0}{\hbar\lambda v_F}\right)} =$$

$$\frac{(E + \xi\Delta)\ i\ \pi\ e^{i\pi(j+1/2)}\left(\frac{p^2 r_0^2}{2l_B^2}\right)^{\frac{-j+1/2}{2}} \Gamma(-p^2) H^{(1)}_{j-1/2}\left(\frac{\sqrt{E^2-\Delta^2}\ r_0}{\hbar\lambda v_F}\right)}{i\ \pi\ e^{i\pi(j+3/2)}\left(\frac{p^2 r_0^2}{2l_B^2}\right)^{\frac{-j-1/2}{2}} \Gamma(1 - p^2) H^{(1)}_{j+1/2}\left(\frac{\sqrt{E^2-\Delta^2}\ r_0}{\hbar\lambda v_F}\right)},$$

$$\Rightarrow \frac{2(\lambda\hbar v_F)^2 \left(\frac{p_v^2 r_0^2}{2l_B^2}\right)^{\frac{1}{2}} J_{j-1/2}(\beta r_0)}{l_B^2(E+V_0-\xi\Delta)\ J_{j+1/2}(\beta r_0)} = -\frac{(E+\xi\Delta)\left(\frac{p^2 r_0^2}{2l_B^2}\right)^{\frac{1}{2}} H^{(1)}_{j-1/2}(\beta' r_0)}{-p^2\ H^{(1)}_{j+1/2}(\beta' r_0)},$$

$$\Rightarrow \frac{2(\lambda\hbar v_F)^2 \left(\frac{l_B\sqrt{(E+V_0)^2-\Delta^2}}{\sqrt{2}\hbar\lambda v_F}\right) J_{j-1/2}(\beta r_0)}{l_B^2(E+V_0-\xi\Delta)\ J_{j+1/2}(\beta r_0)} = \frac{(E+\xi\Delta)\ H^{(1)}_{j-1/2}(\beta' r_0)}{\left(\frac{l_B\sqrt{E^2-\Delta^2}}{\sqrt{2}\hbar\lambda v_F}\right) H^{(1)}_{j+1/2}(\beta' r_0)},$$

$$\Rightarrow \frac{\sqrt{(E+V_0)^2-\Delta^2} J_{j-1/2}(\beta r_0)}{(E+V_0-\xi\Delta)\ J_{j+1/2}(\beta r_0)} = \frac{(E+\xi\Delta)\ H^{(1)}_{j-1/2}(\beta' r_0)}{\sqrt{E^2-\Delta^2} H^{(1)}_{j+1/2}(\beta' r_0)},$$

$$\Rightarrow \frac{\sqrt{(E+V_0)^2-\Delta^2} J_{j-1/2}(\beta r_0)}{(E+V_0-\xi\Delta)\ J_{j+1/2}(\beta r_0)} = \frac{\sqrt{E^2-\Delta^2} H^{(1)}_{j-1/2}(\beta' r_0)}{(E-\xi\Delta) H^{(1)}_{j+1/2}(\beta' r_0)}, \tag{5.41}$$

with $\beta = \frac{\sqrt{(E+V_0)^2-\Delta^2}}{\hbar\lambda v_F}$ and $\beta' = \frac{\sqrt{E^2-\Delta^2}}{\hbar\lambda v_F}$.

Let us take, without loss of generality[1], the valley K_- ($\xi = -$). The energy spectrum consists of a continuum portion for $|E| > \Delta$, and a discrete one for $|E| < \Delta$, where the bound states appear. The first bound state, $E \lesssim \Delta$, corresponds to that related to the smallest centrifugal barrier $j = -1/2$, and appears at an arbitrarily small potential V_0. Under these considerations, the quantities β and β' become imaginary. Defining the new variables

$$X = \frac{E}{\Delta}, \quad Y = \frac{V_0}{\Delta}, \quad R = \frac{\Delta r_0}{\hbar\lambda v_F}, \tag{5.42}$$

and using the relations

$$J_{-n}(z) = (-1)^n J_n(z), \quad H^{(1)}_{-n}(z) = (-1)^n H^{(1)}_n(z), \ J_n(iz) = e^{i\pi n/2} I_n(z),$$

and

$$H^{(1)}_n(iz) = \frac{2}{i\pi} e^{-i\pi n/2} K_n(z),$$

[1]The solution at the K_+ valley is obtained by changing $\Delta \to -\Delta$ and exchanging the spinor components $\psi_A \leftrightarrow \psi_B$.

in Eq. (5.41), we have

$$\frac{i\,\sqrt{1-(X+Y)^2}}{X+Y+1}\frac{(-1)e^{i\pi/2}I_1(\sqrt{1-(X+Y)^2}R)}{I_0(\sqrt{1-(X+Y)^2}R)} =$$

$$\frac{i\,\sqrt{1-X^2}}{X+1}\frac{(-1)e^{-i\pi/2}\frac{2}{i\,\pi}K_1(\sqrt{1-X^2}R)}{\frac{2}{i\,\pi}\,K_0(\sqrt{1-(X+Y)^2}R)},$$

$$\Rightarrow \frac{\sqrt{1-(X+Y)^2}}{X+Y+1}\frac{I_1(\sqrt{1-(X+Y)^2}R)}{I_0(\sqrt{1-(X+Y)^2}R)} = \frac{\sqrt{1-X^2}}{X+1}\frac{-K_1(\sqrt{1-X^2}R)}{K_0(\sqrt{1-(X+Y)^2}R)}.$$

Then, using the asymptotic expressions for $z \to 0$:

$$\lim_{z\to 0} I_n(z) \simeq \frac{1}{\Gamma(n+1)}\left(\frac{z}{2}\right)^n, \quad n \geq 0,$$

$$\lim_{z\to 0} K_n(z) \simeq \begin{cases} -\ln\left(\frac{z}{2}\right) - \gamma, & n = 0, \\ \frac{\Gamma(n)}{2}\left(\frac{2}{z}\right)^2, & n > 0, \end{cases}$$

where γ is the Euler-Mascheroni constant (≈ 0.5772), we have

$$\frac{\sqrt{1-(X+Y)^2}}{X+Y+1}\left(\frac{\sqrt{1-(X+Y)^2}\;R}{2}\right) = \frac{\sqrt{1-X^2}}{X+1}\left(\frac{-1}{\sqrt{1-X}R}\right)\left(\frac{-1}{\ln\left(\frac{\sqrt{1-X^2}R}{2}\right)+\gamma}\right),$$

$$\Rightarrow \frac{\left(1-(X+Y)^2\right)(1+X)}{X+Y+1}\left(\ln\left(\frac{\sqrt{1-X^2}R}{2}\right)+\gamma\right) = \frac{2}{R^2},$$

$$\Rightarrow (-1+X+Y)(1+X)\left(\ln\left(\frac{\sqrt{1-X^2}R}{2}\right)+\gamma\right) = -\frac{2}{R^2},$$

and using that $X \to 1_-$, and the logarithm identity $a\ln(b) = \ln(b^a)$, we have

$$\Rightarrow \ln\left(\frac{(1-X^2)R^2}{4}\right) = -\frac{2}{YR^2} - 2\gamma,$$

$$\Rightarrow \ln\left(\frac{(1-X)R^2}{2}\right) = -\frac{2}{YR^2} - 2\gamma,$$

$$\Rightarrow X = 1 - \frac{2}{R^2}\exp\left[-\frac{2}{YR^2} - 2\gamma\right],$$

$$\Rightarrow E = \Delta\left[1 - 2\left(\frac{\hbar\lambda v_F}{\Delta r_0}\right)^2 \exp\left(-\frac{2(\hbar\lambda v_F)^2}{V_0\Delta r_0^2} - 2\gamma\right)\right]. \tag{5.43}$$

The dependence of the energy with respect to λ of this state with $j = -1/2$ (Eq. (5.43)) is shown in Fig. 5.4. It can be seen that as λ grows, the energy decays more slowly, and requires a higher radius r_0 to reach the minimum value $E = 0$. This is an indicative of the displacement of the angular centrifugal barrier $j = -1/2$ produced by the strain of the lattice. Furthermore, as V_0 grows, the lowest energy

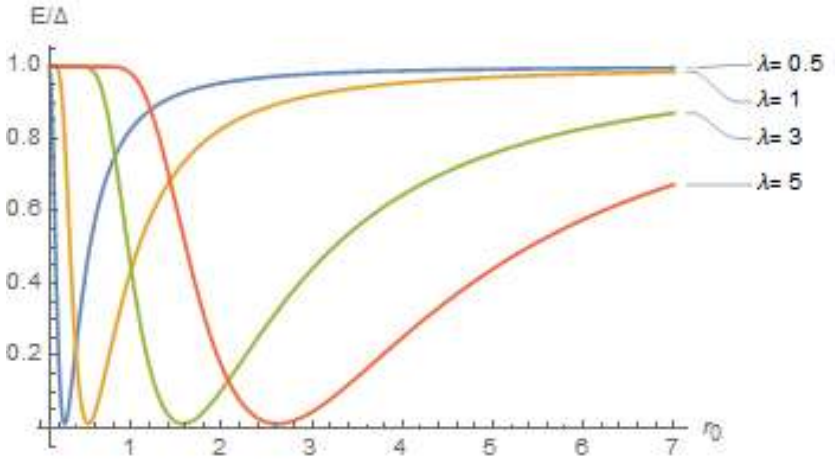

Figure 5.4: Energy E as a function of r_0 for different values of λ for the state with $j = -1/2$.

state ($j = -1/2$) gets closer to the continuum ($E = -\Delta$). Using the defined notation for X, Y and R, Eq. (5.43) for $E = -\Delta$ turns into

$$\frac{\sqrt{(Y-1)^2-1}}{Y}\frac{J_{-1}\left(\sqrt{(Y-1)^2-1}R\right)}{J_0\left(\sqrt{(Y-1)^2-1}R\right)} = \frac{\sqrt{X-1}}{\sqrt{X+1}}\frac{H_{-1}^{(1)}\left(\sqrt{(-1)^2-1}R\right)}{H_0^{(1)}\left(\sqrt{(-1)^2-1}R\right)},$$

where the limit in this case, $X \to -1$, was used. Insomuch as the functions $H_{-1}^{(1)}(0)$ and $H_0^{(1)}(0)$ are nonzero, the condition to find the critical potential value $V_{0,cr}$ is

$$J_0\left(\sqrt{(Y-1)^2-1}R\right) = 0,$$

$$\Rightarrow \sqrt{(Y-1)^2-1}R = j_{0,1},$$

$$V_{0,cr} = \Delta\left[1 + \sqrt{1 + \left(\frac{\hbar\lambda v_F}{\Delta r_0}\right)^2 j_{0,1}^2}\right], \tag{5.44}$$

where $j_{0,1} \approx 2.41$ is the first zero of the function $J_0(x)$[2]. From Eq. (5.44) it can be seen immediately that the value of $V_{0,cr}$ grows or diminishes depending on the value of λ. An expansion of the Landau levels $\lambda > 1$ leads to a higher value of $V_{0,cr}$, whereas for contractions $\lambda < 1$, it gets smaller. In this sense it can be said that strain promotes or inhibits atomic collapse. Below we analyze the case with an external magnetic field B_0. As we will shortly see, the magnetic field has powerful repercussions in collapse.

5.2.2 Collapse with the effects of an external magnetic field

Let us now consider the case treated until now of a potential well of radii r_0 and value V_0 representing a Coulomb impurity in a graphene lattice, but now let us add an external magnetic field B_0 perpendicular to the crystal plane. First of all, if we delete the potential well (taking $r_0 \to 0$ or $V_0 \to 0$), Eq. (5.24) gives the expected Landau levels[3], but with the strain parameter inside

$$E = -\xi\Delta, \quad j \leq -1/2, \tag{5.45}$$

$$E = \pm\sqrt{\Delta^2 + 2n\left(\frac{\hbar\lambda v_F}{l_B}\right)^2}, \quad n = 1, 2, ..., \text{ and } j + 1/2 \leq n. \tag{5.46}$$

It is important to mention that the states are degenerate, as the energy only depends on the principal number n and not on the angular momentum value j. This degeneracy is lifted when a nonzero potential V_0 is considered. This can be seen in Figs. 5.5-5.6, where a set of solutions of Eq. (5.24) with $E = \Delta$ and different angular momentum j are represented as a functions of the potential strength (both, the energy and the potential, are normalized by the mass gap Δ), in the valley $\xi = -$. Each plot also carries information about the strain by the factor λ. In order to make the plot, the values $l_B\Delta/(\sqrt{2}\hbar v_F) = 10$ and $\rho_0^2/2 = 0.02$ were used.

There are some important facts to notice: First, as we said before, the states with different angular momentum are no longer degenerate, and more and more of them decay from $E = \Delta$ to $E = -\Delta$ as V_0 grows. This represents the fact that these states are diving toward the nucleus, taking place the atomic collapse. In addition, comparing with the case of unstrained graphene (Fig. 5.5), a contracting strain causes promotion in atomic collapse (Fig. 5.6(a)), whereas an expansive one makes collapse inhibited (Fig. 5.6(b)). We can think of this observation, as the strain deforms the lattice, the Dirac cones have now an elliptical cross section. Thus, the electrons orbiting near the larger semi-axis last more in their spiral-falling trajectory than those that are near the lower semi-axis. The first crossing to the continuum

[2]Note that for $\Delta = 0$ there are no bound states.

[3]Note that the values $E = \pm\Delta$ are only present at the points $K_\pm$ respectively.

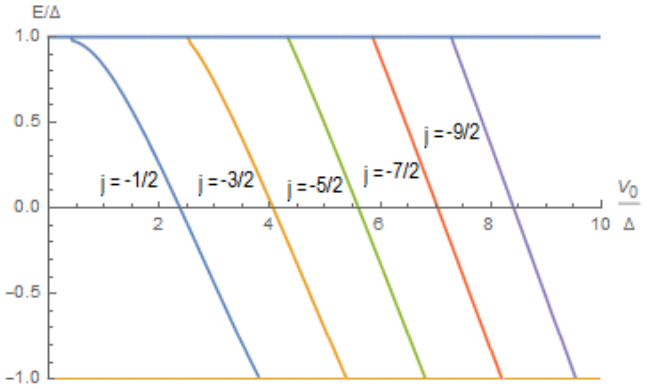

Figure 5.5: Energy E as a function of V_0 (both normalized by the mass gap Δ) for some states with negative angular momentum $j \leq -1/2$, and without strain $\lambda = 1$.

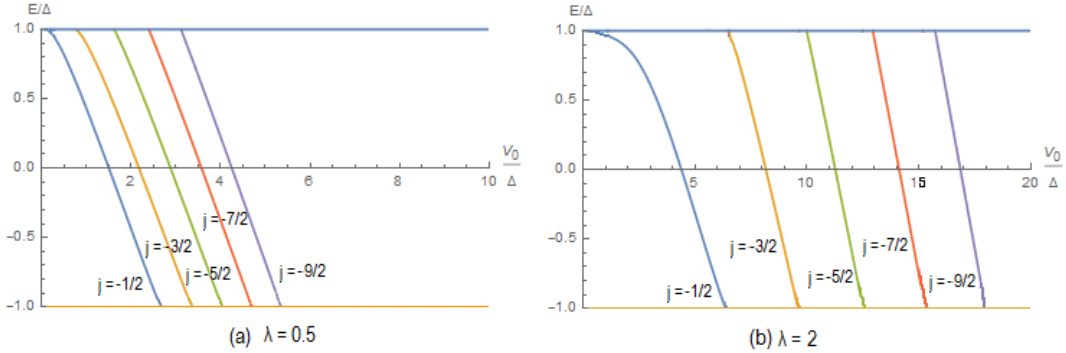

Figure 5.6: Energy E as a function of V_0 (both normalized by the mass gap Δ) for some states with negative angular momentum $j \leq -1/2$, taking into account the strain parameter λ for the values (a) $\lambda = 0.5$ and (b) $\lambda = 2.0$, representing compression and expansion of the Landau levels respectively.

of energy is given by the state with $j = -1/2$. The critical value of the potential $V_{0,cr}$ in which this occurs (when $E = -\Delta$) can be obtained from Eq. (5.24), by noting that in this case $p^2 = 0$, $p_v^2 = l_B^2(V_0^2 - 2\Delta V_0)/2(\hbar\lambda v_F)^2$, and using that $U(0,0;z) = U(0,1;z) = 1$. So, we have[4]

$$V_{0,cr} = 2\Delta \left[1 + \frac{2\ M\left(a, 1; \rho_0^2/2\right)}{\rho_0^2\ M\left(1+a, 2; \rho_0^2/2\right)}\right], \tag{5.47}$$

where $a = l_B^2\ V_{0,cr}(V_{0,cr} - 2\Delta)/2(\hbar\lambda v_F)^2$.

[4]Note that for $B = 0$ we recover the expression given by Eq. (5.44).

The critical potential strength as a functions of the quasiparticle mass gap is plotted in Figs. 5.7-5.8 for different values of the parameters ρ and λ. It is clearly seen that the value of $V_{0,cr}$ decreases with the value of the magnetic field B_0 (as $\rho_0 = r_0/l_B$ and $l_B \sim \sqrt{1/|B_0|}$) for fixed values of r_0 and Δ.

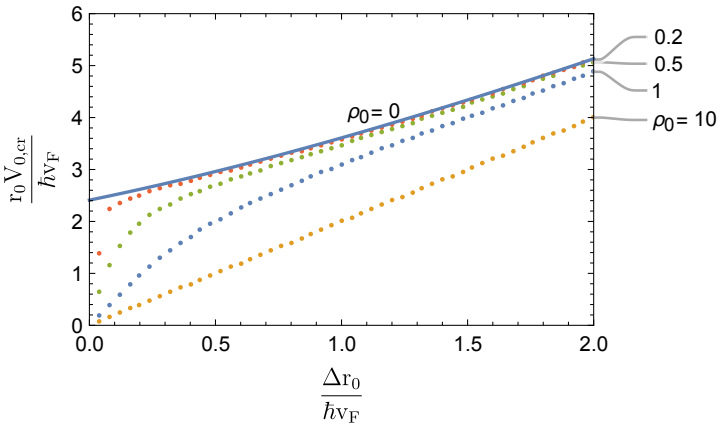

Figure 5.7: $V_{0,cr}$ as function of Δ for different values of ρ_0 (B_0). The case $\rho_0 = 0$ (blue continuous line) corresponds to the system with no magnetic field applied $B_0 = 0$.

Since from the physical point of view, this represents the fact that the external magnetic field B_0 brings electronic orbitals closer to the nucleus, and thus, the attraction between electrons an nucleus gets more intense, lowering the critical value of coupling. In addition, the value of the parameter λ, which contains information about the strain, provokes the critical potential value $V_{0,cr}$ to decrease for $\lambda < 1$ (Fig. 5.8(a)), or to grow for $\lambda > 1$ (Fig. 5.8(b)), for fixed values of r_0, Δ and B_0. This result leads us to conclude that possibility to induce such an strain in the graphene lattice makes electronic collapse easier to take place in one direction and more difficult in the other, being capable to control an effective directed-current. Another observation is that in all the cases with $B_0 \neq 0$, $V_{0,cr}$ goes to zero as Δ decreases arbitrarily. From that, we can conclude that the presence of an homogeneous magnetic field catalyzes atomic collapse of the Coulomb center doped graphene for any strain. In particular, in the case of gapless graphene in the presence of an homogeneous magnetic field, atomic collapse would take place for any value of Ze.

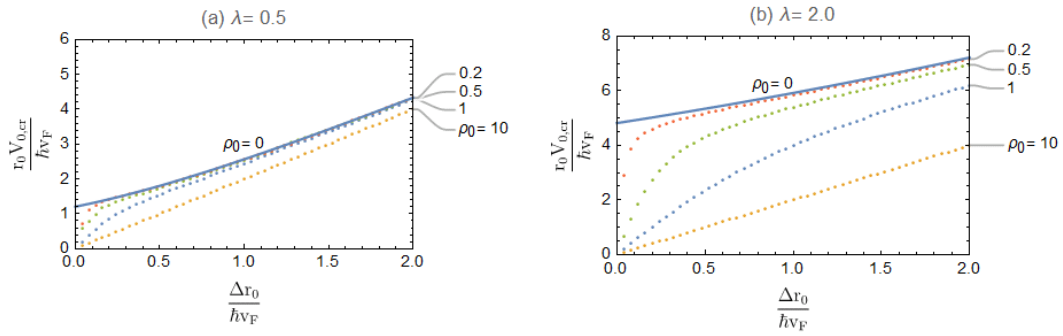

Figure 5.8: $V_{0,cr}$ as function of Δ for different values of ρ_0 (B_0) and including the strain parameter λ with the values (a) $\lambda = 0.5$ and (b) $\lambda = 2.0$, representing compression and expansion of the Landau levels respectively. Just as in the last figure, the case $\rho_0 = 0$ (blue continuous line) corresponds to the system with no magnetic field applied $B_0 = 0$.

5.3 Coulomb impurity in graphene under a strained-generated *pseudomagnetic* field

Even though strains which generate *pseudomagnetic* fields in graphene are way more difficult to model in terms of a tensor Fermi velocity $\mathbf{v}_F$[5], this because the deformation is more complex, it is possible to obtain some qualitative conclusions after the analysis of the previous Section. First, the induced *pseudomagnetic* field leads to the decrease of the critical potential $V_{0,cr}$, turning its value lower as the magnitude of the field increases, thus, catalyzing the atomic collapse phenomenon in graphene. In the case of gapless quasiparticles, it leads the system to atomic collapse always. On the other hand, the "effective strain magnitud" (expansion or compression) has effects over the value $V_{0,cr}$ making it higher or lower. Therefore, globally, the system will be, or under a competition between the strain magnitude of expansion and the magnitude of the *pseudomagnetic* field generated by it, or both effects will "add constructively" in order to make atomic collapse easier. Finally, the fact that the *pseudomagnetic* field generated by strains is of opposite directions in each valley K and K', would give us the opportunity to, with the aid of an external magnetic field, control the dynamics of the quasiparticles in each valley not only by the interference of both-*pseudo*- and external-magnetic fields, but also through an special strain strength different in each valley, thus, conforming a more specialized area of application based in both *Valleytronics* and *Straintronics*.

[5] As for example those considered in [87].

Chapter 6

Strained graphene in presence of a point electric dipole

In this Chapter we treat the case of a point electric dipole placed in a graphene plane (Fig. 6.1) [18, 19], but taking also into account the effect of strain on the Dirac fermions. First, we introduce the potential describing the electric dipole in the distorted lattice and we make the approximation of large distances, where the expression for the potential describes the one of a point electric dipole. Then, we solve the corresponding Dirac equation near the edges $\pm\Delta$, obtaining expressions containing the strain parameter λ explicitly. Some energy plots of the bound states in this case are presented.

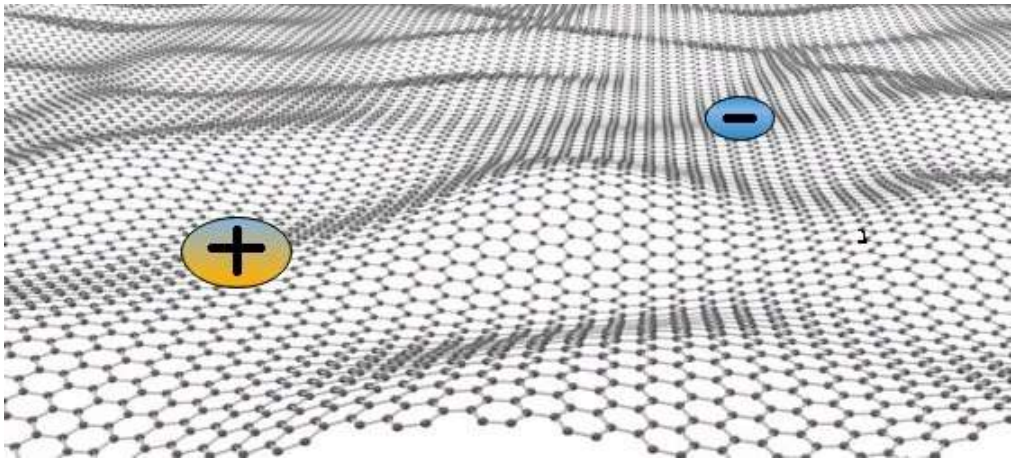

Figure 6.1: Electric dipole in graphene.

The electric dipole consists in two opposite charges $+Q$ and $-Q$ separated a distance d. Thus, its electric potential is given by [88]

$$V(r) = \frac{p/d}{r_+} - \frac{p/d}{r_-}, \tag{6.1}$$

where $p = Qd$ is the dipole moment[1], and

$$r_\pm = \sqrt{(x \pm d/2)^2 + y^2} \tag{6.2}$$

are the length of the vectors $\mathbf{r}_+$, $\mathbf{r}_-$ joining the negative and positive charge positions with the observation point respectively (Fig. 6.2).

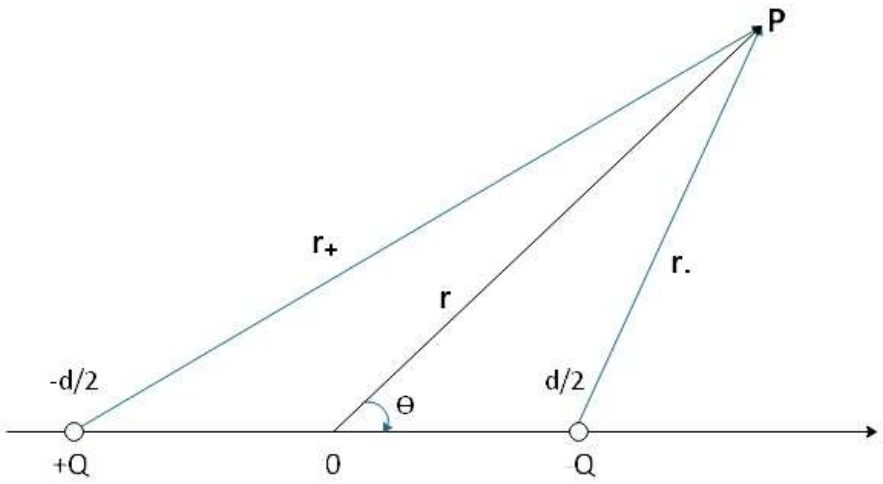

Figure 6.2: Geometry of an electric dipole placed in the x-axis with the opposite charges separated a distance d.

The expressions in Eq. (6.2) can be taken to the form

$$r_\pm^2 = r^2 + \left(\frac{d}{2}\right)^2 \pm rd\cos\theta,$$

$$\Rightarrow \frac{r}{r_\pm} = \left(1 + \left(\frac{d}{2r}\right)^2 \pm \frac{d}{r}\cos\theta\right)^{-1/2}, \tag{6.3}$$

[1]It can be renormalized to include a substrate dielectric constant, as for example in graphene [71].

with r the magnitude of the vector joining the center of the line which connects both charges with the observation point, as shown in Fig 6.2. For $r \gg d$, by using the approximation $(1+x)^{-1/2} \approx 1 - \frac{1}{2}x + \frac{3}{8}x^2 + ...$ in Eq. (6.3), we have

$$\frac{r}{r_\pm} = \left(1 + \left(\frac{d}{2r}\right)^2 \pm \frac{d}{r}\cos\theta\right)^{-1/2} \approx 1 - \frac{1}{2}\left(\frac{d}{2r}\right)^2 \mp \frac{d}{2r}\cos\theta. \tag{6.4}$$

Thus, using these expressions in Eq. (6.1), we obtain the potential of a point electric dipole

$$V_d(r,\theta) = -\frac{p\cos\theta}{r^2}. \tag{6.5}$$

The case of the point electric dipole, in which the distance between the opposite charges $d \to 0$ with fixed dipole moment, has been recently treated in [18, 19], where it was shown the emergence of towers of infinite bound states satisfying a universal Efimov-like scaling hierarchy, with the existence of at least one tower for arbitrary dipole strength. In this work it is found that bounds states do not dive into the lower (higher) continuum for the case of electron (holes), but they first approach each other and then they go away. This leads to the conclusion that supercriticality in graphene under the presence of a point electric dipole is unlikely to occur[2].

From here, we follow the discussion given in [19] for the electric dipole in graphene, but we extend it to include the effects of strain. The (2+1) Hamiltonian for Dirac fermions in graphene in the K_+ valley, with mass gap Δ, and in the presence of a point electric dipole is

$$H = \hbar \mathbf{v}_F \cdot \boldsymbol{\sigma} \cdot \mathbf{p} + \Delta\sigma_z + V_d, \tag{6.6}$$

where we are introducing the strain effects by the tensor Fermi velocity as in the previous Chapter, namely

$$\mathbf{v}_F = v_F \begin{pmatrix} a & 0 \\ 0 & b \end{pmatrix}. \tag{6.7}$$

The Hamiltonian given in Eq. (6.6) has an intrinsic electron-hole symmetry $UHU^\dagger = -H$, with the unitary operator $U = \sigma_x R_x$ satisfying $U^2 = 1$, where R_x is the operator of reflection $x \to -x$. An eigenstate $\Psi_E(x,y)$ with energy E is mapped to another eigenstate with energy $-E$ as

$$\Psi_{-E}(x,y) = U\Psi_E(x,y) = \sigma_x \Psi_E(-x,y). \tag{6.8}$$

[2]The case of a finite-size electric dipole was treated in [89] by using the LCAO technique and the variational Galerkin-Kantarovich method. It was found a migration of the electron wave function from the negatively to the positively charged impurity (and the opposite for the hole), and can be thought as a generalization of the atomic collapse with the positron decaying in the positive charged impurity instead of escaping to infitite.

Hence, all solutions of the Dirac equation come in pairs with $\pm E$, and it is enough to study one of the eigenstates to automatically know the other.

Thus, the Dirac equation governing the system is written as

$$\begin{pmatrix} V_d(r,\theta)+\Delta-E & \hbar v_F(aP_x-ibP_y) \\ \hbar v_F(aP_x+ibP_y) & V_d(r,\theta)-\Delta-E \end{pmatrix}\begin{pmatrix}\psi_A \\ \psi_B\end{pmatrix}=0, \tag{6.9}$$

where $P_x=-i\partial_x$ and $P_y=-i\partial_y$. By using the definitions of λ and ζ given in Eq. (5.3), and the azimuthal-symmetric relations in Eq. (5.8)[3] we have

$$\begin{aligned} aP_x \pm ibP_y &= \lambda\left[\zeta^{1/2}P_x \pm i\zeta^{-1/2}P_y\right] = \lambda\left[-i\zeta^{1/2}\partial_x \pm \zeta^{-1/2}\partial_y\right] \\ &= \lambda\left[-i\left(\cos\phi\partial_r - \frac{\sin\phi}{r}\partial_\phi\right) \pm \left(\sin\phi\partial_r - \frac{\cos\phi}{r}\partial_\phi\right)\right] \\ &= \lambda\left[-i\left(\cos\phi \pm i\sin\phi\right)\partial_r \pm \frac{1}{r}\left(\cos\phi \pm i\sin\phi\right)\partial_\phi\right] \\ &= \lambda e^{\pm i\phi}\left(-i\partial_r \pm \frac{\partial_\phi}{r}\right), \end{aligned} \tag{6.10}$$

thus, the Dirac equation turns into

$$\begin{pmatrix} V_d(r,\theta)+\Delta-E & \hbar\lambda v_F e^{-i\phi}\left(-i\partial_r - \frac{\partial_\phi}{r}\right) \\ \hbar\lambda v_F e^{i\phi}\left(-i\partial_r + \frac{\partial_\phi}{r}\right) & V_d(r,\theta)-\Delta-E \end{pmatrix}\begin{pmatrix}\psi_A \\ \psi_B\end{pmatrix}=0. \tag{6.11}$$

Let us remember that values of the energy $|E|>\Delta$ represent states in the continuum of energy ("scattering states"), and $|E|<\Delta$ represent states with discrete energies ("bound states"). Then, if we consider energies near the edge $-\Delta$, $E=-\Delta+\epsilon$, with $|\epsilon|\ll\Delta$, Eq. (6.11) is written as

$$\begin{pmatrix} \frac{-p\cos\phi}{r^2}+2\Delta-\epsilon & \lambda v_F e^{-i\phi}\left(-i\partial_r - \frac{\partial_\phi}{r}\right) \\ \hbar\lambda v_F e^{i\phi}\left(-i\partial_r + \frac{\partial_\phi}{r}\right) & \frac{-p\cos\phi}{r^2}-\epsilon \end{pmatrix}\begin{pmatrix}\psi_A \\ \psi_B\end{pmatrix}=0, \tag{6.12}$$

where we have taken $\hbar=1$. So that, we have the coupled equations

$$\left(\frac{-p\cos\phi}{r^2}+2\Delta-\epsilon\right)\psi_A = -\lambda v_F e^{-i\phi}\left(-i\partial_r - \frac{\partial_\phi}{r}\right)\psi_B \tag{6.13}$$

[3]The elliptical condition in Eq. (5.9) turns into a circular one because of the fact that for a punctual dipole ($r\gg d$) $a\approx b$ and then $\zeta\approx 1$.

and

$$\left(\frac{-p\cos\phi}{r^2}-\epsilon\right)\psi_B=-\lambda v_F e^{i\phi}\left(-i\partial_r+\frac{\partial_\phi}{r}\right)\psi_A. \tag{6.14}$$

For $p \ll d^2\Delta$, from Eq. (6.13) we have

$$\psi_A \approx \frac{\lambda v_F}{2\Delta}e^{-i\phi}\left(i\partial_r+\frac{\partial_\phi}{r}\right)\psi_B, \tag{6.15}$$

and substituting this in Eq. (6.13) we get the equation for ψ_B

$$\left(\frac{-p\cos\phi}{r^2}-\epsilon\right)\psi_B=-\frac{\lambda^2 v_F^2}{2\Delta}\left(-i\partial_r+\frac{\partial_\phi}{r}\right)\left(i\partial_r+\frac{\partial_\phi}{r}\right)\psi_B$$

$$\Rightarrow\left(-\frac{\lambda^2 v_F^2}{2\Delta}\nabla^2+\frac{p\cos\phi}{r^2}+\epsilon\right)\psi_B=0, \tag{6.16}$$

where $\nabla^2=\partial_r^2+\frac{1}{r}\partial_r+\frac{1}{r^2}\partial_\phi^2$ is the 2D Laplace operator in cylindrical coordinates. This equation can be solved by the method of separation of variables. Let us propose a solution of the form

$$\psi_B(r,\phi)=R(r)\Phi(\phi), \tag{6.17}$$

so, Eq. (6.16) reads

$$-\frac{\lambda^2 v_F^2}{2\Delta}\left(\Phi(\phi)\partial_r^2 R(r)+\frac{1}{r}\Phi(\phi)\partial_r R(r)+\frac{1}{r^2}R(r)\partial_\phi^2\Phi(\phi)\right)+\left(\frac{p\cos\phi}{r^2}+\epsilon\right)R(r)\Phi(\phi)=0, \tag{6.18}$$

and, multiplying this equation by r^2 and dividing by $\psi(r,\phi)$, we obtain the variable-separated equation

$$\frac{r^2}{R(r)}\frac{\partial^2 R(r)}{\partial r^2}-\frac{2\Delta}{\lambda^2 v_F^2}r^2\epsilon=-\frac{1}{\Phi(\phi)}\frac{\partial^2\Phi(\phi)}{\partial\phi^2}+\frac{2\Delta}{\lambda^2 v_F^2}p\cos\phi=\gamma. \tag{6.19}$$

The angular equation

$$\left[\frac{d^2}{d\phi^2}-\frac{2\Delta}{\lambda^2 v_F^2}p\cos\phi+\gamma\right]\Phi(\phi)=0, \tag{6.20}$$

which is independent of the parameter ϵ, corresponds to a Mathieu equation [90, 91] whose solutions,

$$Y_{j,\kappa}(\phi)=\begin{cases} ce_{2j}\left(\frac{\phi}{2},\frac{4p\Delta}{\lambda^2 v_F^2}\right), \text{ for } \kappa=+, \\ \\ se_{2j}\left(\frac{\phi}{2},\frac{4p\Delta}{\lambda^2 v_F^2}\right), \text{ for } \kappa=-, \end{cases} \tag{6.21}$$

where $\kappa = \pm$ is the parity, are 2π-periodic and are only permitted for characteristic values of γ,

$$\gamma_{j,\kappa}(p) = \begin{cases} \frac{1}{4} a_{2j}\left(\frac{4p\Delta}{\lambda^2 v_F^2}\right), \text{ for } \kappa = +, \\ \\ \frac{1}{4} b_{2j}\left(\frac{4p\Delta}{\lambda^2 v_F^2}\right), \text{ for } \kappa = -, \end{cases} \tag{6.22}$$

where the angular momentum $j = 0, 1, 2...$ is unconventional because of the anisotropy, satisfying the relation $j + \kappa \geq 0$. These characteristic values are ordered for a given value of p as $\gamma_{0,+}(p) < \gamma_{1,-}(p) < \gamma_{1,+}(p) < \gamma_{2,-}(p) < ...$

The radial equation is given by

$$\left[\frac{d^2}{dr^2} - \frac{2\delta}{\lambda^2 v_F^2}\epsilon + \frac{1}{r}\frac{d}{dr} - \frac{\gamma}{r^2}\right] R(r) = 0, \tag{6.23}$$

has the form of a MacDonald equation [90]

$$u'' + \frac{1}{z}u' - \left(1 - \frac{\nu^2}{z^2}\right) z = 0, \tag{6.24}$$

whose solutions are the modified Bessel functions $K_\nu(z)$. In our case the Bessel functions are $K_{\sqrt{\gamma}}\left(\frac{r}{\lambda v_F}\sqrt{2\Delta\epsilon}\right)$, where for bound states ($\epsilon > 0$) they have to decay for $r \to 0$ and to be regular at the origin. For this purpose, we use the regularization condition $R(r_0) = 0$, which gives the energy quantization condition within each (j, κ) tower

$$\epsilon_{n,j,\kappa} = \frac{z_n^2 \lambda^2 v_F^2}{2\Delta r_0^2}, \tag{6.25}$$

where z_n are the zeros of the function $K_{\sqrt{\gamma_{j,\kappa}}}(z)$ satisfying $z_1 < z_2 < z_3 < ...$ As this function only has zeros for $\sqrt{\gamma_{j,\kappa}}$ imaginary [90], then the condition $\gamma_{j,\kappa}(p) < 0$ is required for bound states. This is satisfied for values $p > p_{j,\kappa}$ with

$$\gamma_{j,\kappa}(p_{j,\kappa}) = 0. \tag{6.26}$$

These values of $p_{j,\kappa}$ have been already computed in [19], and are shown in Table 1.

By increasing the value of p, each time that p hits a critical value $p_{j,\kappa}$, a new infinite tower of bound states emerges from the continuum. It is possible to expand $K_{is}(z)$ for small z ($s_{j,\kappa}(p) = \sqrt{-\gamma_{j,\kappa}(p)}$ for $p > p_{j,\kappa}$) obtaining an explicit expression for the bound energies near the edges $\pm\Delta$

$$\epsilon_{n,j,\kappa} = \frac{2\lambda^2 v_F^2}{\Delta r_0^2} e^{\phi(s_{j,\kappa})} e^{-2\pi n / s_{j,\kappa}}, \tag{6.27}$$

(j,κ)	$p_{j,\kappa}\Delta$
$(1,-)$	1.89492
$(1,+)$	5.32466
$(2,-)$	10.4819
$(2,+)$	17.3571
$(3,-)$	25.9511
$(3,+)$	36.2639

Table 6.1: Lowest few finite critical dipole moments obtained from the Mathieu eigenvalues (Eq. (6.26)). Adapted from [19].

where $\phi(s) = (2/s)\arg\Gamma(1+is)$, and the values $s_{j,\kappa}$ are given by [19]

$$s_{j,\kappa}(p) = \begin{cases} \frac{\sqrt{2}p\Delta}{\lambda^2 v_F^2}, & (j,\kappa) = (0,+), \\ \\ \frac{\alpha}{\lambda v_F}\sqrt{(p-p_{j,\kappa})\Delta}, & j > 0, \end{cases} \tag{6.28}$$

where $\alpha \approx 0.956$. From Eq. (6.27) it can be seen that it is satisfied a Efimov scaling law as in [19]

$$\frac{\epsilon_{n+1}}{\epsilon_n} = e^{-2\pi/s_{j,\kappa}}, \tag{6.29}$$

but with the λ-dependence inserted in the $s_{j,\kappa}$ terms. Plots of the energy spectrum versus dipole moment p for different values of the strain strength λ are presented in Fig. 6.3. In all of them the first electron, $\epsilon_{n,j,\kappa}$, bound states are presented for each tower, decaying from the continuum to discrete values.

Just as in the case of a single charged impurity seen in the previous Chapter, the role of the strain strength is to promote (for values of $\lambda < 1$) or inhibit (for values of $\lambda > 1$) the decay of the electron and hole bound states, making the collapse in both systems easier or more difficult to occur depending on the strain. Also, for $n \to \infty$ we have that $\epsilon \to 0$, so that the edges $\pm\Delta$ are accumulation points. These facts suggest that electrons can be captured by a dipole potential in graphene, and strain can be used to tune the strength of confinement and to promote or inhibit atomic collapse.

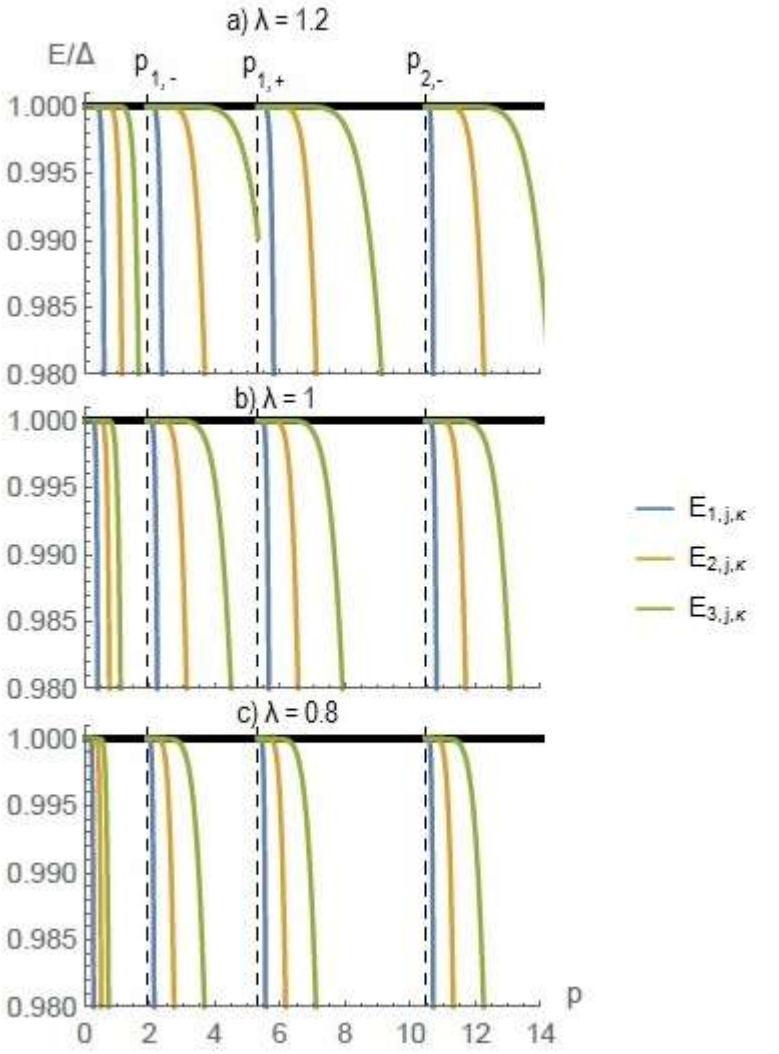

Figure 6.3: Energy of the first electron bound states with respect to the electric dipole moment for different values: a) $\lambda = 1.2$, b) $\lambda = 1.0$, and c) $\lambda = 0.8$. It can be noted the appearance of towers of bound states for each value of the dipole moment $p_{j,\kappa}$. These energy towers decay for higher values of p for $\lambda > 1$, as shown in a), and for lower values of p for $\lambda < 1$, as shown in c).

Chapter 7

Discussion and conclusions

In this thesis we have addressed the problem of atomic collapse of a charged center in graphene immersed in an homogeneous external magnetic field, and under the effects of uniaxial strain. For that purpose, we have extensively reviewed some basics of graphene physics, starting from the electronic and crystallographic properties of the material, going through the Landau problem, and finishing with the effects of lattice strain in its properties.

The hexagonal structure of graphene (and in fact, a full variety of different physical systems) makes of this wonder material an exceptional candidate for technological applications and fundamental Physics research. One of the most remarkable features is that in this material, charge excitations behave as massless Dirac fermions. This is the cornerstone of the thesis.

For the Landau problem, we solved the corresponding Dirac equation. We used the Landau and Symmetric gauges, the minimal coupling of the magnetic vector potential, and the approximation of the tensor Fermi velocity describing strain. This approximation represent the fact that the strain is seen as a renormalization of the Fermi velocity.

We then addressed the problem of graphene in the potential of a Coulomb impurity analytically. We approximate the Coulomb potential by a potential well. We obtained the corresponding wave functions of the system, finding them to be written in terms of Whittaker functions. In addition, the boundary conditions in the border of the potential well dictate a valley-dependent transcendental expression for energy, where again the effects of strain are those of renormalize the Fermi velocity.

In absence of a potential well, we recover the well-known degenerate Landau lev-

els in graphene. This degeneracy is lifted when considering a non-zero potential well, obtaining different energy levels for each value of the angular momentum j, where in the case of graphene $\mathbf{J} = J_z$.

Neglecting the influence of an external magnetic field, we found a splitting of the energy spectrum in two branches, a continuous one for $|E| > \Delta$, and other formed by discrete levels for $|E| < \Delta$, indicating the presence of bound states, as expected by the presence of the potential well. For the case of the first centrifugal barrier of angular momentum ($j = -1/2$), we found that, if the Landau levels suffers an "effective" compression ($\lambda < 1$), the energy decays and reaches its minimum quickly, namely, the critical value of the potential required for collapse is lower, whereas, for an effective expansion ($\lambda > 1$), the scenario of collapse is inhibited. This indicates a displacement of the centrifugal barrier of angular momentum produced by strain. The critical value $V_{0,cr}$, in which the first bound state energy dives into the lower continuum branch, is found to be also dependent of the effective strain magnitude λ, growing for values $\lambda > 1$ and decreasing for values $\lambda < 1$. This tells us again that strain promotes or inhibits atomic collapse in graphene. For realistic samples, the graphene lattice is able to sustain expansions of 25% of the interatomic distance before bond-breaking, and compressions of only 1% before it starts to bend [87], being able to feel more intensely the effects of retardation than those of acceleration of collapse in graphene.

When we turn-on an external magnetic field, it acts as an atomic collapse catalyst as it reduces the value of $V_{0,cr}$, but additionally, just as in the last case of zero-magnetic field, the effective strain magnitude λ plays a role in promoting or inhibiting collapse. Thus, atomic collapse become dependent of both effects, magnetic and strain. Also, it was found that in the case of zero mass gap ($\Delta = 0$), the value of $V_{0,cr}$ goes to zero in all the cases (for all λ), indicating that, for gapless quasiparticles, atomic collapse is present for arbitrary values of Ze and λ.

When considering the case of a charged impurity in graphene under triaxial strain (or any strain producing a non-zero *pseudo-magnetic* field), even though modelling the system by a tensor Fermi velocity would be too difficult, qualitatively we found that, on the one hand, the presence of the *pseudo-magnetic* field leads to the decrease of $V_{0,cr}$, accelerating atomic collapse, but, on the other hand, the effective strain magnitude "interferes" constructively or destructively to collapse. An important conclusion is thus that, as the *pseudo-magnetic* field acts in opposite direction in each Dirac valley K, K', it could be possible to control the dynamics of the quasiparticles independently in each valley by both, the application of an external magnetic field, and by controlling the effective strain magnitude. This mix would lead to conform *Straintronics* and *Valleytronics* into a more specialized field.

In the case of the punctual electric dipole in graphene under strain, it was found that the strain has the same effect in the electron-holes bound states as in the single-impurity problem, that is, to promote or inhibit the decay of these states depending on the strain strength λ. This result strengthens the idea that the effect of strain in atomic collapse is that it renormalizes the Fermi velocity.

As a general conclusion, electronic and magnetic properties of graphene can be controlled through application of magnetic fields (as expected), and through lattice strains, leading to the possible application of graphene as a semiconductor, or even as a circuit itself. This is because the effects of strain can be accounted for by a proper redefinition (renormalization) of the Fermi velocity.

Research on graphene is still recent, and exist hope on a technological revolution based on it. As a future work, we are interested in studying the dynamics of the charge carriers in pure and impurity-doped graphene (monolayer and bilayer) with the aid of Magnetohydrodynamics.

Appendix A

Dirac equation

As we previously discussed in Chapter 2, the low-energy Hamiltonian which describes the electronic properties of the charge carriers in graphene can be approximated near the Dirac points $\mathbf{K}$ and $\mathbf{K}'$ as Eq. (2.15)

$$\hat{H}_{\mathbf{K},\mathbf{K}'} = \hbar v_F \boldsymbol{\sigma} \cdot \mathbf{q}, \tag{A.1}$$

which has the form of a Dirac equation describing relativistic massless fermions. This Appendix is specially devoted to give a brief introduction to Relativistic Quantum Mechanics (RQM), directed to the study of graphene.

We start with an historical review of the elaboration of RQM in the late 20ies of the last century. Then, we focus on the Dirac equation, particularly in the two-dimensional case (two space and one time dimensions), which is important in the case of graphene, deriving some of its properties. Finally, a brief introduction to chirality is presented[1].

A.1 Relativistic quantum mechanics

High energy systems are those in which the particles acquire very high velocities, close to c. So, it is required a relativistic wave equation to describe its quantum dynamics. The new wave equation is required to satisfy both, quantum mechanics and special relativity postulates. In particular, it has to satisfy:

a) The equation has to be invariant under Lorentz transformations.

[1]The discussion about RQM and the Klein-Gordon equation is followed from [65]. On the other hand, the discussion about the Dirac equation in (3+1) and (2+1) dimensions is based on [24, 65], with some historical notes followed from [101]. Finally, The chirality discussion is based on [24].

b) Spatial and temporal coordinates have to be treated equally. From this assumption we immediately see that Schrödinger equation, whose temporal and spatial derivatives are of different order, cannot describe relativistic systems.

c) The Heisenberg uncertainty principle:

$$\Delta x \Delta p > \hbar \Rightarrow \Delta x > \frac{\hbar}{m_0 c}, \tag{A.2}$$

tells us that a relativistic particle cannot be localized more accurately than $\approx \hbar/m_0 c$, otherwise pair creation takes place. Thus, the idea of a free particle only makes sense for particles which are not confined to volumes smaller than approximately the Compton wavelength $\lambda_c = \hbar/m_0 c$. Furthermore, the time is also uncertain since

$$\Delta t \sim \frac{\Delta x}{c} > \frac{\hbar}{m_0 c^2}. \tag{A.3}$$

Therefore, we recognize the necessity to reconsider the concept of probability density, $\rho(\mathbf{r}, t)$, which describes the probability of finding a particle at a definite place $\mathbf{r}$ at a fixed time t. This problem does not occur in the non-relativistic case, where $c \to \infty$, having arbitrarily small values of Δt.

d) At high energies, pair creation (particle-antiparticle pair) and annihilation process occur. In consequence, the particle conservation assumption is no longer valid.

A.2 The Klein-Gordon equation

The first efforts to obtain an equation satisfying these assumptions were made independently by Schrödinger, Klein and Gordon in 1926/27 [92, 93, 94]. They departed from in the relativistic dispersion relation

$$p^2 = \frac{E^2}{c^2} - \mathbf{p}^2 = m_0^2 c^2, \tag{A.4}$$

with $p^\mu = \left(\frac{E}{c}, \mathbf{p}\right)$ is the four-momentum. Replacing this four-momentum by its respective four-momentum operator in Hilbert space:

$$\begin{aligned} \hat{p}^\mu &= i\hbar \left\{ \frac{\partial}{\partial(ct)}, -\frac{\partial}{\partial x}, -\frac{\partial}{\partial y}, -\frac{\partial}{\partial z} \right\} \\ &= i\hbar \left\{ \frac{\partial}{\partial(ct)}, -\nabla \right\} = \left\{ \hat{p}_0, \hat{\mathbf{p}} \right\}, \end{aligned} \tag{A.5}$$

we obtain the Klein-Gordon equation for free particles

$$\hat{p}^\mu \hat{p}_\mu \psi = m_0^2 c^2 \psi, \tag{A.6}$$

where m_0 is the rest mass of the particle and c the speed of light in vacuum. This equation can be brought to the form:

$$\left(\frac{1}{c^2}\frac{\partial^2}{\partial t^2} - \frac{\partial^2}{\partial x^2} - \frac{\partial^2}{\partial y^2} - \frac{\partial^2}{\partial z^2} + \frac{m_0^2 c^2}{\hbar^2}\right)\psi = \left(\Box + \frac{m_0^2 c^2}{\hbar^2}\right)\psi = 0, \tag{A.7}$$

where the d'Alambertian operator $\Box = \frac{1}{c^2}\frac{\partial^2}{\partial t^2} - \frac{\partial^2}{\partial x^2} - \frac{\partial^2}{\partial y^2} - \frac{\partial^2}{\partial z^2}$ is defined. It can be inferred immediately from Eq. (A.6) the Lorentz covariance of the Klein-Gordon equation, as $\hat{p}^\mu \hat{p}_\mu$ is Lorentz invariant. In addition, Eq. (A.7) can be recognized as the classical wave equation including the mass term, whose solutions are

$$\psi = \exp\left[-\frac{\mathrm{i}}{\hbar}(\mathrm{p_0 x^0} - \mathbf{p}\cdot\mathbf{r})\right] = \exp\left[\frac{\mathrm{i}}{\hbar}(\mathbf{p}\cdot\mathbf{r} - Et)\right]. \tag{A.8}$$

Substituting this solution in Eq. (A.6) we recover the dispersion relation

$$\frac{E^2}{c^2} - \mathbf{p}^2 = m_0^2 c^2 \Rightarrow E = \pm\sqrt{m_0^2 c^4 + \mathbf{p}^2 c^2}. \tag{A.9}$$

Therefore, there exist solutions for both positive and negative energies. This unexpected behavior of the spectrum represented a severe problem to the quantum theory in that time, as the ground state may not be correctly defined for an energy spectrum with no lower bound. In principle, a particle in a higher level of energy would "fall" to one of lower energy by the emission of a photon with energy given by the difference in energy between the initial and final states, but without a lower bound, this process would occur infinitely. This "problem" represented an important advance in the field, when it was cleverly interpreted.

Another problem of the Klein-Gordon equation is related to its second order time derivative. To illustrate this point let us construct the four-current connected with Eq. (A.7). Multiplying Eq. (A.7) for the left by ψ^*

$$\psi^*\left[\Box + \left(\frac{m_0 c}{\hbar}\right)\right]\psi = 0. \tag{A.10}$$

Then, taken the complex conjugate of Eq. (A.7) and multiplying for the left by ψ

$$\psi\left[\Box + \left(\frac{m_0 c}{\hbar}\right)\right]\psi^* = 0. \tag{A.11}$$

Subtracting Eq. (A.10) - (A.11), we get

$$\psi^*\Box\psi - \psi\Box\psi^* = 0 \Rightarrow \partial_\mu\left(\psi^*\partial^\mu\psi - \psi\partial^\mu\psi^*\right) \equiv \partial_\mu j^\mu = 0, \tag{A.12}$$

where we have used the covariant and contravariant definitions of the four-gradient

$$\partial^\mu = \left(\frac{\partial}{\partial ct}, \frac{\partial}{\partial x}, \frac{\partial}{\partial y}, \frac{\partial}{\partial z}\right), \tag{A.13}$$

$$\partial_\mu = \left(\frac{\partial}{\partial ct}, -\frac{\partial}{\partial x}, -\frac{\partial}{\partial y}, -\frac{\partial}{\partial z} \right), \tag{A.14}$$

and where we defined the four-current

$$j_\mu \equiv (\rho, \mathbf{j}) = \frac{i\hbar}{2m_0} \left(\psi^* \partial_\mu \psi - \psi \partial_\mu \psi^* \right). \tag{A.15}$$

Explicitly, Eq. (A.12) has the form

$$\frac{\partial}{\partial t} \left[\frac{i\hbar}{2m_0 c^2} \left(\psi^* \frac{\partial \psi}{\partial t} - \psi \frac{\partial \psi^*}{\partial t} \right) \right] + \nabla \cdot \left[-\frac{i\hbar}{2m_0} \left(\psi^* \nabla \psi - \psi \nabla \psi^* \right) \right] = 0, \tag{A.16}$$

which has the form of a continuity equation

$$\frac{\partial}{\partial t} \rho + \nabla \cdot \mathbf{j} = 0, \tag{A.17}$$

with the probability density ρ given by

$$\rho(\mathbf{r}, t) = \frac{i\hbar}{2m_0 c^2} \left(\psi^* \frac{\partial \psi}{\partial t} - \psi \frac{\partial \psi^*}{\partial t} \right). \tag{A.18}$$

Therefore, as the Klein-Gordon equation is of second order in the time derivative, at a given time t, both ψ and $\frac{\partial \psi}{\partial t}$ may have arbitrary values, so that, $\rho(\mathbf{r}, t)$ may be either positive or negative, and thus cannot be interpreted as a probability density. This is the deeper reason to consider the Klein-Gordon equation to be physically senseless. Then, it was required to seek a relativistic wave equation of first order in time.

A.3 The Dirac equation

After the problems with the Klein-Gordon equation, in 1928 Dirac was looking forward to develop a wave equation of the Schrödinger form [95]

$$i\hbar \frac{\partial \psi}{\partial t} = \hat{H} \psi, \tag{A.19}$$

with positive definite probability density. Dirac understood that, in order to satisfy the Lorentz invariance, it has to be constructed an equation which were linear in time-derivatives, and at the same time linear is space-derivatives. So that, the desired equation has to be of the form

$$i\hbar \frac{\partial \Psi}{\partial t} = \left[\frac{\hbar c}{i} \left(\hat{\alpha}_1 \frac{\partial}{\partial x^1} + \hat{\alpha}_2 \frac{\partial}{\partial x^2} \hat{\alpha}_3 \frac{\partial}{\partial x^3} \right) + \hat{\beta} m_0 c^2 \right] \Psi \equiv \hat{H}_D \Psi, \tag{A.20}$$

where $\hat{H}_D$ can be expressed as

$$\hat{H}_D = \frac{\hbar c}{i}\hat{\alpha}\cdot\nabla + \hat{\beta}m_0c^2. \tag{A.21}$$

From equation (A.20), the next conditions have to be satisfied:

1. The objects $\hat{\beta}$, and $\hat{\alpha} = (\hat{\alpha}_1, \hat{\alpha}_2, \hat{\alpha}_3)$ are dimensionless, and, in order to satisfy spatial rotation invariance, they cannot be simple numbers. Actually, they have to be matrices, and therefore, $\hat{H}_D$ is a $n \times n$ matrix.

2. Then, Ψ cannot be a simple scalar function, but has to be a column vector

$$\Psi = \begin{pmatrix} \psi_1 \\ \psi_2 \\ . \\ . \\ . \\ \psi_n \end{pmatrix}. \tag{A.22}$$

3. The probability density is positive definite

$$\rho(x) = \Psi^\dagger\Psi = (\psi_1^*, ..., \psi_n^*)\begin{pmatrix} \psi_1 \\ . \\ . \\ . \\ \psi_n \end{pmatrix} = \sum_i \psi_i^*\psi_i, \tag{A.23}$$

   and it is the temporal component of a conserved four-current $j^\mu = (\rho, \mathbf{j})$, such that the continuity equation is satisfied

$$\partial_\mu j^\mu = 0 \Rightarrow i\hbar\frac{\partial}{\partial t}(\Psi^\dagger\Psi) = \frac{\hbar c}{i}\nabla\cdot(\Psi^\dagger\alpha\Psi), \tag{A.24}$$

   with $\rho = \Psi^\dagger\Psi$ and $\mathbf{j} = \Psi^\dagger\alpha\Psi$.

In order to satisfy the relativistic dispersion relation given by Eq. (A.4), from the square of Eq. (A.20) expressed in components

$$-\hbar^2\frac{\partial^2\psi_\sigma}{\partial t^2} = -\hbar c^2\frac{\alpha_i\alpha_j + \alpha_j\alpha_i}{2}\frac{\partial^2\psi_\sigma}{\partial x^i\partial x^j} + \frac{\hbar m_0c^3}{i}\frac{\alpha_i\beta + \beta\alpha_i}{2}\frac{\partial\psi_\sigma}{\partial x^i} + \beta^2m_0^2c^4\psi_\sigma, \tag{A.25}$$

the next relations are required:

(i) $\alpha_i\alpha_j + \alpha_j\alpha_i = \{\alpha_i, \alpha_j\} = 2\delta_{ij}$, where δ_{ij} is the Kronecker delta.

(ii) $\alpha_i\beta + \beta\alpha_i = \{\alpha_i, \beta\} = 0$.

(iii) $\alpha_i^2 = \beta^2 = \mathbf{I}$, where $\mathbf{I}$ represents the $n \times n$ identity matrix. So that, the eigenvalues of these matrices are always ± 1.

(iv) To accomplish the hermiticity of the hamiltonian, the matrices α_i and β have to be hermitian, and also from condition (ii), they have to be unitary

$$\alpha_i = \alpha_i^\dagger = \alpha_i^{-1} \quad \text{and} \quad \beta = \beta^\dagger = \beta^{-1} \ .$$

(v) By using the trace property $tr[AB] = tr[BA]$ in condition (ii):

$$tr[\alpha_i\beta] = tr[-\beta\alpha_i] \Rightarrow tr[\beta\alpha_i\beta] = tr[\beta^2\alpha_i] = tr[\alpha_i] = tr[-\beta^2\alpha_i] = -tr[\alpha_i]$$

$$\Rightarrow tr[\alpha_i] = 0 = tr[\beta] \ .$$

Thus, they are null-trace matrices, and, as their eigenvalues are only ± 1, it is immediately seen that their dimension n must be pair.

Conditions (i), (ii), and (iii) define the so-called *Clifford* algebra.

In the $(3+1)$ dimensional case, the minimal dimension of the matrices α_i and β is 4. One may satisfy the Clifford algebra by choosing, e.g., the so-called standard representation

$$\beta = \begin{pmatrix} \mathbf{I} & 0 \\ 0 & -\mathbf{I} \end{pmatrix} \quad \text{and} \quad \alpha_i = \begin{pmatrix} 0 & \sigma_i \\ \sigma_i & 0 \end{pmatrix}, \tag{A.26}$$

where the σ_i matrices are the well-known Pauli matrices

$$\sigma_1 = \begin{pmatrix} 0 & 1 \\ 1 & 0 \end{pmatrix}, \quad \sigma_2 = \begin{pmatrix} 0 & -i \\ i & 0 \end{pmatrix}, \quad \sigma_3 = \begin{pmatrix} 1 & 0 \\ 0 & -1 \end{pmatrix}. \tag{A.27}$$

As a consequence, the Dirac Hamiltonian has a matrix structure

$$H_D^{3D} = \begin{pmatrix} m_0c^2 & c\mathbf{p}\cdot\boldsymbol{\sigma} \\ c\mathbf{p}\cdot\boldsymbol{\sigma} & -m_0c^2 \end{pmatrix}, \tag{A.28}$$

and the quantum state must be represented by the *four-spinor* $\Psi = \begin{pmatrix} \psi_1 \\ \psi_2 \\ \psi_3 \\ \psi_4 \end{pmatrix}$. If we represent it as formed by two two-spinors $\Psi = \begin{pmatrix} \phi \\ \xi \end{pmatrix}$, with $\phi = \begin{pmatrix} \phi_1 \\ \phi_2 \end{pmatrix}$ and $\xi = \begin{pmatrix} \xi_1 \\ \xi_2 \end{pmatrix}$, considering a particle in rest, we have the Dirac equation

$$\begin{pmatrix} m_0c^2 & 0 \\ 0 & -m_0c^2 \end{pmatrix} \begin{pmatrix} \phi \\ \xi \end{pmatrix} = E \begin{pmatrix} \phi \\ \xi \end{pmatrix}. \tag{A.29}$$

This equation has four solutions: Two with positive energy $E = m_0c^2$ corresponding to the components of the two-spinor ϕ, and which are related to the particle components of the four-spinor Ψ; the other two solutions, which possess a negative energy value $E = -m_0c^2$, correspond to the components of the two-spinor ξ, related to the antiparticle components of the four-spinor Ψ. This interpretation of the ξ components as antiparticles was proposed by the first time by Dirac in 1931 [96], after Oppenheimer and Tamm argued that electron-proton annihilation in atoms would not be consistent with the stability of ordinary matter [97], breaking down the idea that the ξ components were related to protons, as was first thought by Dirac [98]. The existance of antiparticles was confirmed in 1932, when Anderson discovered the positron [99].

Furthermore, the components ϕ_1, ϕ_2 and ξ_1, ξ_2 of the two-spinors ϕ and ξ, respectively, correspond to both different possible spin states of the particle [100, 101].

By introducing the notation of the Dirac matrices γ^μ

$$\gamma^0 = \beta \ , \quad \gamma^i = \beta\alpha^i \quad \text{and} \quad \{\gamma^\mu, \gamma^\nu\} = 2g^{\mu\nu}, \tag{A.30}$$

and the Feynman "slash" notation

$$\not{a} = a_\mu \gamma^\mu, \tag{A.31}$$

we get the usually found covariant form of the Dirac equation[2]

$$(i\not{\partial} - m_0)\Psi = 0. \tag{A.32}$$

A.3.1 (2+1) dimensional Dirac equation

In the $(2 + 1)$ dimensional case, which is of interest in the case of graphene, the Clifford algebra is satisfied by the identification of the α_i and β matrices with the Pauli matrices

$$\alpha_1 = \sigma_1, \quad \alpha_2 = \sigma_2, \quad \beta = \sigma_3, \tag{A.33}$$

so, the $(2 + 1)$ Dirac equation for massless particles can be written as

$$H_D^{2D} = c\sigma \cdot \mathbf{p}, \tag{A.34}$$

which, by the identification of c with the Fermi velocity v_F, has the same form as the Hamiltonian describing graphene, obtained in Chapter 2.

[2]The K-G equation is obtained by multiplying Eq. (A.32) by $(i\not{\partial} + m_0)$.

If we consider the $(2+1)$ Dirac equation for $m \neq 0$, it can be rewritten in the form

$$H_D^{2D} = \epsilon \begin{pmatrix} \cos\beta & \sin\beta\ e^{-i\phi_{\mathbf{p}}} \\ \sin\beta\ e^{i\phi_{\mathbf{p}}} & -\cos\beta \end{pmatrix}, \tag{A.35}$$

where we have defined the quantities

$$\epsilon = \sqrt{m_0^2 + \mathbf{p}^2},\ \cos\beta = \frac{m_0}{\epsilon},\ \sin\beta = \frac{|\mathbf{p}|}{\epsilon},\ \phi_{\mathbf{p}} = \arctan\left(\frac{p_y}{p_x}\right), \tag{A.36}$$

where additionally, we have taken the values $\hbar = c = 1$. The matrix in the right side of Eq. (A.35) is a unitary matrix, whose eigenvalues are $\lambda = \pm 1$, corresponding to the positive and negative energy states found earlier $E^\lambda = \lambda E = \lambda\sqrt{m_0^2 + \mathbf{p}^2}$.

A.3.2 Chirality

In high-energy physics it is defined the *helicity* [100, 101] of a particle as the projection of its spin onto the direction of propagation

$$h_{\mathbf{p}} = \frac{\mathbf{p} \cdot \boldsymbol{\sigma}}{|\mathbf{p}|}. \tag{A.37}$$

It is an hermitian and unitary operator with eigenvalues $\eta = \pm 1$:

$$h_{\mathbf{p}} \left|\eta = \pm 1\right\rangle = \pm \left|\eta = \pm 1\right\rangle. \tag{A.38}$$

In this case, σ describes the real physical spin of the particle. In absence of a particle mass m_0, the helicity operator $h_{\mathbf{p}}$ commutes with the Dirac hamiltonian, and it is therefore a good quantum number.

In the case of graphene, the Pauli matrices no longer describe the real spin, but the sublattice isospin. In this case the helicity operator is called *chirality* operator.

The $(2+1)$ Dirac hamiltonian for graphene can be rewritten in terms of the chirality operator as

$$H_D^{2D} = |\mathbf{p}| h_{\mathbf{p}}\ , \quad H_D^{2D,\xi} = \xi H_D^{2D} = \xi |\mathbf{p}| h_{\mathbf{p}}\ , \tag{A.39}$$

where ξ refers to the two-fold *valley isospin degeneracy* ($\xi = \pm$). Then, the band index λ, which describes the valence and the conduction bands, is entirely determined by the chirality and the valley isospin

$$\lambda = \xi\eta\ . \tag{A.40}$$

This expression can be graphically seen in Fig. A.1, where the valence and conduction bands for each valley ($\mathbf{K}$ and $\mathbf{K}'$) are shown, and define the chirality of the particles in them.

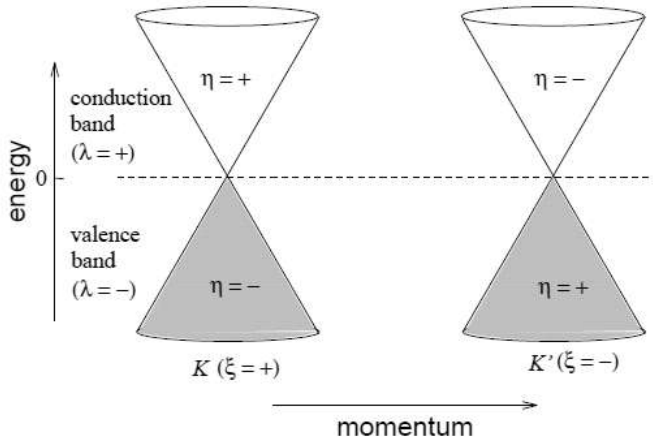

Figure A.1: Relation between the band index λ, valley isospin ξ, and chirality η. Image adapted from [24].

Appendix B

Landau levels in the symmetric gauge

In this appendix, we show in detail the computation of the Landau levels for the non-relativistic and the graphene cases (Eqs. (3.18), (3.29) and (3.30)).

B.1 Non-relativistic Landau levels for the Symmetric gauge

In this case $\mathbf{A}$ is given in Eq.(3.5). So, the Hamiltonian is

$$\begin{aligned} H &= \frac{1}{2M}\left[\left(p_x - \frac{eB_0}{2c}y\right)^2 + \left(p_y + \frac{eB_0}{2c}x\right)^2\right] \\ &= \frac{1}{2M}\left[p_x^2 + p_y^2 - \frac{eB_0}{2c}\left(p_x y - y p_x\right) + \frac{eB_0}{2c}\left(p_y x - x p_y\right) + \frac{e^2B_0^2}{4c^2}\left(x^2+y^2\right)\right]. \end{aligned} \quad \text{(B.1)}$$

Since $[p_i, x_j] = 0$ for $i \neq j$

$$H = \frac{p_x^2}{2M} + \frac{p_y^2}{2M} + \frac{eB_0}{2Mc}\left(x p_y - y p_x\right) + \frac{e^2B_0^2}{8Mc^2}\left(x^2+y^2\right), \quad \text{(B.2)}$$

and, by using the definition of the z-component of the angular momentum $\hat{L}_z = \hat{x}\hat{p}_y - \hat{y}\hat{p}_x$, and $\omega_B = \dfrac{eB_0}{M}$ is the cyclotron frequency introduced in Chapter 3, we have

$$\begin{aligned} H &= \frac{p_x^2}{2M} + \frac{p_y^2}{2M} + \frac{\omega}{2}\mathrm{L}_z + \frac{M\omega^2}{8}\left(x^2+y^2\right) \\ \Rightarrow \hat{H}\psi(x,y) &= \left[\frac{\hat{p}_x^2}{2M} + \frac{\hat{p}_y^2}{2M} + \frac{\omega}{2}\hat{L}_z + \frac{M\omega^2}{8}\left(\hat{x}^2+\hat{y}^2\right)\right]\Psi(x,y) = E\Psi(x,y), \end{aligned} \quad \text{(B.3)}$$

and, using that $\hat{p}_i = \dfrac{\hbar}{i}\dfrac{\partial}{\partial x_i}$

$$\left[-\frac{\hbar^2}{2M}\left(\frac{\partial^2}{\partial x^2}+\frac{\partial^2}{\partial y^2}\right)+\frac{\omega}{2}\hat{L}_z+\frac{M\omega^2}{8}\left(x^2+y^2\right)\right]\psi(x,y)=E\psi(x,y). \tag{B.4}$$

For the sake of simplicity, it is better to use cilindrical coordinates

$$\begin{cases} x=\rho\,\cos\theta \\ y=\rho\,\sin\theta \quad \Rightarrow x^2+y^2=\rho^2, \\ z=z \end{cases}$$

for which the Laplacian operator is written

$$\nabla^2=\frac{1}{\rho}\frac{\partial}{\partial\rho}\left(\rho\frac{\partial}{\partial\rho}\right)+\frac{1}{\rho^2}\frac{\partial^2}{\partial\theta^2}. \tag{B.5}$$

So, Eq. (B.4) is written as

$$-\frac{\hbar^2}{2M}\left[\frac{1}{\rho}\frac{\partial}{\partial\rho}\left(\rho\frac{\partial\psi(\rho,\theta)}{\partial\rho}\right)+\frac{1}{\rho^2}\frac{\partial^2\psi(\rho,\theta)}{\partial\theta^2}\right]+\frac{\omega}{2}\hat{L}_z\psi(\rho,\theta)+\frac{M\omega^2}{8}\rho^2\psi(\rho,\theta)=E\psi(\rho,\theta). \tag{B.6}$$

Also, we know that the $\hat{L}_z$ operator in the position representation is given by

$$\hat{L}_z=-i\hbar\frac{\partial}{\partial\theta}\Rightarrow\hat{L}_z^2=-\hbar^2\frac{\partial^2}{\partial\theta^2}. \tag{B.7}$$

Thus, using this operator, we rewrite Eq. (B.6) as

$$-\frac{\hbar^2}{2M}\left[\frac{1}{\rho}\frac{\partial}{\partial\rho}\left(\rho\frac{\partial\psi(\rho,\theta)}{\partial\rho}\right)+\frac{1}{\rho^2}\frac{\partial^2\psi(\rho,\theta)}{\partial\theta^2}\right]-\frac{i\hbar\omega}{2}\frac{\partial\psi(\rho,\theta)}{\partial\theta}+\frac{M\omega^2}{8}\rho^2\psi(\rho,\theta)=E\psi(\rho,\theta). \tag{B.8}$$

Thus, the function $\psi(\rho,\theta)$ has to be an eigenfunction of the $\hat{L}_z$ operator

$$\hat{L}_z\psi(\rho,\theta)=\hbar m\psi(\rho,\theta)\Rightarrow\psi(\rho,\theta)=e^{im\theta}R(\rho), \tag{B.9}$$

and we only have a radial equation to solve. It has the form

$$-\frac{\hbar^2}{2M}\left[\frac{1}{\rho}\frac{dR(\rho)}{d\rho}+\frac{d^2R(\rho)}{d\rho^2}-\frac{m^2}{\rho^2}R(\rho)\right]+\frac{\hbar m\omega}{2}R(\rho)+\frac{M\omega^2}{8}\rho^2R(\rho)=ER(\rho)$$

$$\Rightarrow\frac{d^2R(\rho)}{d\rho^2}+\frac{1}{\rho}\frac{dR(\rho)}{d\rho}+\left[\frac{2ME}{\hbar^2}-\frac{m^2}{\rho^2}-\frac{Mm\omega}{\hbar}-\frac{M^2\omega^2}{4\hbar^2}\rho^2\right]R(\rho)=0. \tag{B.10}$$

We now introduce the change of variable $\xi = \frac{M\omega}{2\hbar}\rho^2 \Rightarrow d\xi = \frac{M\omega}{\hbar}\rho d\rho$, so, Eq. (B.10) takes the form

$$\xi R'' + R' + \left[\beta - \frac{m^2}{4\xi} - \frac{\xi}{4}\right] R = 0, \tag{B.11}$$

where $R' = \frac{dR}{d\xi}$ and $\beta = \frac{E}{\hbar\omega} - \frac{m}{2}$.
Let us write the function $R(\xi)$ as

$$R(\xi) = \xi^{-1/2} y(\xi) \Rightarrow \begin{cases} R' = y'(\xi)\xi^{-1/2} - \frac{1}{2} y(\xi)\xi^{-3/2} \ , \\ R'' = y''(\xi)\xi^{-1/2} - y'(\xi)\xi^{-3/2} + \frac{3}{4} y(\xi)\xi^{-5/2} \ . \end{cases}$$

Substituting this in Eq. (B.11) we have

$$\begin{aligned} & y''(\xi)\xi^{1/2} + \frac{1}{4} y(\xi)\xi^{-3/2} + \left[\beta - \frac{m^2}{4\xi} - \frac{\xi}{4}\right] \xi^{-1/2} y(\xi) = 0, \\ \Rightarrow\ & y''(\xi) + \frac{1}{4} y(\xi)\xi^{-2} + \left[\beta - \frac{m^2}{4\xi} - \frac{\xi}{4}\right] \xi^{-1} y(\xi) = 0, \\ \Rightarrow\ & y''(\xi) + \left[\frac{-1}{4} + \frac{\beta}{\xi} + \frac{\frac{1}{4} - \frac{m^2}{4}}{\xi^2}\right] y(\xi) = 0, \end{aligned} \tag{B.12}$$

which is a Whittaker equation, with solutions

$$y(\xi) = A e^{-\xi/2} \xi^{|m|/2} M\left(\frac{|m|}{2} + \frac{1}{2} - \beta, |m| + 1; \xi\right), \tag{B.13}$$

where A is a normalization constant and M is the function which is solution of the confluent-hypergeometric equation. Using the relation between M and the associated Laguerre Polinomials

$$M(-n, \alpha + 1, x) = \frac{n!\alpha!}{(n+\alpha)!} L_n^\alpha(x), \tag{B.14}$$

and recalling that $R(\xi) = \xi^{-1/2} y(\xi)$, we obtain the solution for $R(\xi)$

$$R(\xi) = A \frac{n_\rho! |m|!}{(n_\rho + |m|)!} e^{-\xi/2} \xi^{|m|/2} L_{n_\rho}^{|m|}(\xi), \tag{B.15}$$

where

$$n_\rho = \frac{E}{\hbar\omega_B} - \frac{m}{2} - \frac{|m|}{2} - \frac{1}{2}. \tag{B.16}$$

The constant A is obtained from the relation

$$\int_0^\infty \rho d\rho |R|^2 = 1. \tag{B.17}$$

So, with $\xi = \frac{M\omega_B}{2\hbar}\rho^2 = \frac{\rho^2}{2a_B^2} \Rightarrow d\xi = \frac{M\omega_B}{\hbar}\rho d\rho = \frac{\rho d\rho}{a_B^2}$, where $a_B = \sqrt{\frac{\hbar}{M\omega_B}} = \sqrt{\frac{\hbar}{eB_0}}$ is the Larmor radius, we have

$$\int_0^\infty \left(\frac{n_\rho!|m|!}{(n_\rho+|m|)!}\right)^2 |A|^2 e^{-\xi}\xi^{|m|}\left(L_{n_\rho}^{|m|}(\xi)\right)^2 a_B^2 dx = 1,$$

$$\Rightarrow \left(\frac{n_\rho!|m|!}{(n_\rho+|m|)!}\right)^2 |A|^2 a_B^2 \int_0^\infty e^{-\xi}\xi^{|m|}\left(L_{n_\rho}^{|m|}(\xi)\right)^2 dx = 1.$$

Using the ortogonalization relation of the associated Laguerre Polinomials [35]

$$\int_0^\infty e^{-x}x^m L_n^m(x)L_{n'}^m(x)dx = \frac{(n+m)!}{n!}\delta_{n,n'}, \tag{B.18}$$

we have

$$\left(\frac{n_\rho!|m|!}{(n_\rho+|m|)!}\right)^2 |A|^2 a_B^2 \frac{(n_\rho+|m|)!}{n_\rho!} = |A|^2 \frac{n_\rho!(|m|!)^2}{(n_\rho+|m|)!}a_B^2 m = 1,$$

$$\Rightarrow A = \frac{1}{a_B|m|!}\sqrt{\frac{(n_\rho+|m|)!}{n_\rho!}}. \tag{B.19}$$

Hence, collecting all results we have

$$R(\rho) = \frac{n_\rho!}{(n_\rho+|m|)!}\frac{1}{a_B^{|m|+1}}\sqrt{\frac{(n_\rho+|m|)!}{2^{|m|}n_\rho!}}e^{-\rho^2/4a_B^2}\rho^{|m|}L_{n_\rho}^{|m|}\left(\frac{\rho^2}{2a_B^2}\right), \tag{B.20}$$

and, finally we have the normalized wave function of the system

$$\Psi(r,\theta,z) = e^{ik_z z}\frac{e^{im\theta}}{\sqrt{2\pi}}\frac{n_\rho!}{(n_\rho+|m|)!}\frac{1}{a_B^{|m|+1}}\sqrt{\frac{(n_\rho+|m|)!}{2^{|m|}n_\rho!}}e^{-\rho^2/4a_B^2}\rho^{|m|}L_{n_\rho}^{|m|}(\frac{\rho^2}{2a_B^2}). \tag{B.21}$$

The energy spectrum comes from Eq. (B.16)

$$E_n = \hbar\omega_B\left(n_\rho + \frac{|m|}{2} + \frac{m}{2} + \frac{1}{2}\right). \tag{B.22}$$

B.2 Landau levels in graphene for the Symmetric gauge

In this case $\mathbf{A} = \frac{B_0}{2}(-y, x, 0)$. Thus

$$\pi_x = p_x - \frac{eB_0}{2}y, \quad \pi_y = p_y + \frac{eB_0}{2}x, \tag{B.23}$$

and

$$[\hat{\pi}_x, \hat{\pi}_y] = \left[\hat{p}_x - \frac{eB_0}{2}\hat{y}, \hat{p}_y + \frac{eB_0}{2}\hat{x}\right] = \frac{eB_0}{2}\left([\hat{p}_x, \hat{x}] + [\hat{p}_y, \hat{y}]\right) = -ieB_0, \tag{B.24}$$

where the relations $[\hat{p}_i, \hat{p}_j] = 0 = [\hat{x}_i, \hat{x}_j]$ and $[p_i, x_j] = -i\delta_{ij}$ where used. Substituting these results in Eqs. (3.21) and (3.22) we have

$$\left[\left(\hat{p}_x - \frac{eB_0}{2}\hat{y}\right)^2 + \left(\hat{p}_y + \frac{eB_0}{2}\hat{x}\right)^2\right]\Psi_A = \left(E^2 - eB_0\right)\Psi_A, \tag{B.25}$$

and

$$\left[\left(\hat{p}_x - \frac{eB_0}{2}\hat{y}\right)^2 + \left(\hat{p}_y + \frac{eB_0}{2}\hat{x}\right)^2\right]\Psi_B = \left(E^2 + eB_0\right)\Psi_B, \tag{B.26}$$

expanding the left-hand side, which is the same for both equations:

$$\begin{aligned}\left(\hat{p}_x - \frac{eB_0}{2}\hat{y}\right)^2 + \left(\hat{p}_y + \frac{eB_0}{2}\hat{x}\right)^2 &= \hat{p}_x^2 + \hat{p}_y^2 + \frac{e^2B_0^2}{4}\left(\hat{x}^2 + \hat{y}^2\right) + eB_0[\hat{x}\hat{p}_y - \hat{y}\hat{p}_x] \\ &= \hat{p}_x^2 + \hat{p}_y^2 + \frac{e^2B_0^2}{4}\left(\hat{x}^2 + \hat{y}^2\right) + eB_0\hat{L}_z, \end{aligned} \tag{B.27}$$

where it was used that $\hat{p}_x\hat{y} = \hat{y}\hat{p}_x$ and $\hat{p}_y\hat{x} = \hat{x}\hat{p}_y$. So that, Eqs. (B.25) and (B.26) take the form

$$\left[\hat{p}_x^2 + \hat{p}_y^2 + \frac{\omega_B^2}{16}\left(\hat{x}^2 + \hat{y}^2\right) + \frac{\omega_B}{2}\hat{L}_z\right]\Psi_A = \tilde{E}\Psi_A, \tag{B.28}$$

and

$$\left[\hat{p}_x^2 + \hat{p}_y^2 + \frac{\omega_B^2}{16}\left(\hat{x}^2 + \hat{y}^2\right) + \frac{\omega_B}{2}\hat{L}_z\right]\Psi_B = \tilde{E}'\Psi_B, \tag{B.29}$$

respectively, where $\omega_B = 2eB_0$, $\tilde{E} = E^2 - eB_0$ and $\tilde{E}' = E^2 + eB_0$. We can see that the left-hand sides of Eqs. (B.28) and (B.29) are the same as the left side of Eq. (B.3) with $M = 1/2$. So the procedure and the results are the same, just with diferent energy in the right side of the equations ($\tilde{E}$ and $\tilde{E}'$ in this case). Therefore, for the A-sublattice

$$n_\rho = \frac{\tilde{E}}{\omega_B} - \frac{|m|}{2} - \frac{m}{2} - \frac{1}{2} = \frac{E_{A,n}^2 - eB_o}{\omega_B} - \frac{|m|}{2} - \frac{m}{2} - \frac{1}{2},$$

$$\Rightarrow E_{A,n} = \sqrt{2eB_0 \left(n_\rho + 1 + \frac{|m|}{2} + \frac{m}{2} \right)}. \tag{B.30}$$

Analogously for the B-sublattice:

$$E_{A,n} = \sqrt{2eB_0 \left(n_\rho + \frac{|m|}{2} + \frac{m}{2} \right)}. \tag{B.31}$$

Bibliography

[1] L. D. Landau, *Zur Theorie der phasenum wandlungen II*, Phys. Z. Sowjetunion, **11**, 26-35 (1937).

[2] R. E. Peierls, *Quelques proprietes typiques des corpses solides*, Ann. I. H. Poncaire **5**, 177 (1935).

[3] N. D. Mermin, *Crystalline order in two dimensions*, Phys. Rev. **176**, 250 (1968).

[4] P. R. Wallace, *The Band Theory of Graphite*, Phys. Rev. **71**, 622 (1947).

[5] K. S. Novoselov *et al.*, *Electric field effect in atomically thin carbon films*, Science **306**, 666 (2004).

[6] J. C. Meyer *et al.*, *The structure of suspended graphene sheets*, Nature **446**, 60 (2007).

[7] D. R. Nelson, T. Piran and S. Weinberg, *Statistical Mechanics of Membranes and Surfaces*, World Scientific, Singapore (2004).

[8] K. S. Novoselov and A. K. Geim, *The rise of graphene*, Nature Materials, 2007.

[9] N. Levy, S. A. Burke, K. L. Meaker, M. Manlasigui, A. Zettl, F. Guinea, A. H. Castro Neto, and M. F. Crommie, *Strain-induced pseudomagnetic fields greater than 300 Tesla in graphene nanobubbles*, Science **329**, 544 (2010).

[10] I. Pomeranchuk, Y. Smorodinsky, J. Phys. USSR **9**, 97 (1945).

[11] Y. Wang, D. Wong, A. V. Shytov, V. W. Brar, S. Choi, Q. Wu, H.-Z. Tsai, W. Regan, A. Zettl, R. K. Kawakami, S. G. Louie, L. S. Levitov, and M. F. Crommie, *Observing Atomic Collapse Resonances in Artificial Nuclei on Graphene*, Science **340**, 734 (2013).

[12] A. V. Shytov, M. I. Katsnelson, and L. S. Levitov, *Vacuum Polarization and Screening of Supercritical Impurities in Graphene*, Phys. Rev. Lett. **99**, 236801 (2007).

[13] A. V. Shytov, M. I. Katsnelson, and L. S. Levitov, *Atomic Collapse and Quasi-Rydberg States in Graphene*, Phys. Rev. Lett. **99**, 246802 (2007).

[14] V. M. Pereira, J. Nilsson, and A. H. Castro Neto, *Coulomb Impurity Problem in Graphene*, Phys. Rev. Lett. **99**, 166802 (2007).

[15] O. V. Gamayun, E. B. Gorbar, and V. P. Gusynin, *Magnetic field driven instability of a charged center in graphene*, Phys. Rev. B **83**, 235104 (2011).

[16] D. Valenzuela, S. Hernandez-Ortiz, M. Loewe, and A. Raya, *Atomic collapse in graphene: lost of unitarity*, J. Phys. A: Math. Theor. **49**, 495302 (2016).

[17] P. Ghosh and P. Roy, *Collapse of Landau levels in graphene under uniaxial strain*, Mater. Res. Express **6**, 125603 (2019).

[18] D. Klöpfer, A. De Martino, D. Matrusalov, and R. Egger, *Scattering theory and ground state energy of Dirac fermions in graphene with two Coulomb impurities*, Eur. Phys. J. B **87**, 187 (2014).

[19] A. De Martino, D. Klöpfer, D. Matrusalov, and R. Egger, *Electric-Dipole-Induced Universality for Dirac Fermions in Graphene*, Phys. Rev. Lett. **112**, 186603 (2014).

[20] A. Vargas Chavez, *Estructura Supersimetrica de los Estados de Landau en Grafeno*, 2018.

[21] A. H. Castro Neto, F. Guinea, N. M. R. Peres, K. S. Novoselov, and A. K. Geim, *The electronic properties of graphene*, Rev. Mod. Phys. **81**, 109 (2009).

[22] Charles Kittel, *Introduction to Solid State Physics*, John Wiley & Sons, Inc., New York, 6th edition, 1986.

[23] M. I. Katsnelson, *Graphene: Carbon in Two Dimensions*,Cambridge University Press, 1st edition, 2012.

[24] J.-N. Fuchs and M.O. Goerbing, *Introduction to the Physical Properties of Graphene*, Lecture Notes, 2008.

[25] L. Pauling, *The nature of the chemical bond*, Journal of American Chemical Society, 1931.

[26] A. Apicella *et al.*, *Hybrid Ceramo-Polymeric Nano-Diamond Composites*, American Journal of Engineering and Applied Sciences **11(2)**, 766 (2018).

[27] L. F. Torres, S. Roche, and J.-C. Charlier, *Introduction to Graphene-Based Nanomaterials. From Electronic Structure to Quantum Transport*, Cambridge University Press, New York, 2014.

[28] D. W. Boukhvalov, M. I. Katsnelson, and A. I. Lichtenstein, *Hydrogen on graphene: Electronic structure, total energy, structural distortions and magnetism from first-principles calculations*, Phys. Rev. B **77**, 035427 (2008).

[29] A. Bostwick, T. Ohta, T. Seyller, K. Horn, and E. Rotenberg, *Quasiparticle dynamics in graphene*, Nature Physics 3, 2007.

[30] Kerson Huang, *Statistical Mechanics*, Jhon Wiley Sons, Inc., Second Edition, 1987.

[31] H. Falomir, J. Gamboa, M. Loewe and M. Nieto, *Graphene and non-Abelian quantization*, J. Phys. A: Math. Theor. **45**, 135308 (2012).

[32] S. Reich, J. Maultzsch, C. Thomsen, and P. Ordejón, *Tight-binding description of graphene*, Phys. Rev. B **66**, 035412 (2002).

[33] L. Landau, *Diamagnetismus der Metalle*, Zeitschrift für Physik **64**, 629-637 (1930).

[34] https://www.nist.gov/programs-projects/measuring-magneto-electronic-properties-graphene-nanometer-scale.

[35] George B. Arfken, *Mathematical Methods for Physicists*, Academic Press, New York, 7th edition, 2005.

[36] J. W. McClure, *Diamagnetism of Graphite*, Phys. Rev. **104**, 666 (1956).

[37] K. S. Novoselov, A.K. Geim, S.V. Morozov, D. Jiang, M.I. Katsnelson, I.V. Grigorieva, S.B. Bubonos, and A.A. Firsov, *Two-dimensional gas of massless Dirac fermions in graphene*, Nature Volume 438 (2005).

[38] Y. Zhang, Y.-W. Tan, H. L. Stormer, and P. Kim, *Experimental observation of the quantum Hall effect and Berry's phase in graphene*, Nature Volume 438 (2005).

[39] G. Li and E. Y. Andrei, *Observation of Landau levels of Dirac fermions in graphite*, Nature Physics Volume 3 (2007).

[40] V. P. Gusynin and S. G. Sharapov, *Unconventional Integer Quantum Hall Effect in Graphene*, Phys. Rev. Lett. **95**, 146801 (2005).

[41] E. Cadelano, P. L. Palla, S. Giordano, and L. Colombo, *Nonlinear Elasticity of Monolayer Graphene*, Phys. Rev. Lett. **102**, 235502 (2009).

[42] A. Fasolino, J. H. Los, and M. I. Katsnelson, *Intrinsic ripples in graphene*, Nature Materials volume 6 (2007).

[43] N. A. Vinogradov, A. A. Zakharov, V. Kocevski, J. Rusz, K. A. Sinonov, O. Eriksson, A. Mikkelsen, E. Lundgren, A. S. Vinogradov, N. Martensson, and A. B. Preobrajenski, *Formation and Structure of Graphene Waves on Fe(110)*, Phys. Rev. Lett. **109**, 026101 (2012).

[44] M. Oliva-Leyva and G. G. Naumis, *Generalizing the Fermi velocity of strained graphene from uniform to nonuniform strain*, Phys. Lett. A **379**, 2645-51 (2015).

[45] G. G. Naumis, D. Barraza-Lopez, M. Oliva-Leyva, and H. Terrones, *Electronic and optical properties of strained graphene and other similar 2d materials: A review*, Rep. Prog. Phys. **80** (2017).

[46] C. Si, Z. Sun and F. Liu, *Strain engineering of graphene: a review*, Nanoscale **8**, 3207 (2016).

[47] V. M. Pereira, A. H. Castro Neto, and N. Peres, *A tight-binding approach to uniaxial strain in graphene*, Phys. Rev. B: Condens. Matter **80**, 045401 (2009).

[48] S.-M. Choi, S.-H. Jhi, and Y.-W. Son, *Effects of strain on electronic properties of graphene*, Phys. Rev. B: Condens. Matter **81**, 081407 (2010).

[49] M. Farjam and H. Rafii-Tabar, *Comment on "Band structure engineering of graphene by strain: First-principles calculations"*, Phys. Rev. B: Condens. Matter **80**, 167401 (2009).

[50] R. Ribeiro, V. M. Pereira, N. Peres, P. Briddon, And A. H. Castro Neto, *Strained graphene: tight-binding and density functional calculations*, New J. Phys. **11**, 115002 (2009).

[51] G. Cocco, E. Cadelano and L. Colombo, *Gap opening in graphene by shear strain*, Phys. Rev. B: Condens. Matter **81**, 241412 (2010).

[52] I. Y. Sahalianov, T. M. Radchenko, V. A. Tatarenko, G. Cuniberti, and Y. I. Prylutskyy, *Straintronics in graphene: extra large electronic band gap induced by tensile and shear strains*, J. Appl. Phys. **126**, 054302 (2019).

[53] F. Guinea, M. I. Katsnelson, and A. K. Geim, *Energy gaps and a zero-field quantum Hall effect in graphene by strain engineering*, Nature Physics volume **6**, 30 (2010).

[54] F. Guinea, A. K. Geim, M. I. Katsnelson, and K. S Novoselov, *Generating quantizing pseudomagnetic fields by bending graphene ribbons*, Phys. Rev. B **81**, 035408 (2010).

[55] L. Landau, E. Lifshitz, *Theory of Elasticity*,Pergamon, Oxford, 1976.

[56] A. L. Kitt, V. M. Pereira, A. K. Swan and B. B. Goldberg, *Erratum: Lattice-corrected strain-induced vector potentials in graphene (Phys. Rev. B 85, 115432 (2012)*, Phys. Rev. B **87**, 159909 (2013).

[57] J. L. Mañes, *Symmetry-based approach to electron-phonon interactions in graphene*, Phys. Rev. B **76**, 045430 (2007).

[58] A. J. Heeger, S. Kivelson, J. R. Schrieffer and W.-P Su, *Solitons in conducting polymers*, Rev. Mod. Phys. **60**, 781 (1988).

[59] M. A. H. Vozmediano, M. I. Katsnelson and F. Guinea, *Gauge fields in graphene*, Phys. Rep. **496**, 109 (2010).

[60] C. L. Kane and E. J. Mele, *Z_2 Topological Order and the Quantum Spin Hall Effect*, Phys. Rev. Lett. **95**, 146802 (2005).

[61] C. L. Kane and E. J. Mele, *Quantum Spin Hall Effect in Graphene*, Phys. Rev. Lett. **95**, 2268012 (2005).

[62] Y. Betancur-Ocampo, M. E. Cifuentes-Quintal, G. Cordourier-Maruri, and R. de Coss, *Landau levels in uniaxially strained graphene: A geometrical approach*, Annals of Physics, 2008.

[63] E. Díaz-Bautista and Y. Betancur-Ocampo, *Phase-space representation of Landau and electron coherent states for uniaxially strained graphene*, arXiv:1910.09696v1 (2019).

[64] E. N. Economou, *Green's Functions in Quantum Physics*, Third edition, Springer, Berlin, 2006.

[65] W. Greiner, B. Muller, J. Rafelski, *Quantum Electrodynamics of Strong Fields*, Springer, Berlin, 1985.

[66] Y. B. Zeldovich, V. S. Popov, *Electronic structure of superheavy atoms*, Sov. Phys. Usp. **14**, 673 (1972).

[67] S. S. Gershtein and Y. B. Zeldovich, Sov. Phys. JETP **30**, 358 (1970).

[68] J. Rafelski, L. P. Fulcher, and W. Greiner, Phys. Rev. Lett. **27**, 958 (1971).

[69] B. Müller, H. Peitz, J. Rafelski, and W. Greiner, Phys. Rev. Lett. **28**, 1235 (1972).

[70] https://crommie.berkeley.edu/research/imrel/atomcollapse/

[71] S. Hernandez-Ortiz, *Sobre la Transición Semimetal-Aislante en Grafeno*, 2013.

[72] D. S. Novikov, *Elastic scattering theory and transport in graphene*, Phys. Rev. B **76**, 245435 (2007).

[73] I. S. Terekhov, A. I. Milstein, V. N. Kotov, and O. P. Sushkov, *Screening of Coulomb impurities in graphene*, Phys. Rev. Lett. **100**, 076803 (2008).

[74] M. M. Fogler, D. S. Novikov, and B. I. Shklovskii, *Screening a hypercritical charge in graphene*, Phys. Rev. B **76**, 233402 (2007).

[75] Y. Wang et *al.*, *Mapping Dirac Quasiparticles near a Single Coulomb Impurity on Graphene*, Nat. Phys. **8**, 653 (2012).

[76] Ch.-L. Ho and V. R. Khalilov, *Planar Dirac electron in Coulomb and magnetic fields*, Phys. Rev. A **61**, 032104 (2000).

[77] A. Raya, E. Reyes, *Fermion condensate in vacuum current density induced by homogeneous and inhomogeneous magnetic fields in (2+1) dimensions*, Phys. Rev. D **82**, 016004 (2010).

[78] D. V. Kheveshchenko, *Magnetic-Field-Induced Insulating Behaviour in Highly Oriented Pyrolitic Graphite*, Phys. Rev. Lett. **87**, 206401 (2001).

[79] E. V. Gorbar, V. P. Gusynin, V. A. Miransky, and I. A. Shovkovy, *Magnetic field driven metal-insulator phase transition in planar systems*, Phys. Rev. B **66**, 045108 (2002).

[80] V. P. Gusynin, V. A. Miransky, S. G. Sharapov, and I. A. Shovkovy, *Rxcitonic gap, phase transition, and quantum Hall effect in graphene: strong-coupling regime*, Phys. Rev. B **74**, 195429 (2006).

[81] I. F. Herbut, *Theory of Integer quantum Hall effect in graphene*, Phys. Rev. B **75**, 165411 (2007).

[82] I. F. Herbut, $SO(3)$ *symmetry between Néel and ferromagnetic order parameters for graphene in a magnetic field*, Phys. Rev. B **76**, 094701 (2007).

[83] J.-N. Fuchs and P. Lederer, *Spontaneous Parity Breaking of Graphene in the Quantum Hall Regime*, Phys. Rev. Lett. **98**, 016803 (2007).

[84] M. Ezawa, *Intrinsic Zeeman Effect in Graphene*, J. Phys. Soc. Jpn. **70**, 094701 (2007).

[85] V. N. Oraevskii, A. I. Rex and V. B. Semikoz, Sov. Phys. JETP **45**, 428 (1977).

[86] P. Schlutter et *al.*, *Bound electrons in critical magnetic fields*, J. Phys. B **18**, 1685 (1985).

[87] A. Contreras-Astorga, V. Jakubský, A. Raya, *On the propagation of Dirac fermions in graphene with the strain-induced inhomogeneous Fermi velocity*, arXiv:1912.00675v1, Condensed Matter (2019).

[88] J. D. Jackson, *Classical Electrodynamics*, Third Edition, John Wiley Sons, Inc. (1999).

[89] E. V. Gorbar, V. P. Gusynin, and O. O. Sobol, *Supercritical electric dipole and migration of electron wave function in gapped graphene*, Europhys. Lett. **111**, 37003 (2015).

[90] I. S. Gradshteyn and I. M. Ryzhik, *Table of Integrals, Series, and Products*, Academic Press, New York (2007).

[91] M. Abramowitz and I. A. Stegun, *Handbook of Mathematical Functions*, Dover, New York (1965).

[92] E. Schrödinger, Ann. Phys. **79**, 361, 489; **80**, 437; **81**, 109 (1926).

[93] O. Klein, Z. f. Phys. **37**, 895 (1926).

[94] W. Gordon, Z. f. Phys. **40**, 117 (1926).

[95] P. A. M. Dirac, Proc. Roy. Soc. **A 117**, 610; **A 118**, 351 (1928).

[96] P. A. M. Dirac, Proc. Roy. Soc. **133**, 60 (1931).

[97] J. R. Oppenheimer, Phys. Rev. **35**, 562 (1930); I.Tamm, Z. f. Phys. **62**, 545 (1930).

[98] P. A. M. Dirac, First W. R. Crane Lecture at the University of Michigan, April 17, 1989, unpublished.

[99] C. D. Anderson, Science **76**, 238 (1932); Phys. Rev. **43**, 491 (1933).

[100] C. Itzykson and J.-B. Zuber, *Quantum Field Theory*, McGraw-Hill (1985).

[101] S. Weinberg, *The Quantum Theory of Fields I*, Cambridge UP (1995).